FAST HISTORY MATCHING OF TIME-LAPSE SEISMIC AND PRODUCTION

DATA FOR HIGH RESOLUTION MODELS

A Dissertation

by

ALVARO JOSE REY AMAYA

Submitted to the Office of Graduate Studies of
Texas A&M University
in partial fulfillment of the requirements for the degree of

DOCTOR OF PHILOSOPHY

August 2011

Major Subject: Petroleum Engineering

Fast History Matching of Time-Lapse Seismic and Production Data for High Resolution

Models

FAST HISTORY MATCHING OF TIME-LAPSE SEISMIC AND PRODUCTION

DATA FOR HIGH RESOLUTION MODELS

A Dissertation

by

ALVARO JOSE REY AMAYA

Submitted to the Office of Graduate Studies of
Texas A&M University
in partial fulfillment of the requirements for the degree of

DOCTOR OF PHILOSOPHY

Approved by:

Chair of Committee,	Akhil Dattagupta
Committee Members,	Yousef Jafarpour
	Ahmed Ghassemi
	Yalchin Efendiev
Head of Department,	Stephen A. Holditch

August 2011

Major Subject: Petroleum Engineering

ABSTRACT

Fast History Matching of Time-Lapse Seismic and Production-Data for High Resolution
Models. (August 2011)

Alvaro Jose Rey Amaya, B.S., Universidad Industrial de Santander;

M.S., Universidad de los Andes, Colombia

Chair of Advisory Committee: Dr. Akhil Dattagupta

Seismic data have been established as a valuable source of information for the
construction of reservoir simulation models, most commonly for determination of the
modeled geologic structure, and also for population of static petrophysical properties (e.g.
porosity, permeability). More recently, the availability of repeated seismic surveys over
the time scale of years (i.e., 4D seismic) has shown promising results for the qualitative
determination of changes in fluid phase distributions and pressure required for
determination of areas of bypassed oil, swept volumes and pressure maintenance
mechanisms. Quantitatively, and currently the state of the art in reservoir model
characterization, 4D seismic data have proven distinctively useful for the calibration of
geologic spatial variability which ultimately contributes to the improvement of reservoir
development and management strategies. Among the limited variety of techniques for the
integration of dynamic seismic data into reservoir models, streamline-based techniques
have been demonstrated as one of the more efficient approaches as a result of their
analytical sensitivity formulations. Although streamline techniques have been used in the
past to integrate time-lapse seismic attributes, the applications were limited to the
simplified modeling scenarios of two-phase fluid flow and invariant streamline geometry
throughout the production schedule.

This research builds upon and advances existing approaches to streamline-based seismic
data integration for the inclusion of both production and seismic data under varying field
conditions. The proposed approach integrates data from reservoirs under active reservoir

management and the corresponding simulation models can be constrained using highly detailed or realistic schedules. Fundamentally, a new derivation of seismic sensitivities is proposed that is able to represent a complex reservoir evolution between consecutive seismic surveys. The approach is further extended to manage compositional reservoir simulation with dissolution effects and gravity-convective-driven flows which, in particular, are typical of CO_2 transport behavior following injection into deep saline aquifers. As a final component of this research, the benefits of dynamic data integration on the determination of swept and drained volumes by injection and production, respectively, are investigated. Several synthetic and field reservoir modeling scenarios are used for an extensive demonstration of the efficacy and practical feasibility of the proposed developments.

DEDICATION

This work is dedicated to my wife who has been the support and motivation during the good and difficult times during my adulthood. Pilar, this dissertation is not my work. We made it together.

ACKNOWLEDGEMENTS

TABLE OF CONTENTS

LIST OF FIGURES

FIGURE   Page

LIST OF TABLES

CHAPTER I

INTRODUCTION AND STUDY OBJECTIVES

Seismic data have been a valuable source of information for the construction of reservoir models and widely used for the determination of the structure, and for the population of petrophysical properties (e.g. porosity, permeability) when combined with well information. More recently the availability of repeated seismic surveys in conjunction with refined high resolution seismic processing methods and seismic inversion algorithms have shown promising results for determination of the changes in fluid distribution and pressure as the reservoir evolves through time. Imaging techniques and sophisticated visualization software have made the 4D seismic an attractive monitoring tool that can be used for quantitative evaluation of the state of the reservoir. Geologists, geophysicists and reservoir engineers study the effects of changes detected in a variety of seismic attributes and the elastic properties of the rock in order to design effective reservoir management strategies to optimize production and increase recovery.

The next natural step is to calibrate the static model using the seismic surveillance data. This is particularly attractive because of the large areal coverage of the seismic data. This large quantity of information can be utilized to infer reservoir properties far from the wells. However, this is a complex task. First, the areal resolution of the seismic data must be comparable with the horizontal size of the cells in the geologic model (i.e., to make effective use of this information we should consider a high resolution inversion). The amount of information and the variability of the pressure and fluid saturation changes are major challenges for the implementation of derivative-free techniques for inversion. Other methods that have traditionally been recognized for their efficiency in

This dissertation follows the style of *SPE Journal*.

sensitivity calculation, such as the adjoint techniques, can be computationally prohibitive when dealing with large 4D seismic data sets (Dong and Oliver, 2005). More recent methods such as the Ensemble Kalman Filter have problems with sampling error due to the large amount of dynamic data and practical limitations related to the ensemble size.

Streamline techniques have proven to be particularly efficient to calibrate static properties from dynamic well responses (e.g. tracer data, water cut, gas oil ratio and interference tests). They have also been applied for integrated changes using seismic amplitude. However, the application was limited to the case of minimal changes in pressure and field conditions between the base and consecutive seismic surveys (Vasco et al., 2004). One of the most attractive properties of the streamline-based data integration algorithms is their ability to calculate analytical sensitivities of the production data with respect to continuous reservoir parameters (Vasco and Datta-Gupta, 1997). Furthermore, data integration based on travel time sensitivities leads to a minimization procedure that exhibits quasi-linear properties, converging in a smaller number of iterations and with better performance (in the context of getting trapped into a local minima) compared to amplitude inversion algorithms (Luo and Schuster, 1991; Vasco et al., 1999; Cheng et al., 2005a). The advantages of streamline methods in relation to the calculation of sensitivities, even under complex geological descriptions, make them appealing for history matching procedures using high resolution seismic data.

This research aims to extend the previous streamline-based history matching workflows for the inclusion of production and seismic data under varying field conditions. The proposed approach integrates data from reservoirs under active reservoir management, and the corresponding simulation models can be constrained using highly detailed schedules. We propose a new set of seismic sensitivities that can represent a complex reservoir evolution between consecutive seismic surveys, and we have extended the approach to handle compositional reservoir simulation with dissolution effects and

gravity-convective-driven flows typical of CO2 injection into deep saline aquifers. One of the practical and practically relevant characteristics of our approach is the ability to use seismic inverted attributes (e.g., soft maps of water saturation) expressed as differences between consecutive seismic surveys instead of absolute values, i.e., we can perform the inversion on data expressed as a change in time rather than as maps of the fluid distribution at a particular time. We also study the effects of noise associated with the results of a geophysical seismic inversion (Feng and Mannseth, 2010) on the performance of the proposed methods. Finally, we investigate the benefits obtained by data integration in the determination of swept and drained volumes. Synthetic and field examples are used extensively to demonstrate the power and practical feasibility of our proposed approaches.

1.1. Overview of Model Calibration and Reservoir Management

Reservoir engineers dedicate their efforts to increase petroleum recovery and maximize the return on investment. The main objective is to "understand" the reservoir and learn the mechanisms that provide energy (flow potential that drives the movement of hydrocarbons) and the underlying heterogeneity (that affects the pathways of the fluids from the sources to the producers). Reservoir simulation is the most comprehensive tool applied to design strategies that modify the fluid motion in the subsurface (e.g. infill wells, changes in injection and production rates, external driving mechanisms, smart wells) in order to improve recovery. The model is constructed using all possible sources of data (including seismic, well logs, cores, etc.) to make the best possible representation of the physical system. Of all data types, seismic data are fundamental to infer the structure of the reservoir. Geological analogs are often used to determine the facies distribution. Core data are used to determine flow and transport properties. The seismically constrained model is typically up-scaled and prepared for reservoir simulation. Reservoir simulation is the exercise of numerically solving a set of partial differential equations (PDE's) that define the conservation laws (mass, momentum and

energy) and a set of constitutive equations that determine the behavior of fluids in the formation (thermodynamic properties, special core analysis [SCAL] properties), subject to a set of boundary conditions (well locations, rates, pressures, aquifer, gas cap, etc) and initial conditions (oil water contacts, gas oil contact, initial pressure, fluids in place, etc), in order to forecast the production of fluids at the field facilities. The objective is to generate multiple scenarios for the development of the field and also multiple realizations of the reservoir model for uncertainty assessment. The responses are used to select a business development plan which aims to maximize the recovery while minimizing the operational cost with some acceptable level of risk.

The reservoir surveillance data play a fundamental role in the improvement of the reliability of the predictions, reducing the uncertainty of the model and enhancing our understanding of the drive mechanisms of the reservoir. The main objective of this research is to develop an efficient workflow that can integrate areally sparse production data with seismic-derived parameters such as acoustic impedance to reduce the uncertainty associated with the reservoir model; thus, improving the ability to assess the changes resulting from reservoir management activities.

1.2. Objectives

We'll now outline the stages of this research and the specific objectives associated with each phase.

1.2.1. Model Calibration with Production Data

Although the benefits of the GTTI technique have been extensively covered in the past (He et al., 2002; Wu and Datta-Gupta 2002; Cheng et al, 2005a; Cheng et al, 2005b); a common problem for the misfit calculation is the performance of the cross-correlation with highly detailed production data. Under the influence of rapid variations of the

production responses, the cross-correlation may present non-convexity making it difficult to determine the maximum. The common procedure to avoid this limitation is to smooth the production responses; however, a time-domain smoothing does not guarantee the elimination of the high frequency details. It can quickly deteriorate the resolution of the production responses, thereby reducing the GTTI technique into a single travel time inversion. We present a new approach for re-sampling of the production information that eliminates the high frequency details while preserving the shape of the production responses.

1.2.2. Two Phase Time-lapse Seismic Data Integration

We propose an approach that deals with seismic-derived information in two phase reservoirs. The workflow utilizes maps of changes in the saturation state of the reservoir between two different seismic surveys or changes in acoustic impedance. We assume that those changes have been obtained as a result of a previous geophysical inversion and use a poroelastic model for relating the reservoir dynamic variables with the seismic-derived acoustic impedance. This information is then integrated with other sources of dynamic data (specifically the arrival of water at the producers). In order to utilize the seismic data in the calibration of the static model, we develop a set of sensitivities of the changes in seismic attributes with respect to continuous reservoir parameters (e.g., porosity and permeability). These sensitivities incorporate the effects of varying field conditions that can drastically affect the state of the velocity field in the reservoir (e.g., changes in rate, infill wells, aquifer interaction, etc.).

We investigate the use of seismic-derived information as either the sole source of surveillance data, or in combination with the arrival time of the water phase at the producers. Our aim is to propose an efficient method of jointly integrating the seismic surveillance data and production data at the well level.

1.2.3. Compositional Seismic Data Integration

We extend the algorithms developed for the seismic data integration using streamline-derived sensitivities to the case of injection of CO_2 (e.g. sequestration in deep saline aquifers). In the proposed approach, we overcome the limitations of the streamline techniques related to their inability to capture transverse dynamic effects that are not aligned to the streamlines. This transverse component of the driving force is particularly significant in the case of CO_2 movement due to the buoyancy effects originating from the difference in densities between the fluids in the reservoir. We use compositional streamlines that capture the state of the reservoir dynamics at any particular time. The streamlines are traced using the fluxes from a compositional reservoir simulator that includes all the significant physical and chemical effects associated with the injection of CO_2. We calculate the sensitivities of the changes of the CO_2 plume with respect to the permeability. In order to formulate our sensitivity calculations, we use the relationship between the streamlines, the underlying heterogeneity and the location of the CO_2 plume. Finally, we use the sensitivities to perform a gradient based minimization using a least squares algorithm, to calibrate the movement of the CO_2 plume using seismic data.

We investigate the effects of the buoyancy forces in the performance of our proposed inversion workflow. These effects can be captured by analyzing the influence of the viscous-gravity ratio number in the inversion procedure. Finally, we are interested in the benefits of integrating the dynamic data to better understand the underlying heterogeneity and the capacity to store CO_2.

CHAPTER II

ASSISTED HISTORY MATCHING IN THE PRESENCE OF FREQUENT WELL
INTERVENTION[*]

Streamline based assisted and automatic history matching techniques have shown great potential in reconciling high resolution geologic models to production data. Several field applications have demonstrated the efficiency of streamline-based sensitivity calculations together with the generalized travel time inversion (GTTI) for history matching. The GTTI has been shown to be particularly effective because of its quasi-linear properties. However, a limitation of the current GTTI based production data misfit calculations is that it is best suited for continuous and monotonic production histories. Field applications very often include reservoir management decisions that involve well shut-in, recompletions and pattern conversions. These introduce significant discontinuities and non-monotonic effects in the production response.

In this chapter we propose an efficient and novel technique that handles production discontinuities through a re-sampling of the production data, eliminating high frequency production details in a transform domain. The technique also reduces non-monotonic behavior and results in a response more suitable for the GTTI based misfit calculations. Our proposed approach has been applied to an offshore turbidite reservoir with extensive well intervention resulting in highly detailed production responses. The static model contains more than three-hundred-thousand cells, complex sand depositional distribution combined with fault structures, four pairs of injector-producers, deviated producing

---

[*] Part of this chapter is reprinted with permission from "Assisted History Matching in an Offshore Turbidite Reservoir with Active Reservoir Management" by Rey, A., Ballin, P., Park, J., Vitalis, C., Kim, J. and Datta-Gupta, A., 2009. Paper SPE 92873 presented at the 2009 SPE ATCE, New Orleans, LA, 4-7 October. Copyright 2009 by the Society of Petroleum Engineers.

wells and more than 8 years of production history. Previous history matching attempts using traditional approaches had difficulties matching production response at the individual well level. With our proposed modifications to the GTTI approach, a significant improvement was obtained on the well level match quality. Most importantly, by visualizing the streamlines and the dynamic adjustment of flow paths during history matching, we could easily identify the areas of inconsistency between the geologic model and the production data. The calibrated geologic model and streamline trajectories provided important insight about communication within sand channels, differences in flow paths and barriers that have not been included in the previous geologic and seismic interpretation.

2.1. Chapter Introduction

Reconciling geological models with the field production information is one of the most demanding tasks in reservoir characterization. The information contained in the dynamic data such as transient pressure, tracer or multiphase production histories can be used to identify high permeability channels and low permeability barriers in the geologic model. In addition, the dynamic information is fundamental to our understanding of the interaction between heterogeneity and fluid flow in the reservoir and the boundary conditions such as the interaction between the aquifer and the reservoir. It is well known that the geological features play a key role in decisions related to reservoir management and field development strategies (Landa et al., 2000). Traditionally the integration of production data has been performed by reservoir engineers using local and regional multipliers of reservoir properties such as permeability and porosity. This procedure is highly subjective, requires a great deal of experience and can lead to loss of geologic realism (Williams et al., 1998). More recently assisted or automatic history matching using inverse modeling has shown potential benefits related to preserving spatial continuity and geologic realism during history matching (Yang and Watson, 1988, Cheng et al., 2004; Reynolds et al., 1999; Landa and Horne., 1997; Brun et al., 2001).

However, the solution of the inverse problem can be computationally expensive as it involves multiple solutions of the flow and transport equation to establish the relationship between the production response and the uncertain reservoir parameters (Datta-Gupta and King, 2007).

Related to the process of reconciling the model response and the historical production data, several algorithms have been proposed in the literature. These can be categorized into three distinct groups: Gradient-based methods, sensitivity-based methods and derivative-free methods. Although the derivative free methods are the simplest to implement, they are generally limited to a small number of parameters because of the computational demand (Oliver et al., 2001). Gradient-based methods are robust but they generally exhibit slow convergence rates (Gill et al., 1981, McCormick and Tapia, 1972). The sensitivity based methods have the fastest convergence rates but require the calculation of the parameter sensitivities which are partial derivatives of the production response with respect to the reservoir parameters. This collection of techniques is often referred to as automated history matching methods in the literature (Cheng et al., 2005a).

Parameter sensitivities are an integral part of history matching as they quantitatively relate the changes in the production response to the changes in the reservoir properties. Several techniques have been proposed for calculating the sensitivities and these can be broadly categorized into three groups. First, the perturbation methods that are based on introducing small changes in the reservoir properties and computing the corresponding changes in the production response through flow simulation. For large number of parameters, the perturbation method can be computationally prohibitive. Second, the adjoint methods (Li et al. 2003) that use the optimal control theory. Although computationally efficient, they are mathematically complex and require access to the source code of the forward simulator which may not be available. Finally, the streamline-based sensitivities utilize an analytic approach that involves 1-D integral along streamlines to efficiently compute the parameter sensitivities using a single

forward simulation. Because the streamlines can be readily obtained from the fluid fluxes, the approach can be implemented using both finite-difference or streamline simulators. (Cheng et al., 2005b).

The streamline-based travel time inversion for history matching of production data uses a direct analogy between the streamlines methods and the seismic waveform inversion (Vasco et al., 1999; Datta-Gupta et al., 2001). There are several advantages to the travel time inversion compared to the more traditional 'amplitude' inversion during history matching (Cheng et al, 2005a). Among them, particularly noteworthy are the properties related to the quasilinear behavior and rapid convergence during the minimization of the misfit between the observed and computed production response(Luo and Schuster, 1991; Cheng et al., 2005a). The travel time matching approach was extended to changing field conditions by Wu and Datta-Gupta (2002) and He et al (2002). In the proposed generalized travel time inversion (GTTI), an analogy with the travel time tomography is exploited to preserve the favorable characteristics of the travel time inversion and at the same time to obtain an improved match to the production history. Thus, instead of matching a particular time in the production history, the misfit is calculated as the 'optimal' shift in time that maximizes the correlation between the simulated and the observed production responses at all times. Because the GTTI approach leads to a single time misfit per well for the whole production history, the parameter sensitivities for this time misfit has been shown to be averages over all available time points of the production history (He et al., 2002).

The GTTI history matching technique has been applied in a large number of field cases with two-phase oil-water flow (Qassab et al., 2003; Cheng et al., 2004; Hohl et al., 2006) and more recently to three-phase and compressible conditions (Cheng et al., 2007). Oyerinde et al. (2009) reported the difficulties in the calculation of the 'optimal' time shift in the presence of non-monotonic production profiles, particularly for the gas-oil ratios at the wells. Similar difficulties are also encountered with highly detailed and

discontinuous production histories resulting from active reservoir management and interventions leading to well shut-ins and production/injection re-allocations. In this chapter, we focus on generalizing the GTTI calculations for history matching highly non-monotonic production histories arising from continuous reservoir management. Specifically, we propose a new and robust methodology to calculate the GTTI misfit and improved calculations of the GTTI sensitivities.

In this chapter we first introduce the fundamentals of the GTTI technique. After that, the concept of a 'production time' is introduced. This concept is used for resampling the dynamic data and to compute the parameter sensitivities. Next, we introduce the modifications in the calculation of the GTTI sensitivities, and illustrate the general workflow using a synthetic example. We then review the mathematical formulation of the sensitivities in the streamline coordinate system. Finally, the results from data integration in a highly faulted field application with frequent intervention are discussed demonstrating the power and applicability of the proposed methodology.

2.2. Approach

The streamline-based history matching is a maturing technique that has evolved in parallel with the streamline simulation. It has been successfully applied to inversion of production data with high resolution geologic models using streamline simulators. In recent years the technique has been generalized to allow the use of finite difference simulators (FDS) (Cheng et al 2005b, Hohl et al. 2006). In this approach, the FDS is used for solving the pressure equations and calculating the phase fluxes which are then utilized for the streamline tracing. Using the streamline trajectories, we transform the computation domain from the Eulerian finite difference formulation to the Lagrangian perspective. This representation is well suited for convection dominated flows in the reservoir (for example, the tracer transport or the water-oil displacement). Embedded in this transformation is the concept of the streamline travel time or time of flight

coordinate system, which allows expressing the conservation or the saturation equations as a series of one dimensional transport equations (Datta-Gupta and King, 2007). Decoupling the complex flow geometry of the cellular grid into 1-D streamlines is the fundamental element in the computation of streamline-based sensitivity coefficients. This is mainly because the sensitivities are evaluated as numerical integrals along the streamlines. Once the sensitivities are mapped back into the geo-cellular grid, the dynamic data integration is performed utilizing an iterative least squares minimization of a generalized travel time misfit (He et al. 2002; Cheng et al., 2005a). To ensure spatial continuity and geologic realism the misfit function is generally augmented by additional regularization terms, (Yoon et al., 2001.). In this research, our goal is to extend the applicability of the streamline-based generalized travel time inversion to highly detailed and non-monotonic production profiles as commonly encountered in reservoirs under active managements. For this, our proposed modifications to the standard GTTI history matching technique are discussed below.

2.2.1. Resampling the Production Response: Time vs Cumulative Production

Reservoir responses in highly detailed schedules contain rapid fluctuations in production data that it is not well-suited for the GTTI technique (**Fig. 2.1**). This is because the GTTI misfit calculation relies on cross-correlating the observed and computed production response and high frequency content of the data frequently lead to false correlations. Also, much of the fluctuations in the production data are often reflection of the operating conditions and well interventions rather than reservoir heterogeneity. For history matching purposes we have to resample the production data to reflect the reservoir flow patterns. Specifically we need to emphasize the early time that contain information about the flow pattern and barriers. The conventional resampling based on equal time intervals attempts to reduce the high frequency detailed based on coarsening the time intervals into larger time periods. However, such sampling does not ensure removal of production discontinuities such as shut in periods (**Fig. 2.2**). To circumvent this difficulty, the longer periods of well inactivity enforce longer smoothing time periods and higher

information loses. This eventually compromises the quality of sampling of the production data, especially at the beginning of the well history when the majority of the produced volumes and the higher production rates occur. To overcome this problem, we propose a resampling based on expressing the production response at equal volumes of oil produced at surface conditions.
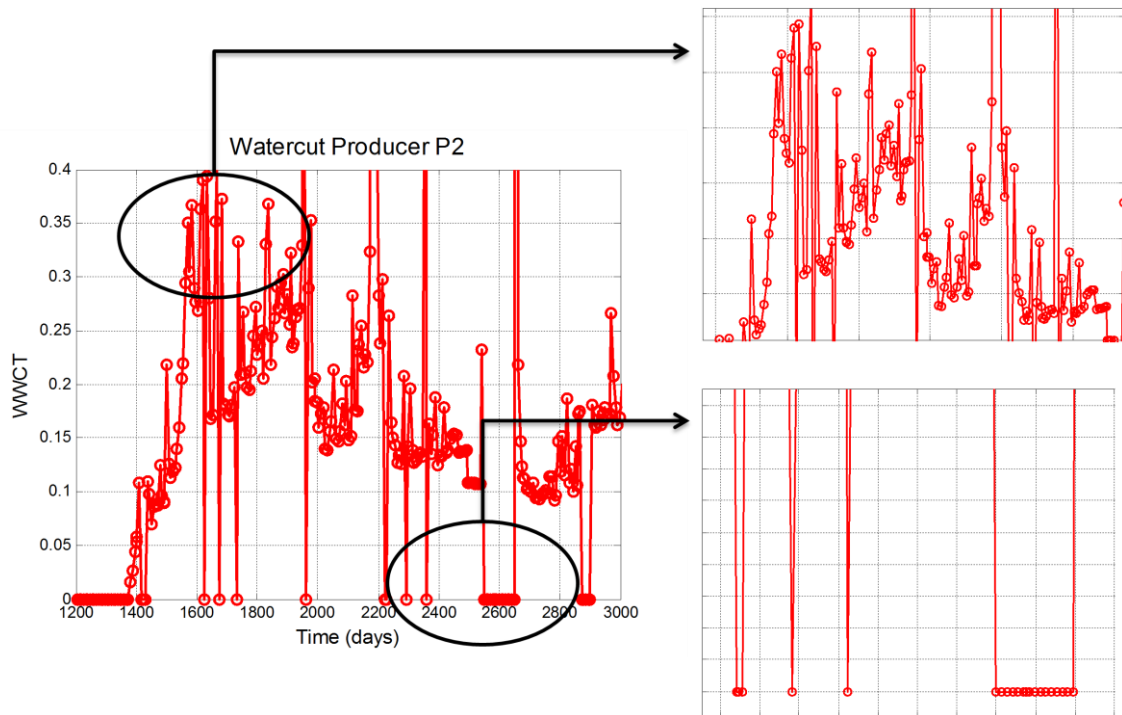
Fig. 2.1—Water cut response under active reservoir management, details of the high frequency information and the discontinuities in the production history.

There are several benefits associated with the use of cumulative oil produce instead of time for production data resampling. This is illustrated in **Fig. 2.3**. The advantages became apparent when we compare **Fig. 2.3** with **Fig. 2.2**. First, the operational conditions are decoupled from the actual state of the reservoir and do not introduce discontinuities in the production history. Expressing the production history at 'equal volumes of produced oil' makes the time intervals more flexible, longer towards the end of the production history when well interventions are potentially more frequent, and shorter at the early times of production when the majority of the large scale

heterogeneity can be captured (Datta-Gupta et al., 1998; Vasco and Datta-Gupta, 1997). Second, the discontinuities in the production history resulting from well shut-in are automatically eliminated. This makes the production history more suitable for the generalized travel time misfit calculations.
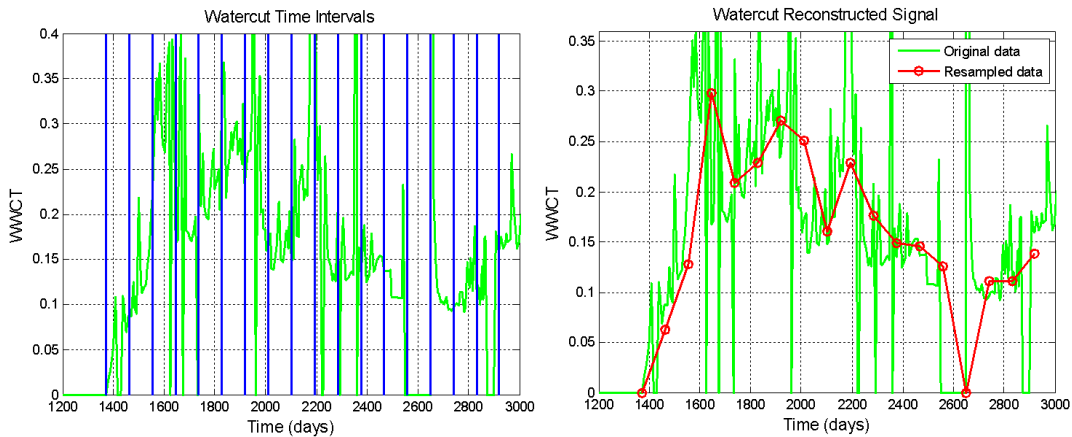
Fig. 2.2—Resampling of production data based in equal intervals in time: Green line is the original signal, red line the smoothed version.
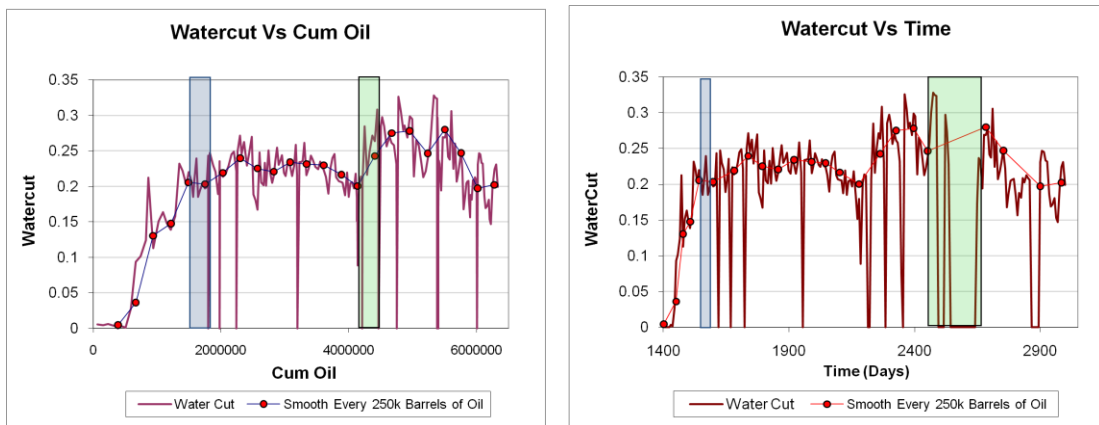
Fig. 2.3—Comparison between equal volumes of oil produced and the corresponding time intervals.

2.2.2. An Illustration of the Method

We will discuss the mathematical details in the next section. To start with, we first illustrated the benefits of our proposed approach using a synthetic example. The

Synthetic example consists of waterflooding in a nine spot pattern with one injector located at the center and eight producers in the periphery. The geological model consists of a two dimensional 50x50 cellular grid with constant porosity and a lognormal permeability distribution with a north-east direction of continuity (**Fig. 2.4a.**). The example involves two phase flow with voidage balance and the hydrocarbon phase is undersaturated oil for the entire production history. For introducing non-monotonicity and discontinuities in the production response as will be the case for a reservoir under active management, a series of shut in times were introduced for the wells located at the corners. However, the wells located on the sides of the model were treated as control wells exhibiting a continuous production profile. The initial permeability field used for history matching is shown in **Fig. 2.4b**.
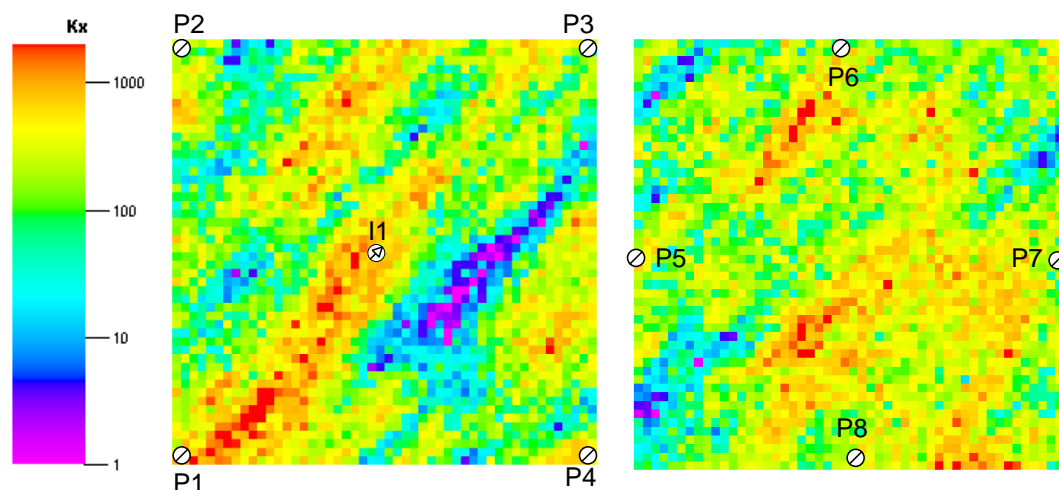
Fig. 2.4—(a) Reference permeability field and distribution of producers and injectors in the nine spot synthetic example, (b) Initial permeability field used in inversion.

The water cut responses from the initial model and the reference model are shown in the **Fig. 2.5**. The presence of production discontinuities introduces higher frequencies in the observed and model production response. In the conventional GTTI technique, these production responses will be used in order to determine the best shift in time which maximizes the correlation between the two responses (**Fig. 2.6a**).
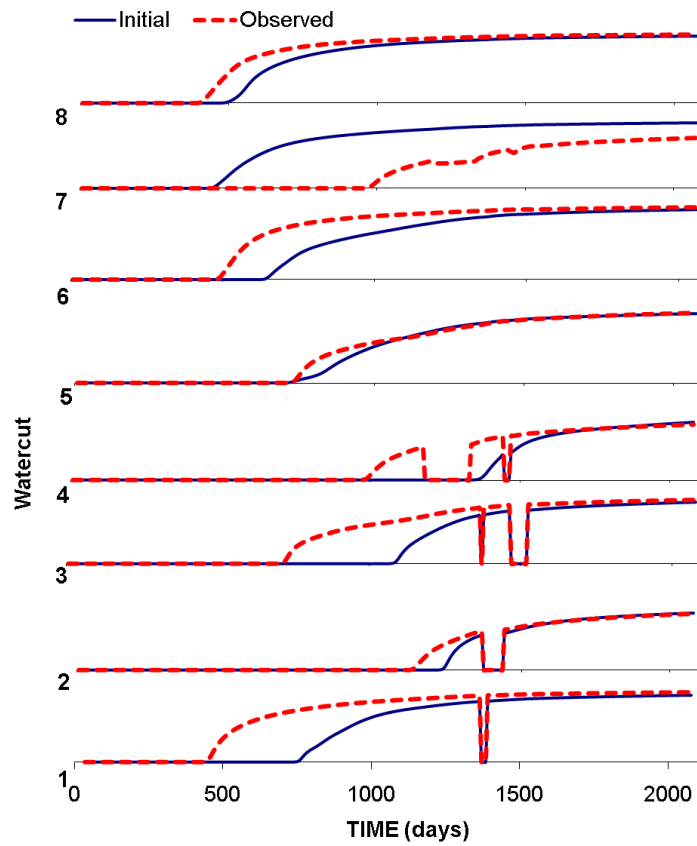
Fig. 2.5—Original production response illustrating the discontinuities in the production profile. The discontinuous pattern is only present in the corner wells of the nine spot synthetic example.

(a)   (b)
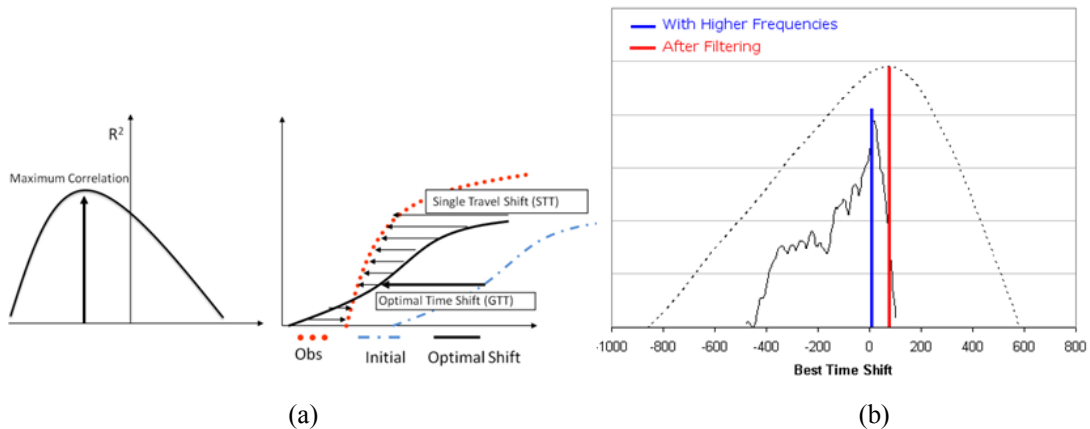
Fig. 2.6— (a) Schematic of the GTTI procedure (b) GTTI misfit calculations. The figure presents the calculation when signals include high frequency components, and after filtering using the proposed procedure.

However the presence of higher frequencies introduces multiple peaks in the cross-correlation curve and no clear shift time can be identified. After resampling the time based on the cumulative oil production, we only retain the low frequency components of the signal, making it more suitable for the GTTI misfit computation (**Fig. 2.6b**). **Fig. 2.7** shows the water cut responses after filtering the production response using the proposed approach.
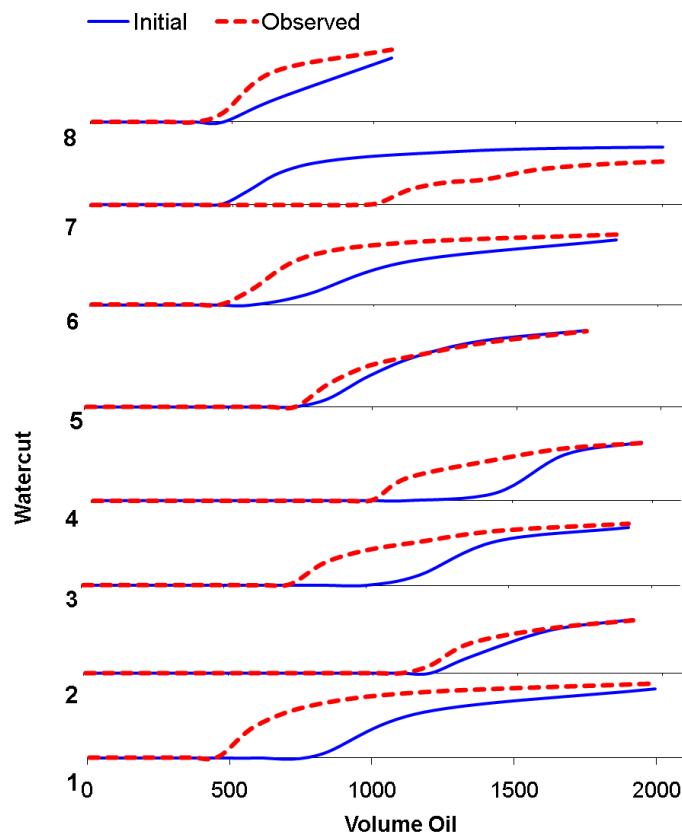
Fig. 2.7—Water cut response after applying a resampling based on volumes of oil produced at the surface conditions.

Fig. 2.8a shows the match on the water cut using our proposed time resampling technique while **Fig. 2.8b** shows the match on the original time space. Clearly, the proposed approach makes the shape of the production curves more suitable for the GTTI technique. Also, matching the resampled data has also resulted in an equally good match in the original time domain.

Fig. 2.9 shows the original permeability field and the updated permeability field obtained via inversion of the water cut data. **Fig. 2.9a** is the initial permeability, and **Fig. 2.9b** is the final model after the inversion procedure. The difference between the initial model and the reference model is shown in **Fig. 2.9c**.
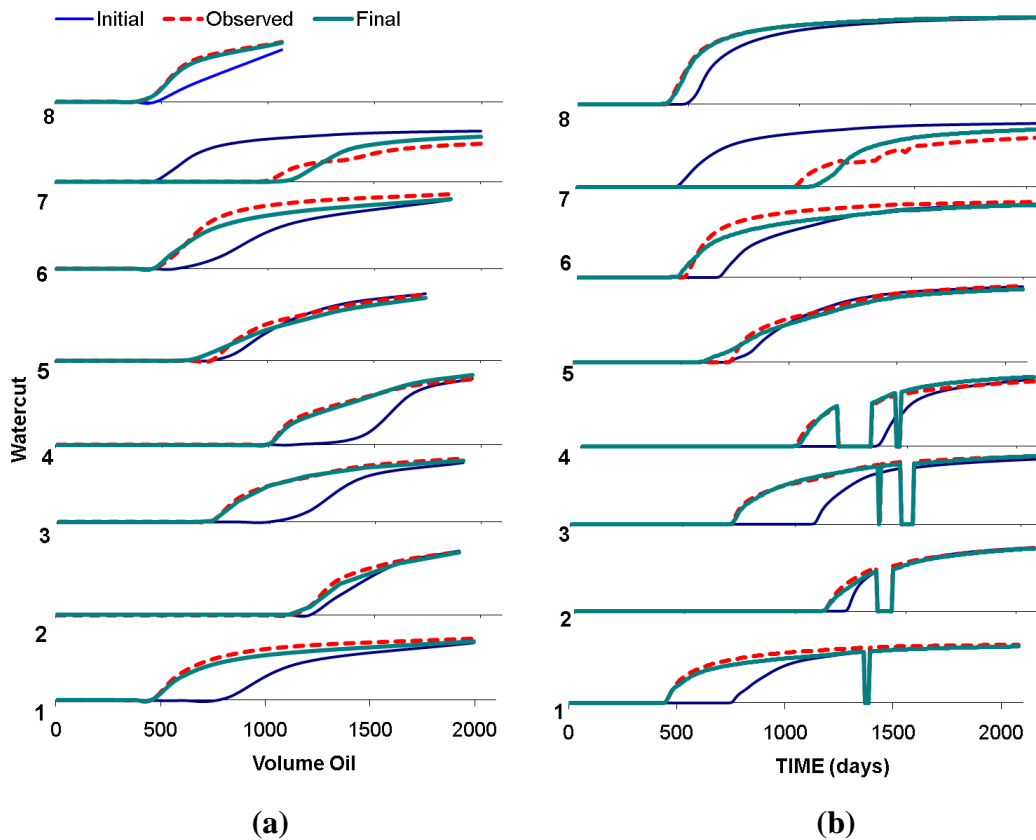
Fig. 2.8—History match in the transformed domain. (a) Matching of water cut data at the resampled times based on equal volumes of oil produced (b) Corresponding matches. using all times.

This difference represents the changes needed in the initial model. **Fig. 2.9d** shows the difference between the initial model and the final update. This difference represents the changes made during inversion. On comparing the figures **Fig 2.9c** and **Fig. 2.9d**, we can see that many of the features in the reference permeability field are captured after inversion.
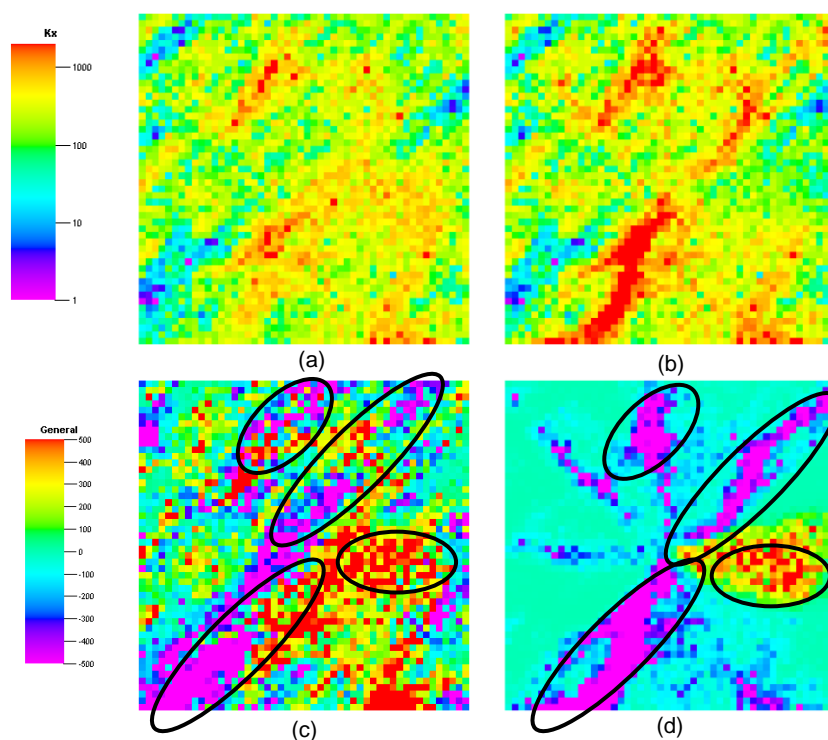
Fig. 2.9— **(a) Initial Permeability, (b) Final Updated Permeability, (c) Changes Needed, (d) Changes Made.**

2.3. Mathematical Formulation

In this section we briefly discuss the basic mathematical formulation for the proposed history matching workflow. More details can be found out in published papers (He et al, 2002; Vasco and Datta-Gupta, 1997; Cheng et al, 2005a; Cheng et al, 2005b). We first define the sensitivities of the fractional flow with respect to reservoir parameters, followed by the determination of the best time shift and the resampling of the water cut response.

2.3.1. Sensitivity Calculation for the Fractional Flow

The streamline time of flight (TOF) variable, τ is the pivotal concept that allow us to transform the flow domain from the three dimensional physical coordinate system to the

streamline coordinates (Datta-Gupta and King, 2007). Conceptually, the time of flight is simply the travel time of a neutral tracer along streamlines and can be expressed as.

$$\tau = \int_{\Sigma} s(x)dx$$ ....(2.1)

Here the variable s(x) is called the "slowness" and is defined as the reciprocal of the interstitial velocity as follows.

$$s(x) = \frac{1}{v(x)}$$ ....(2.2)

With the definition of the time of flight, we can derive the operator identity for the coordinate transformation from the physical coordinate to the streamline coordinate. It is given by (Datta-Gupta and King, 2007)

$$\vec{u} \cdot \nabla = \frac{\partial}{\partial \tau}$$ ....(2.3)

Using the time of flight operator identity in Eq. (2.3), we can write the mass balance equation along streamlines for a two phase incompressible flow as follows (Datta-Gupta and King, 2007),

$$\frac{\partial S_w}{\partial t} + \frac{\partial F_w}{\partial \tau} = 0$$ ....(2.4)

Assuming that small local changes in the reservoir properties, for example individual grid block porosities or permeabilities, will not shift the streamline paths (negligible

changes in the pressure/velocity field), a perturbation in the time of flight can be written as follows,

$$\delta\tau = \int_{\Sigma} \delta s(x) dx$$

....(2.5)

$$\delta s(x) = \frac{\partial s(x)}{\partial \phi} d\phi + \frac{\partial s(x)}{\partial k} dk$$

....(2.6)

In Eq. (2.5), by relating the change in time of flight to local changes in slowness, we have assumed that the streamline trajectories have not changed because of the perturbation. This has been shown to be a reasonable approximation for most practical situations (Cheng et al., 2005a). Unlike porosity, permeability can range over orders of magnitude within a reservoir. Hence, in this work we will treat reservoir permeability as the primary unknown. Thus, we are interested in the relationship between the streamlines time of flight to a producer and cell permeability.

$$\frac{\delta\tau}{dk(x)} = \int_{\Sigma} \frac{\partial s(x)}{\partial k} dx$$

....(2.6a)

Equation (2.6a) relates the reservoir property (permeability) to a streamline variable, viz. the time of flight (Vasco et al., 1999). We can further relate the time of flight to the waterfront arrival time, t_f in the mass balance equation in Eq. (2.4) through the chain rule (He et al, 2002).

$$\frac{\partial t_f}{\partial k} = \left(\frac{\partial t_f}{\partial \tau}\right)\left(\frac{\delta\tau}{dk(x)}\right)$$

....(2.6b)

This completes the derivation of the sensitivity of the waterfront arrival time with respect to cell permeability. It is important to realize that these sensitivities are 1-D

integrals along streamlines and can be readily computed after each flow simulation. No additional simulation runs are needed.

2.3.2. The GTTI Sensitivities

He et al. (2002) showed that the generalized travel time sensitivity can be computed as the averaged value of the sensitivities for all time points at which production data is available. Thus, we can utilize the results from Equation (2.6) to obtained the generalized travel time sensitivity as follows,

$$\frac{\partial \Delta \tilde{t}}{\partial k_j} = \frac{\sum_{i=1}^{N_d}\left(\frac{\partial t_j}{\partial k_j}\right)}{N_d} \quad \dots (2.7)$$

In the above expression, m is the reservoir parameter which is permeability for our case. Typically, the GTTI sensitivity is computed by evaluating Equation (2.7) by sampling production data at equal time intervals. This accentuates the problems associated with discontinuities in the production data arising from well shut-ins. Such discontinuities also complicate the GTTI calculations. In this work, instead of sampling the production data at equal time intervals, we compute the GTTI sensitivities based on time intervals defined by equal volumes of oil production at surface conditions.

$$\Delta V_o = \int_{t_j}^{t_{j+1}} q_o(t)dt \quad \dots (2.8)$$

Thus, the time points are chosen in terms of equal ΔV_o and the time intervals are no longer the same. This approach naturally removes discontinuities in the production response associated with well shut-ins and improves the GTTI calculations. As an added

benefit, the proposed approach also results in more frequent sampling at early times compared to the later times in the reservoir life when well interventions tend to be more frequent.

2.3.3. Transformation of the Production Variables

In the GTTI approach production data misfit is defined in terms of an 'optimal' shift in time that maximizes the correlation between the observed and calculated production responses. It is mathematically defined in Eq. (2.9) for the continuous case and the discrete form is expressed in the Eq. (2.10).

$$g^{cal}(t) * g^{obs}(t) = \int g^{cal}(t + d\tau) g^{obs}(t) d\tau$$ ....(2.9)

$$\rho_i(\Delta\tau) = \sum_{j=1}^{N_d} g_i^{cal}(t_j + \Delta\tau) g_i^{obs}(t_j)$$ ....(2.10)

The cross correlation function (CCF) reflects the shared frequencies between two signals. The maximum value of the CCF contains the shift in time that also maximizes the relation in the frequency domain. Unfortunately, higher frequency components can add levels of complexity in the calculation of the best time shift (Marple, 1987). Similarly, production discontinuities are potential source of complexity that must be eliminated because it cannot be correctly captured by the cross correlation function. **Fig. 2.10** shows the power spectral density for the original and the filtered signal for a very complex reservoir response (the reservoir will be described in more detail in the field application section). Integrating the data using appropriate time intervals will eliminate the high frequency detail, retaining the lower frequency components which are more suitable for the cross-correlation calculations.

Considering the observed and calculated fractional flow in time as the input signals, we consider two options for smoothing the data. If we consider a fixed time interval, then
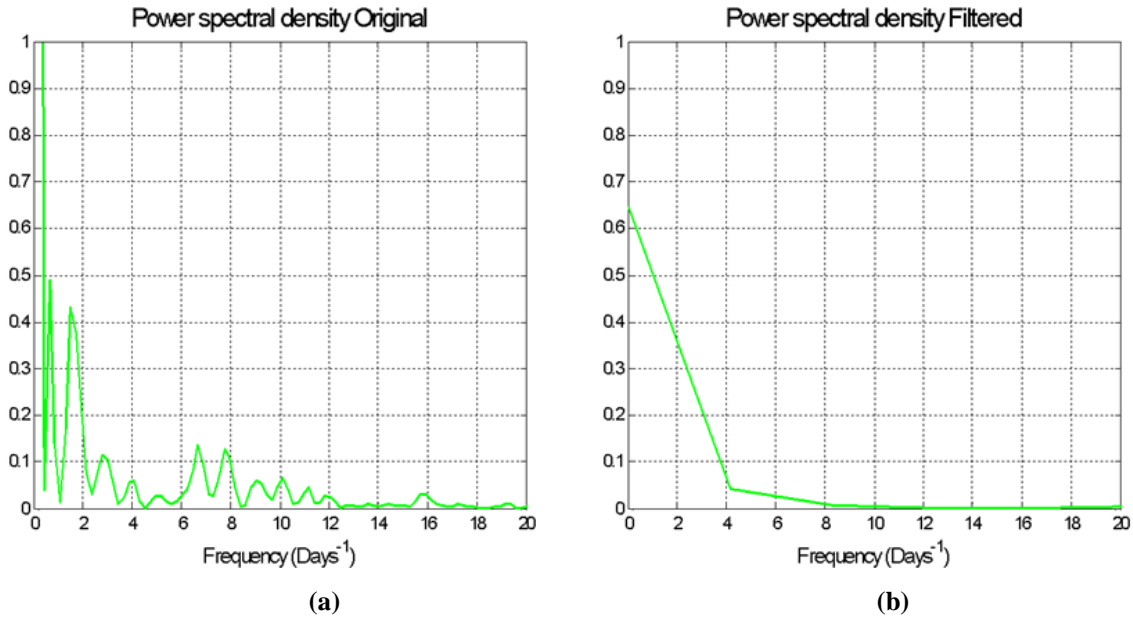
Fig. 2.10—Frequency details of the signals: (a) Frequency components of a signal before the smoothing, (b) Frequency components after smoothing.

$$fw_n = \left(\frac{\int\limits_{t}^{t+\Delta t} q_w dt}{\int\limits_{t}^{t+\Delta t} q_o dt + \int\limits_{t}^{t+\Delta t} q_w dt} \right)_n \dots\dots\dots\dots\dots\dots\dots\dots\dots\dots\dots\dots\dots\dots\dots\dots\dots\dots\dots\dots (2.11)$$

In Eq. (2.11), cumulative volumes of water and oil produced during a fixed time interval are used for smoothing the response signal. An alternative and preferred approach is to fix a desired incremental volume of oil produced and then to calculate the incremental production time and the volume of produced water as follows,

$$fw_n = \frac{\int\limits_{t}^{t+\Delta t_n} q_w dt}{\Delta Vo + \int\limits_{t}^{t+\Delta t_n} q_w dt} \dots\dots\dots\dots\dots\dots\dots\dots\dots\dots\dots\dots\dots\dots\dots\dots\dots\dots\dots\dots (2.12)$$

2.4. Field Example

The proposed approach has been applied to an offshore turbidite reservoir with frequent reservoir intervention and highly detailed production information. The static model contains more than three-hundred-thousand cells, complex sand depositional distribution combined with fault structures, four pairs of injector, deviated producing wells, and more than 8 years of production history. Previous history match attempts using traditional approaches achieved good results at the field level for the reservoir and well pressure data, but were not as successful in matching the oil and water rates at an individual well level. The biggest challenge was matching water cut timing and trend in the wells. More details about the model, results previously obtained, and the results achieved particularly regarding the improved reservoir characterization are presented below.

2.4.1. Field Description

The selected offshore turbidite reservoir has a depositional sequence of multiple sands with highly variable levels of overlap or superposition resulting in a very complex interconnected system. A detailed seismic interpretation integrated with well log and core data was performed in order to identify and map individual sand occurrences. **Fig. 2.11a** shows a schematic representation of the depositional concept used in this interpretation combined with individual sands identified in a seismic cross-section.

The reservoir quality variation inside individual sands was captured in the static model by the net to gross distribution, which was then used to populate the attribute parameter NETG in the 3D grid – **Fig. 2.11b** shows a top view. The contrast on the petrophysical properties among the multiple sands was captured by the average property values estimated from their corresponding intersections with well log data.

(a) (b) (c)
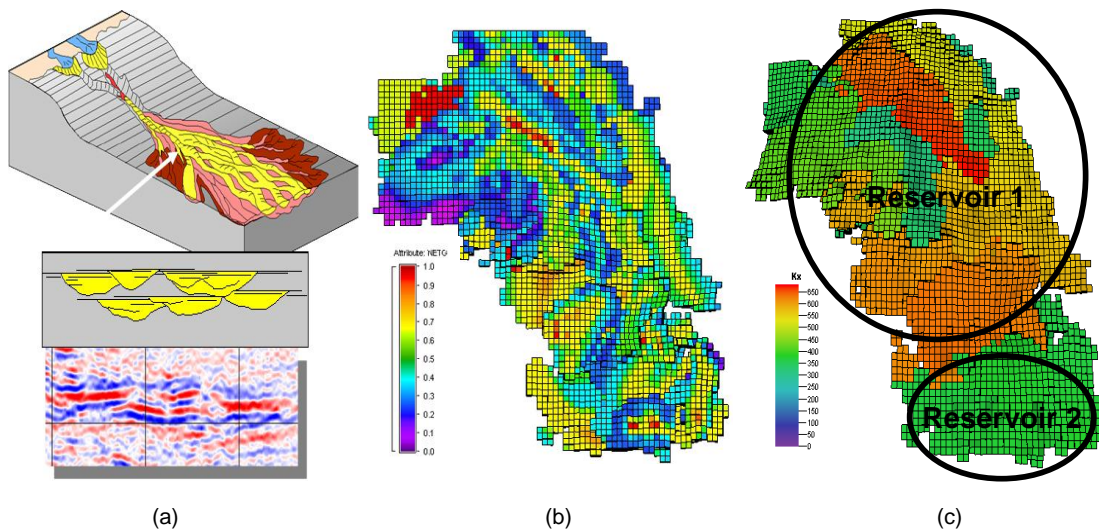
Fig. 2.11— (a) Schematic representation of the depositional concept used in the interpretation and individual sands identified in a selected seismic cross-section, (b) Net to gross over the multiple sands – top view, (c) Horizontal permeability populated as average by individual sand occurrence – top view.

Fig. 2.11c shows the distribution of horizontal permeability in the x direction (KX) populated into the 3D grid from a top view. This figure also shows the location of the vertical well injectors (I wells) and the highly deviated well producers (P wells). The calibration of these estimated individual average property value by sands was one of the targets of the history match previously performed in the field (PHM).

This complex interconnected depositional system is combined with a system of sub-parallel faults present mainly in the lower part of the field. **Fig. 2.12** displays this fault system also indicating the well locations. The available production and pressure data in the field allowed identifying that the sequence of faults between P1 and P4 were completely isolating the reservoir region around the latter; such that it can be subdivided into Reservoir 1 and Reservoir 2 as indicated in **Fig. 2.11c**. However, the transmissibility across the other faults was uncertain and their calibrations were other targets of the history match previously performed.

The significant achievement of the reservoir characterization described above and the history match previously performed led to the ability of reproducing individual well RFT data, which had not been achieved in any modeling attempts performed for this field before. **Fig. 2.13** shows the final RFT match for well P3.
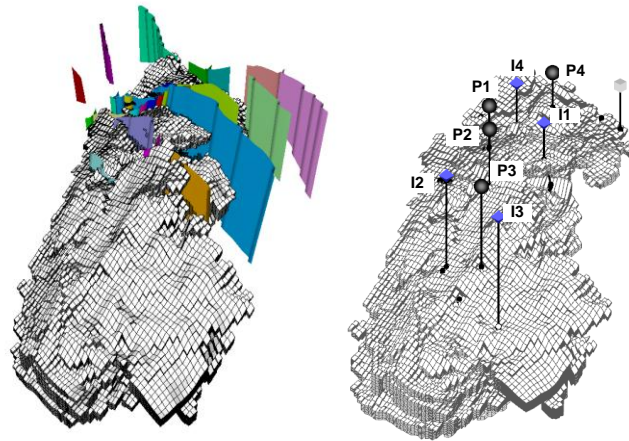
Fig. 2.12—Reservoir fault structure with well locations.
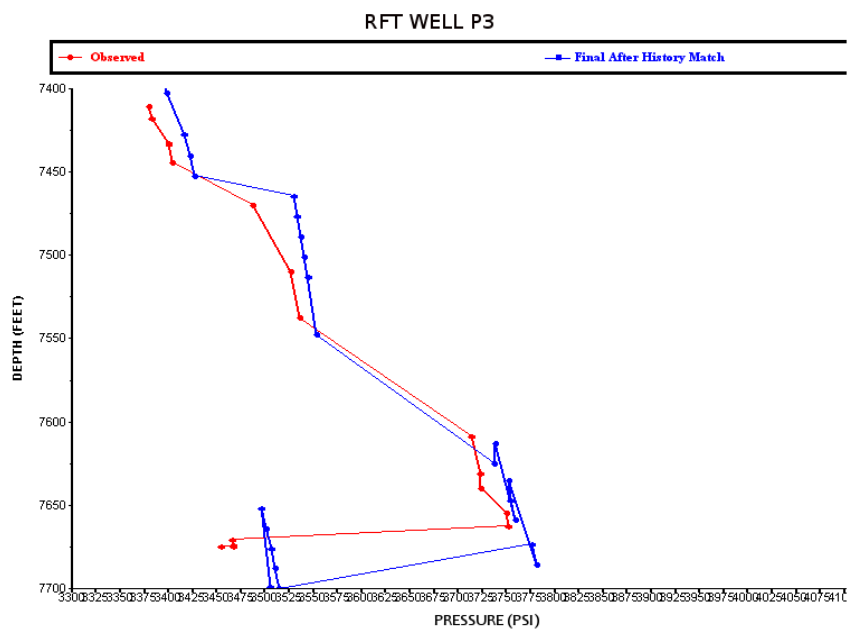
Fig. 2.13—Reservoir RFT history match for the well P3: Red line is observed data and blue line is the simulated data.

2.4.2. Characteristics of the Water Cut Responses on the Field

The water cut response for all the wells is characterized by a rather continuous profile at the beginning of production with an intense well intervention towards the end. Some of these well operations are associated with changes in the active completions on the producers and injectors. The recompletions are introduced in order to isolate areas with early water breakthrough. A recompleted well presents production responses with non monotonic profiles and complex dynamic responses.
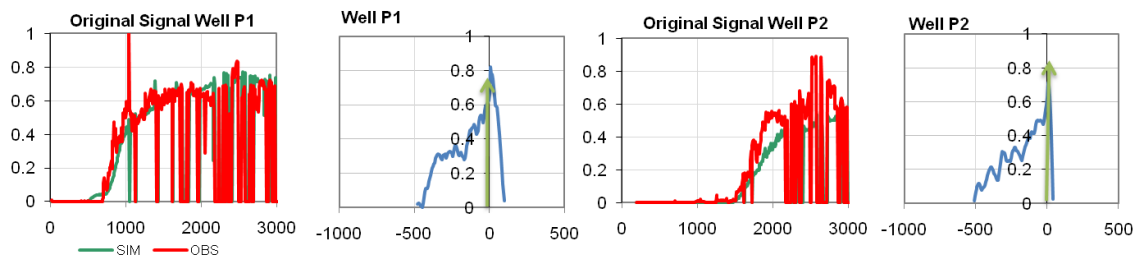
Fig. 2.14—Initial water cut response and the corresponding cross correlation calculation for the complete data in the wells P1 and P2.

We want to investigate the effects of these complex responses when calculating the cross correlation between observed and simulated data during the GTTI misfit calculations. In **Fig. 2.14** the water cut and the corresponding cross correlation calculation for the wells P1 and P2 are plotted. We can clearly observe how the higher frequency components present in the original data contaminates the cross-correlation, producing a maximum near the zero shifts in time. This behavior underscores the inability to deconvolve the lower frequencies and the noise between observe and simulated responses. As a result, the best shift in time is erroneously computed to be zero.

Production data filtering can improve the cross-correlation calculations. For example, sampling the production data at coarse time intervals can reduce the effects of high frequency components. **Fig. 2.15** shows the result of introducing a different time sampling in the shape of the cross correlation function. By smoothing the data, the best time shift is gradually moving away from the zero position for the well P1. However,

there are still some difficulties to determine the maximum correlation for the well P2. The cross correlation calculation now has multiple peaks making it impossible to determine a unique value for the GTTI misfit.
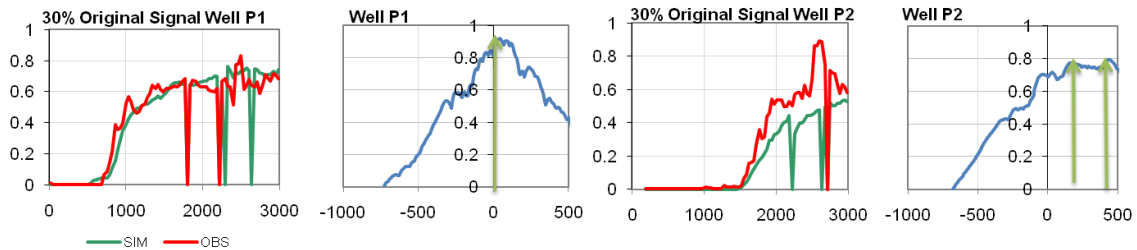
Fig. 2.15—Water cut response and the corresponding cross correlation calculation after resampling the schedule in an equal time base for the wells P1 and P2.
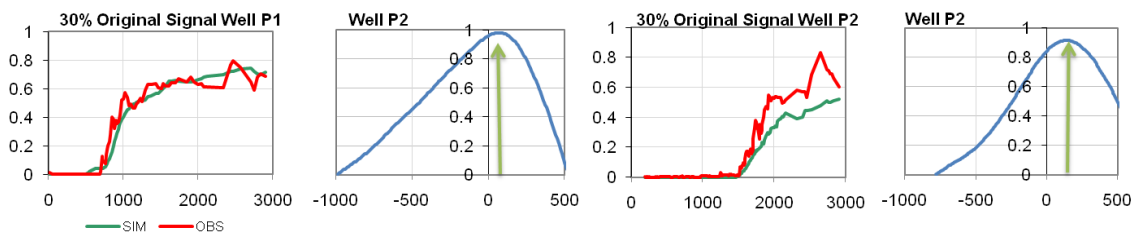
Fig. 2.16—Water cut response and cross correlation calculation using the proposed transformation. Wells P1 and P2

Fig. 2.16 shows the water cut profiles and the cross correlation curve using the proposed data resampling. The cross correlation now presents a smooth shape that allows us to easily identify the maximum and therefore, the best time shift that maximizes the correlation between the two responses. This smooth behavior is not related to any particular threshold in terms of volumes of oil produced. **Fig. 2.17** shows the cross correlation calculation for different levels of produced oil volume used for filtering the well response. Observing the shape of these curves, it can be concluded that the proposed transformation is able to make the production responses suitable for the GTTI inversion and is not very sensitive to the cumulative produced volume of oil interval used while sampling the data
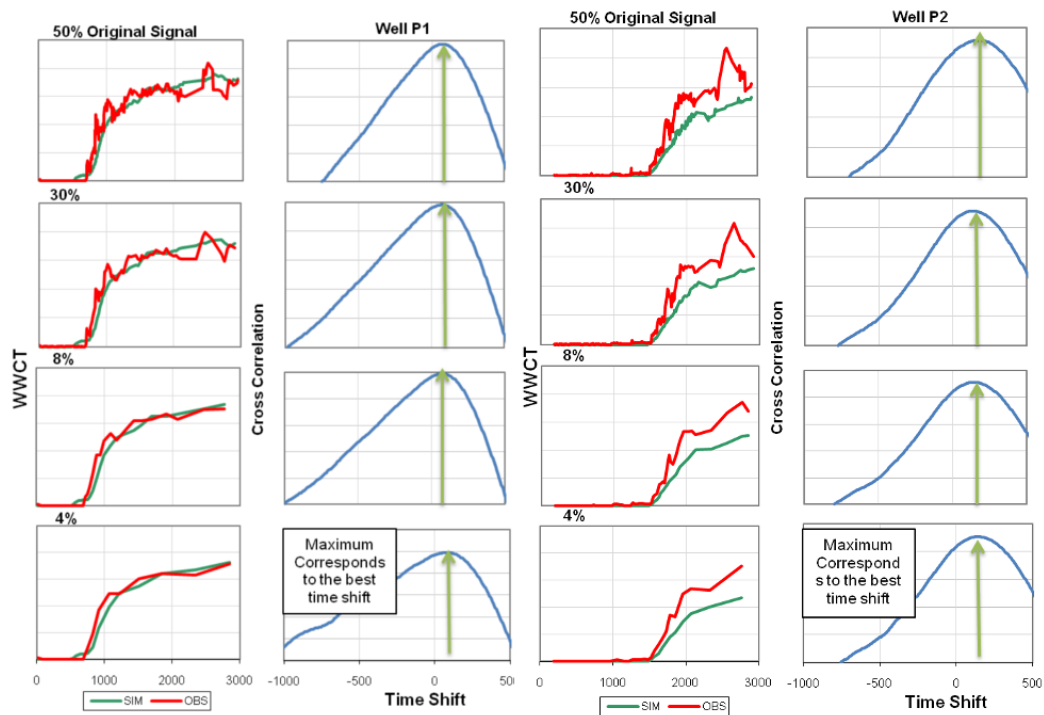
Fig. 2.17—Shape of the cross correlation function after resampling for different values of cumulative oil for different wells of the reservoir.
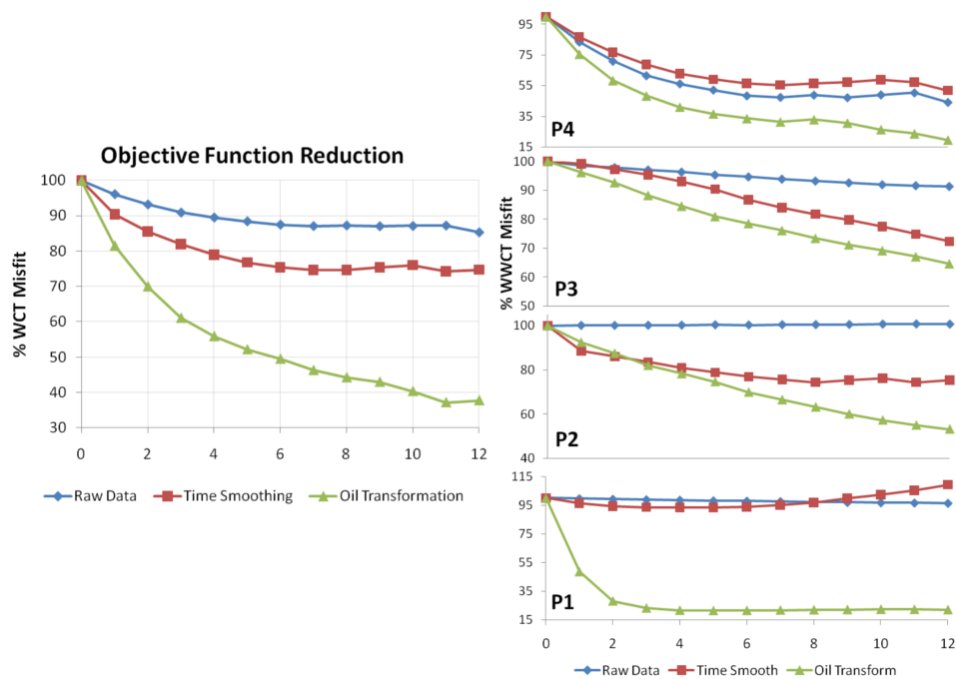
Fig. 2.18—Objective function behavior during the minimization process, on the left the sum of squares for the misfit over all the wells, on the right objective function behavior on a well basis.

Fig. 2.18 shows the performance of the data integration for various sampling approaches. The blue line represents the inversion algorithm using the complete data set. After twelve iterations the minimization has only reduce the initial misfit by a fifteen percent. When we observe the individual well performance it becomes clear that the wells P1, P2 and P3 do not show any significant signs of improvement. The red line shows the results of the minimization using a smoothing in time. This procedure improves the performance when compared to the results of using the original data set and the objective function decreases by twenty five percent. However, some of the wells show minor improvements. In fact, the well P1 is diverging and finishes the history matching with a higher misfit than the original. Finally the red curve represents the minimization using the proposed data transformation based on equal volumes of incremental oil produced.
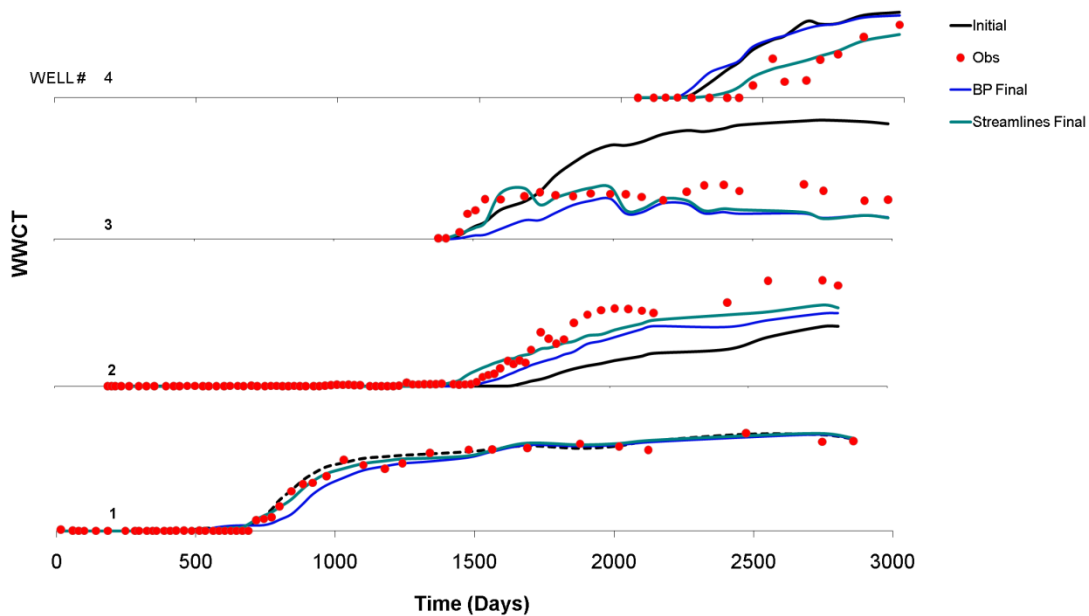
Fig. 2.19—Fine tuned history match of water cut starting from the previous model calibration (PHM) in the Transform Space (smooth version of the original signal). Blue lines represent the observed data, dashed red lines the initial model response, solid green lines the response after the streamline proposed procedure.

By selecting samples at equal intervals of produced oil, we substantially improve the history matching, reducing the objective function by more than 60 percent. The improved matches can also be seen on an individual well basis.

Fig. 2.19 shows the results of the final history match of water cut. Initial geologic model for this case is a previously history matched model obtained from the business unit. The objective of this exercise was to improve the individual well match quality, allowing the inversion algorithm to perform large changes in the reservoir parameters in order to investigate the previous reservoir architecture description. **Fig. 2.20a** shows the history match in terms of the normalized produced cumulative volumes of water and the improvements are more clearly visible here. Finally, **Fig. 2.20b** shows the water cut history match in the original time domain. Clearly, a better quality match using the resampled data is also reproduced in the original time space.
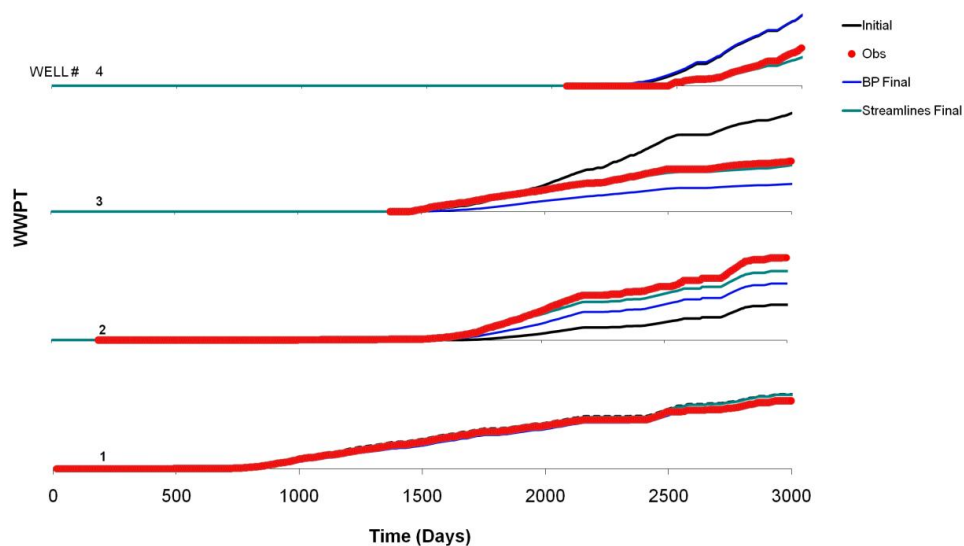
(a)

Fig. 2.20—Comparison of the different history match models, including the previous history match and the fine tuned using the streamlines inversion (a) Water cut per well (WWCT) vs Time, (b) Normalized cumulative water produced per well (WWPT) Vs Time.
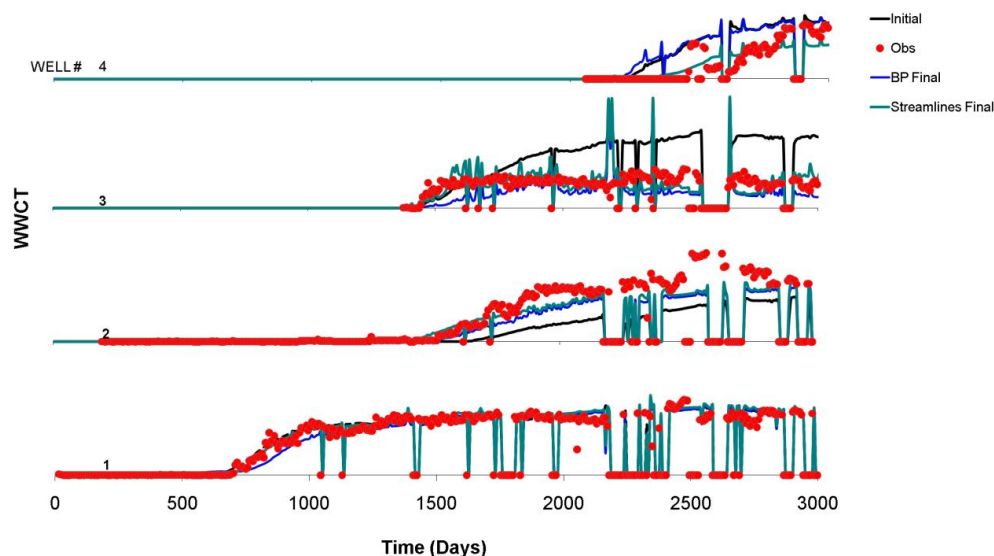
(b)

Fig. 2.20—(cont.)

2.4.3. Impact of the Improved History Match on the Geologic Model

The application of streamlines enables the identification and display of flow paths as well as the characterization of different sources of energy support to any individual well producer. **Fig. 2.21** displays the streamline time of flight (TOF) at a production time when all four wells are producing; in the color scale purple indicates the reservoir regions with smaller time of flight, that is, faster communication. The analysis of TOF for all producers indicates that well P4 has the fastest connectivity region, followed by wells P3 and P2. **Fig. 2.22** displays different energy sources identified for each well producer also labeled as well-pair regions. **Fig. 2.22a** shows the interaction of the well-pairs with the main aquifer region (purple color cells), which significantly supports most of the producers. **Fig. 2.22b** however, shows almost no interaction with the small gas-cap (red color cells).
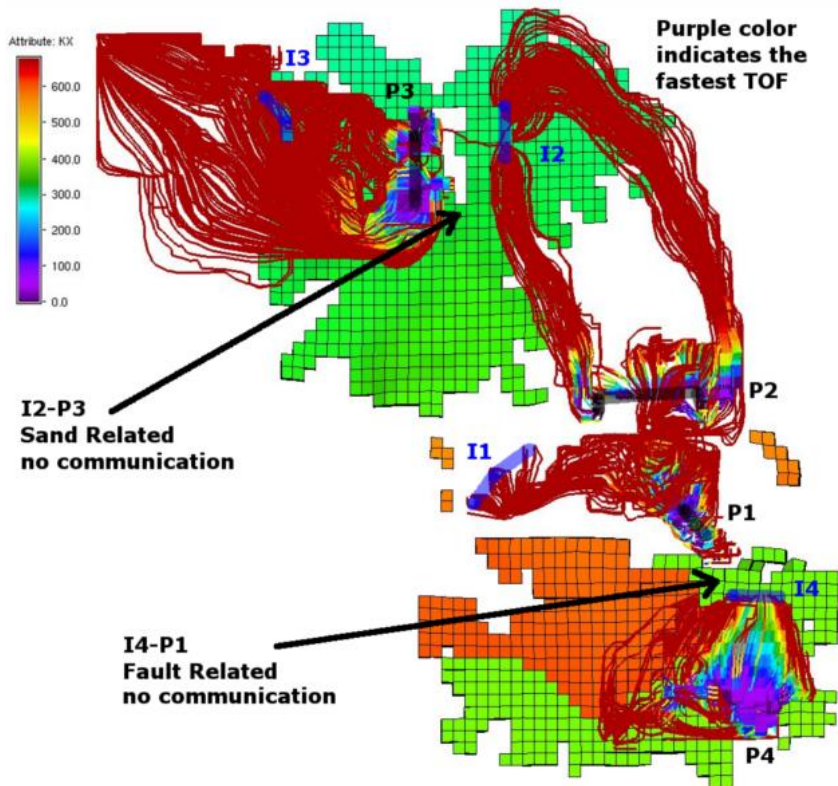
Fig. 2.21—Streamline time of flight (TOF) indicating intersand and well communications. Sand related and fault related non- communication.

(a)   **(b)**
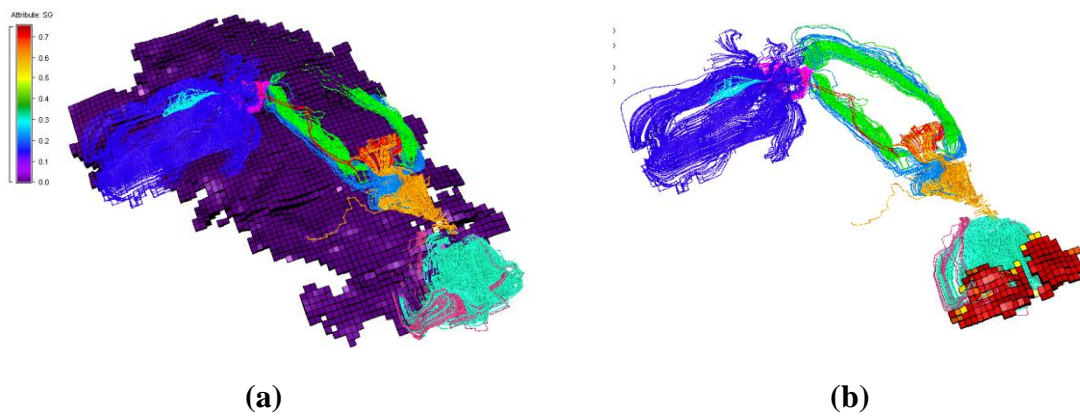
Fig. 2.22—Streamlines colored by well-pair regions and their interaction with (a) aquifer and (b) gas cap.

The fine-scale model calibration with the streamline-based inversion described here had basically no impact on the reservoir area in the vicinity of the injector I1 and the

producer well P1, which already had a good match from the previous history match. **Fig. 2.23** displays model KX before and after the streamline based inversion for a selected representative grid layer indicating minor changes. As desired, the streamline-based inversion process did not affect reservoir regions already having good characterization.
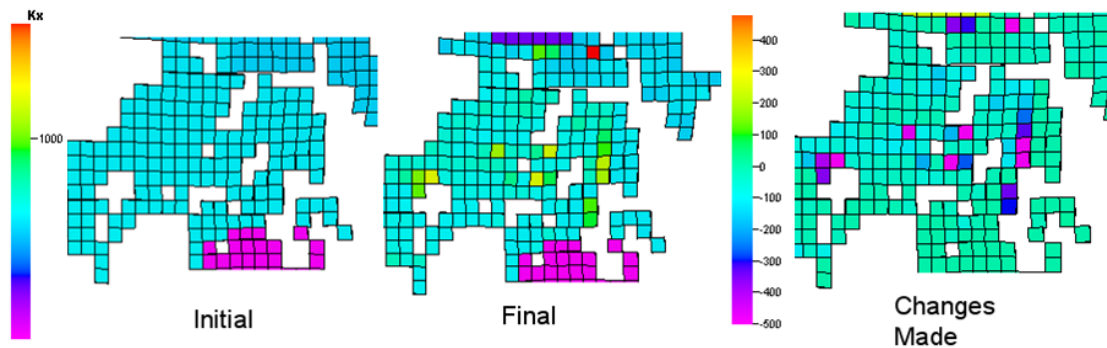
Fig. 2.23—Details of the history match at well P1 showing minor changes in KX from the previous HM for a selected representative layer.

However, the reservoir regions around the other well producers were more affected by the streamline-based inversion. **Fig. 2.24** displays the characteristics of the horizontal permeability KX in three different stages: a) in the initial geological model; b) the final result with streamline-based inversion for the region around producer well P3 c) the differences between the initial and the final permeability field. The streamlines TOF for the model after previous HM and after final inversion are also displayed indicating that in the final model: a) there is an enhanced support of the aquifer region from the lower sand (indicated by the arrows), and b) there is a reduced interaction with injector I3, shown by fewer faster TOF streamlines with purple color inside the grey circles corresponding to the region between injector and producer.
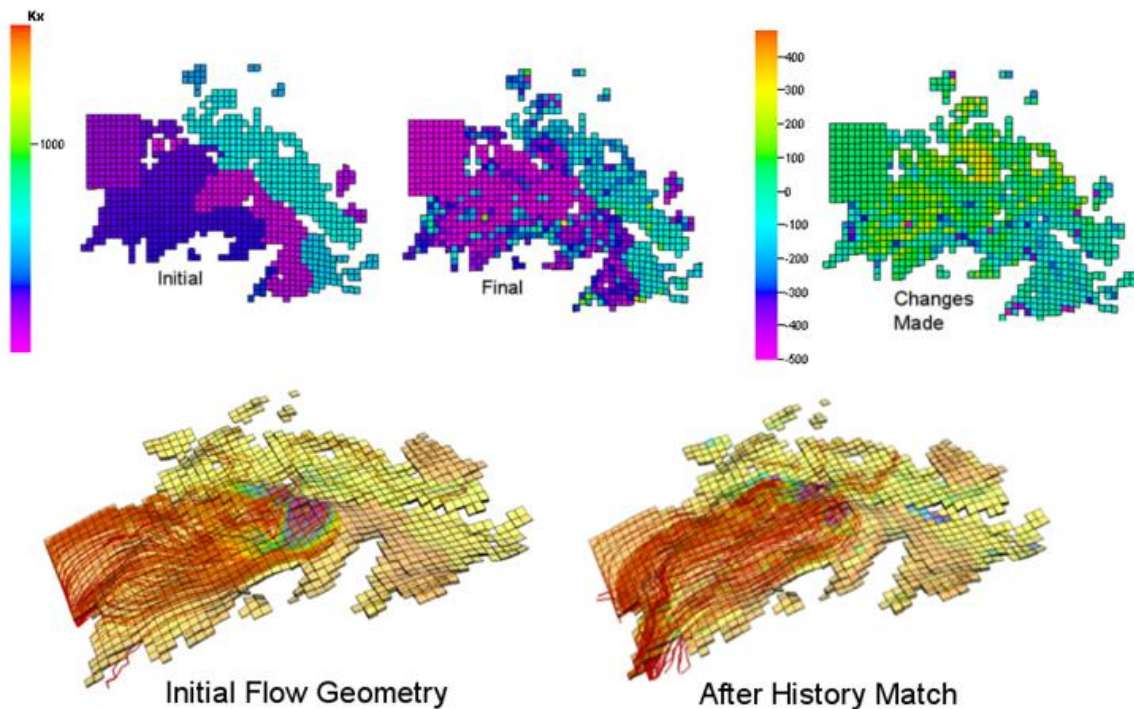
Fig. 2.24—Details of the history match at the well P3 showing the horizontal permeability for initial model, and after streamline calibration. Corresponding streamline TOF indicate increase on aquifer support (arrows) and reduction on injector support (circles) from previous HM.

Fig. 2.25 displays the horizontal permeability KX in the region around producer well P4 (this well is located close to the gas cap in the upper region of the reservoir). This well has a strong direct communication with the injector I4. The final model was able to improve the liquid production match by significantly reducing the direct support from the injector, This systematic reduction in conductivity is related with the late arrival of the water observed at the producer. However, other sources of dynamic data (e.g. bottom hole pressure) were not consistent with this results. Another scenario consistent with the late arrival of the water is the possibility of a different thickness of the sand body where the pair injector-producer is located. This scenario was investigated through a structural reinterpretation of the reservoir.
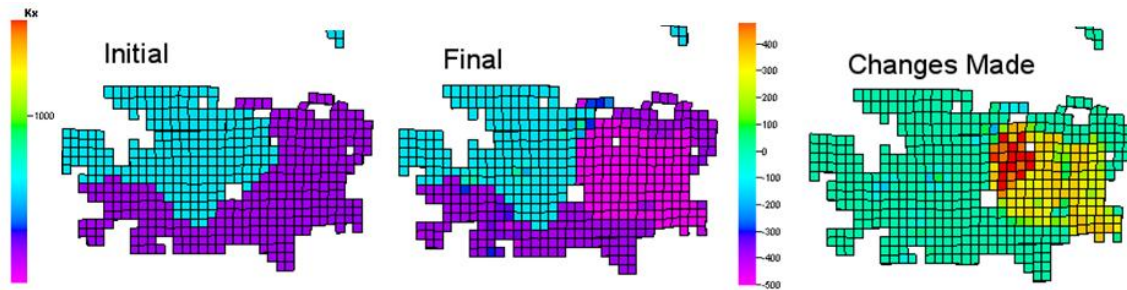
Fig. 2.25—Details of the history match at the well P4 showing the horizontal transmissibility for initial model, previous HM and after streamline calibration. Corresponding streamline TOF indicate a significant reduction on injector support and an increase on aquifer support from previous HM, but still at lower level than in the initial model.

Fig. 2.26 displays similar analysis of the 3 models for the reservoir region around producer well P2. This was the well that required the most significant changes from the model generated by the previous HM. Since the construction of the model was based on the average permeability values for each sand, in order to achieve an improved match on the well liquid productions it was necessary to expand the flexibility in terms of permeability changes in the streamline based inversion. This was done by allowing minimum and maximum values estimated from the inversion to be outside the actual value ranges in the initial model or from the previous HM. The estimated changes from the inversion are local grid cell values that are closer to the limits observed in the well log data than to the whole sand average values used in the model. Minimum and maximum limits used were 0.2 mD and 2D respectively. Those limits however, were not enough for well P2 and the model was rerun removing the fault transmissibilities used in the previous HM, which resulted in some improvements. For additional model investigation and fine tuning, the maximum permeability limit was expanded to 10 D, which provided the best match. **Fig. 2.26** also shows locations with transmissibility increases and the cells in the 3D grid filtered with permeability above the realistic limit of 2D. The filtered cells show a localized feature with many cells still reaching the upper limit of 10 D (in red color). This region is near well P2 and possibly indicates a structural interpretation error being compensated by the large permeability increase. Potential sources of error in this region can be a higher net to gross value or a thicker

interval than in the original interpretation used in the model. The procedure used for opening the uncertainty limits demonstrates that if done properly, it can be very helpful in identifying major discrepancies in the model. Another important feature of **Fig. 2.26** is the systematic transmissibility increase in the extreme right, mid to upper part of the sand, which indicates an increase of communication between the injector to the producer along the longer path which impacts the later water production at well P2. This systematic increase is consistent with the presence of a larger or more conductive channel in that part of the model. The identification of potential local features is a unique characteristic of the streamline-based inversion that is one of its major advantages when compared with other inversion techniques.
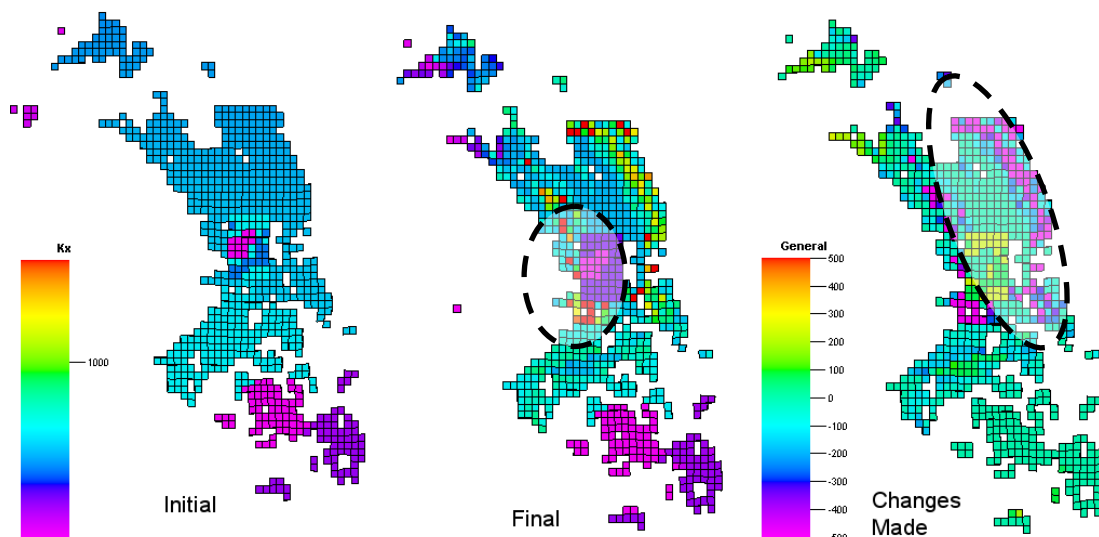
Fig. 2.26—Details of the history match at the well P2 showing horizontal permeability initial, final and the difference for a selected representative layer indicating increase connectivity with injector (potential channel), and an increase on permeability in the vicinity of the producer beyond actual KX limit from field data.

The model changes identified and described in this study preceded significant production and 4D seismic data that became available later. When presented to the field Asset Team it was acknowledged that these observations were consistent with the newly obtained data except for well P4, and that most of the changes in the model were consistent with the geological depositional system and corresponding uncertainties.

2.5. Chapter Summary

In this research, we propose a method for production data integration using the generalized travel time inversion in the presence of active reservoir management. Because of frequent well interventions, the production data can be highly non-monotonic with multiple shut-ins and production discontinuities. The high frequency components in the production data introduce difficulties in computing the data misfit in terms of a travel time shift. We propose a smoothing via resampling of the production data in terms of equal volumes of oil produced at surface conditions. This approach naturally removes production discontinuities and makes the production response more amenable to a travel time inversion. A comparison of the proposed transformation of the production data with the traditional equal time interval filtering is also presented. Finally, the robustness of the proposed approach is first demonstrated using a synthetic example and then on a real field application with active production management characterized by many shut-in's and several recompletions at different sands.

The application of the streamline-based assisted HM allowed a refined reservoir characterization from a previous history match and provided improved production match quality at individual well level. The refined reservoir characterization was achieved by localized and targeted changes only when and where needed to improve the production match. The localized changes also helped identify places with potential interpretation problems either in terms of reservoir quality (net to gross) or sand thickness. Most of the changes proposed by this study were consistent with the geological depositional system and corresponding uncertainties as well as with later production data and 4D seismic survey.

CHAPTER III

RAPID STREAMLINE-BASED INTEGRATION OF TIME-LAPSE SEISMIC AND
PRODUCTION DATA INTO HIGH-RESOLUTION GEOLOGIC MODELS

In this chapter we present an efficient history matching approach that simultaneously integrates 4D repeat seismic surveys with well production data. This approach is particularly well-suited for the calibration of the reservoir properties (porosity and permeability) of high-resolution geologic models because the field-scale seismic data are areally dense while the production data are effectively averaged over inter-well spacing. The joint history matching procedure is performed using streamline-based sensitivities derived from either finite-difference or streamline-based flow simulation.

In our proposed approach the inverted seismic data (i.e., changes in elastic impedance or fluid saturations) are distributed as a 3D high-resolution grid cell property or as a vertically integrated two-dimensional map. We compute the sensitivities of the seismic and production surveillance data to perturbations in absolute permeability at individual grid cells using efficient analytical streamline techniques. We generalize previous formulations of streamline-based seismic inversion to incorporate realistic field situations such as changing field conditions due to infill drilling, pattern conversion, etc. A commercial finite-difference flow simulator is used for reservoir simulation and to generate the time dependent velocity fields from which we compute streamlines and multi-parameter sensitivity coefficients. The commercial simulator allows us to incorporate detailed physical processes including compressibility and non-convective forces, e.g., capillary pressure effects, while the streamline trajectories provide a rapid evaluation of the sensitivities.

The efficacy of our proposed approach is demonstrated with synthetic and field applications. The synthetic example is the SPE benchmark Brugge field case. The field

example involves waterflooding of a North Sea reservoir with multiple seismic surveys. For both the synthetic and the field cases, the advantages of incorporating the time-lapse variations are clearly demonstrated through improved estimation of the permeability distribution, fluid saturation evolution and swept and drainage volumes. The value of the seismic data is clearly demonstrated in terms of identifying the spatial continuity of reservoir sands and barriers, and the preservation of geologic realism during the history matching process.

3.1. Chapter Introduction

Seismic data is extensively used in the oil and gas industry, occupying a fundamental role in the exploration for and development of reservoirs. These data provide one of the principal sources of information for the determination of reservoir structure, and at sub-structural scales are also of considerable use for reducing the uncertainty associated with inter-well reservoir heterogeneity characterization, particularly when used in combination with high vertical resolution well logs (Behrens et al., 1998). However, the potential application of seismic data as a source of dynamic data was only assessed in the mid 1980s when rock physics studies (Nur et al., 1984; Wang and Nur, 1986; Nur, 1989) proved the concept that repeated seismic images can be used to infer changes in rock elastic properties that result from changes in fluid saturation, pressure and temperature. Early applications of dynamic seismic data were constrained to high contrast fluid property interactions such as steam flooding (Pullin et al., 1987; Eastwood et al., 1994; Jenkins et al., 1997), CO_2 injection (Arts et al., 2000) and gas injection (Johnstad et al., 1995). Later, developments in seismic processing combined with the introduction of techniques that improve repeatability and noise filtering made possible the use of 4D seismic for the monitoring of reservoir waterflood performance (Wang et al., 1991; Behrens et al., 2002; O'Donovan et al., 2000; Khazanehdari et al., 2005). The application of time lapse seismic data has subsequently evolved proving unique value as a reservoir management tool (Fanchi, 2001; Clifford et al., 2003), with published

guidelines describing the feasibility and applicability of these techniques (Lumley and Behrens, 1998).

There are many technical challenges associated with the use of repeated 3D seismic surveys to infer changes in the state of the reservoir (Lumley, 2001; Behrens et al., 2002). Nonetheless, 4D seismic data have demonstrated success as a monitoring tool for mapping changes in phase saturations and pressure and, therefore, the inference of areas of bypassed oil, fluid contacts and pressure compartmentalization (Foster, 2007). Appropriately, 4D seismic is at present most commonly recognized as a reservoir management tool, where a number of successful field experiences of reservoir management have used time lapse seismic information (Behrens et al., 2002; Cooper et al., 2005; Landro et al., 1999). The logical progression of this technology is for the application of the dynamic information, inferred through time lapse seismic interpretation, in reservoir model calibration. Specifically, in high-resolution geologic models the areally dense characteristics of the seismic data are expected to compensate for the lack of production data resolution, particularly away from well locations. Nonetheless, the reconciliation of reservoir model heterogeneity with temporal changes in seismic attributes is a remarkably complex task (Gosselin et al., 2001). Several such dynamic data integration algorithms have been proposed in the literature, which we categorize as two distinct types: (1) methods that use direct seismic attributes (e.g., reflection amplitude) and (2) methods that use seismic inverted properties derived from a geophysical inversion (e.g., elastic acoustic impedance, compressional velocity, saturation changes, etc).

The former group, or methods that use direct seismic data, have the advantage of not bearing the uncertainties associated with a seismic inversion to litho-physical properties. It general they require the computation of the reservoir properties at the grid cell scale and later the use of a rock physics model to relate the elastic properties of the rock with the state of the reservoir (Mavko et al., 1998; Dadashpour et al., 2007; Falcone et al.,

2004). A typical workflow begins with the population of acoustic impedance as a grid cell reservoir model property. Then, a seismic wave propagation model is applied to the reservoir interval (vertical thickness) and the overburden rock in order to calculate the seismic attributes throughout the high resolution grid. This is a computationally demanding process as it requires the iterative application of the seismic propagation model and may be prohibitive for an inversion workflow (Gosselin et al., 2003), as to date there are few publications that use direct seismic attributes for model calibration. Huang et al. (1997) used the reflection amplitude obtained from seismic forward modeling over a volume of synthetic acoustic impedance and matched both production and seismic data by updating porosity and permeability maps using simulated annealing together with the Metropolis-Hasting algorithm for parameter update acceptance. Vasco et al. (2004) also used reflection amplitude to update grid cell porosity and permeability, although with a gradient based algorithm in which the sensitivity of seismic amplitude to reservoir properties is analytically computed using streamline trajectories. The tradeoff to the efficiency of their sensitivity formulation is the requirement of streamline invariance between the base and monitoring surveys. Kjelstadli et al. (2005) used maps of the summation of negative amplitude (SNA) as the observation data and calibrated zonal heterogeneity multipliers with a Genetic Algorithm. For the integration of the estimated reservoir properties with the seismic data, they used the convolution of a wavelet with the seismic reflection coefficients, creating a set of synthetic amplitude traces, from which the maps of SNA were subsequently generated.

In the second category of seismic data integration approaches are the workflows that evaluate the seismic match quality in terms of inverted seismic parameters. The inverted parameters can be derived from the traditional post stack data inversion such as the sparse spike inversion (e.g., seismic volumes of acoustic impedance), or from direct saturation and pressure front detection using an amplitude versus offset inversion of pre stack seismic data (Tura and Lumley, 2000; Landro et al., 2001). From a computational stand point, these methods are preferred because of the improved efficiency with respect

to the use of the seismic reflection attributes, which require only a single inversion of the seismic volumes as a separate component of the model calibration workflow. Gosselin et al. (2003) emphasize this benefit in terms of the consistency maintained between the geophysical inversion and the calibration workflow when the data misfit is expressed in terms of rock properties. In support of these assertions, there are at present a greater number of publications that apply seismic inverted parameters for reservoir model calibration compared to those that apply direct seismic attributes. For example, Landa and Horne (1997) used saturation changes as the calibration dataset that they assume can be obtained directly from inverted time lapse seismic data. Gosselin et al. (2001) applied synthetic acoustic impedance maps generated with a rock physics model, together with a heterogeneity parameterization based on grad zone analysis, for model calibration. Arenas et al. (2001) used the compressional velocity to calibrate the permeability field at a set of pilot points, which were used as conditioning data at each iteration of a gradient-based data misfit reduction for population of the complete field by Kriging. They additionally investigated the effects of the uncorrelated noise associated with the geophysical inversion of seismic volumes on calibration performance. Dong and Oliver (2005) assumed the availability of differences in acoustic impedance after a geophysical seismic inversion, data with which they calibrated grid cell porosity and permeability using a quasi-Newton method, computing the objective function gradient by an adjoint method. In a stochastic approach, Skjervheim et al. (2007) used the Ensemble Kalman Smoother to assimilate time lapse seismic data of changes in acoustic impedance and compressional velocity. Fahimuddin et al. (2010) similarly used seismic impedance as the observation data with the Ensemble Kalman Filter with a covariance localization strategy. Finally, Feng and Mannseth (2010) applied pseudo-seismic data in the form of maps of saturation changes and investigated the impact of the seismic data in the presence of noise on permeability estimation.

Building upon these approaches, in this chapter we present a streamline-based methodology for 4-D seismic data integration in the presence of varying field conditions and non convective forces. The method is based on the streamline techniques and the

trajectory-based analytical sensitivities previously presented by Vasco et al. (2004). Notably, we modify the streamline formulation to allow for seismic data integration under varying field conditions, including vertical segregation forces. The method is particularly efficient as only a single reservoir simulation is required to calculate the multiple parameter sensitivities applied in a gradient-based inversion. Further, we combine the seismic data with production data, and also investigate the benefits of the inclusion of aerelly dense seismic information with different levels of background noise. Finally, the method can integrate seismic information both as saturation changes or as changes in the elastic rock properties, e.g., changes in acoustic impedance.

The outline of this chapter is as follows. We first introduce the general workflow for the seismic and production data integration into high-resolution reservoir models under water flood condition, illustrating the essential components of our proposed reservoir heterogeneity calibration using a two-dimensional synthetic example. We next review the mathematical formulations of our technique for computing the analytical, trajectory-based sensitivity of seismic-derived attributes to high-resolution reservoir heterogeneity, including the simplifying assumptions required for use in fields with varying boundary conditions from infill drilling, reservoir management and changes in reservoir drive mechanisms. Next, we present the rock physics model and the elastic properties used to generate the synthetic acoustic impedance that we require for the inversion, and also the sensitivity of the acoustic impedance to perturbations of the pertinent reservoir parameters. Last, we apply the technique in synthetic and field applications. The synthetic application is the Brugge comparative field study, where seismic data is provided as grid cell properties of fluid saturation and pressure changes inverted from pseudo-seismic data. Of note, this application illustrates the benefits of the incorporation of seismic information in combination with production data. For the production (water cut) data integration we utilize the Generalize Travel Time Inversion (GTTI) technique together with our proposed seismic data integration. This application highlights the benefits of the dynamic time-lapse information on improvement in the calibrated front

location and also on the general improvement of the geological realism of the calibrated model. We also present the difference in the swept and drainage volumes before and after the calibration, stressing the benefit to reservoir management. In a final case study, the proposed approach is applied to a set of interpreted acoustic impedance differences together with production data from the Norne field located in the Norwegian Sea.

3.2. Approach

In this section we review our proposed approach to the joint integration of time lapse seismic and production data in water flooded reservoirs. Presented first is an overview of the complete data integration workflow in which the key components and contributions of this study are highlighted. Then, before a presentation of the corresponding mathematical formulations, we illustrate the inversion workflow in a stepwise manner using a simple synthetic example.

3.2.1. Seismic Data Integration

The first step of the data integration workflow is to compute the sensitivity of the state variables, such as saturation, to perturbations in the continuous reservoir parameters. Depending on the type of seismic data available, the partial derivative of the seismic attribute with respect to the state variable (i.e., derivatives of the acoustic impedance with respect to the saturation of water, gas or pressure) may also require calculation.

Sensitivity of Time-Lapse Attributes to Reservoir Properties. The streamline-based approach of seismic attribute integration into high resolution models is founded upon the analytical relationship between the arrival time of a propagating fluid front in the reservoir and the properties of the medium, e.g., porosity and permeability, through which the front traverses (Vasco et al., 2004). Using an asymptotic solution for the problem of the propagation of a two phase front, it is possible to define a self similar variable along the characteristic curves (i.e., the streamlines) that has the property of

transforming the spatial perspective of fluid propagation from an Eulerian to a Lagrangian representation (Vasco and Datta-Gupta, 2001). In the transform domain, which is defined by the trajectory of the particles and the travel time, or Time of Flight (TOF), along the defined path, the coordinate transformation enables an expression of the equations governing fluid motion as a series of one-dimensional equations. The simplicity of the sensitivity formulation then manifests from an analytical relationship between the travel time and the location of the fluid front along the streamline trajectories. The technique is remarkably efficient as it requires only a single forward simulation to compute the sensitivities (Vasco et al., 2004). We present the mathematical formulation of the analytically computed sensitivities following the demonstration of our proposed approach.

Seismic Data Misfit and Petro Elastic Model (PEM). When the time lapse seismic data are presented in the form of changes in acoustic impedance, we use a PEM to calculate the elastic properties of the rock that vary in time as a result of changes in the fluid saturation or reservoir pressure. The seismic responses of the rock such as reflection amplitude are directly correlated to the rock elastic properties; therefore, a geophysical inversion delivers seismic cubes of reservoir properties such as the acoustic impedance. This dependency is characterized by Gassmann's equations (Gassmann, 1951) for computation of the elastic modulus of the saturated rock. The model uses the fluid, solid rock and matrix elasticity, where the matrix has the effect of rock stiffness reduction caused by porosity. We also assume that the shear velocity is almost unaffected by changes in the pore fluid. In our field application, a linear relationship is assumed between the frame bulk modulus and the porosity of the rock (Mavkov et al., 1998). The mathematical form and the specific values for the properties are presented in the appropriate section of this chapter.

3.2.2. Production Data Integration

After definition of the parameter sensitivities and of the objective function defined from the seismic data misfit, the production data are included in the inversion workflow in one of two approaches. The inclusion can be performed in sequence, after the seismic data history match, or by augmenting the objective function with a production data misfit term, thereby facilitating a joint inversion. In the latter case, consideration must be given to the difference in the convergence rates of the two dynamic data terms.

Sensitivity of the Water Arrival at the Producers. We use the grid cell fluxes extracted from a finite difference black oil simulator to trace streamline trajectories originating at wells using a generalization of the Pollock algorithm for corner point geometry (Pollock 1988; Jimenez et al., 2007). It is important to understand that the streamline trajectories and time of flight implicitly characterize the underlying heterogeneity of the field relevant to flow and transport. If each streamline trajectory is assumed invariant to small variations in transport properties, then an increment in the conductivity or velocity will decrement the arrival time inside the reservoir, therefore establishing a relationship between the parameters and the time of flight along the streamlines. That is, production data sensitivity to heterogeneity along streamlines at grid cell resolution is posed in terms of time of flight to producers. Furthermore, through the mass conservation equations when posed in a Lagrangian form, the relationship between the propagation of a sharp front (e.g., water-oil or oil-gas displacement) and the arrival time of a neutral tracer can be computed for each phase, thereby enabling heterogeneity calibration to individual phase production rates. As these concepts have been developed in parallel with streamline simulation techniques, a rich body of literature exists that addresses the details, assumptions and relevant applications of the streamline-based approach (Vasco et al., 1999; Cheng et al., 2005a; Cheng et al., 2007).

Generalized Travel Time Misfit Calculation. The concept of streamline-based travel time inversion is a technique inspired by seismic travel time tomography. In this approach,

the calibration objective function does not consider the amplitude of the surface response at the producer, but rather measures the temporal difference between the simulated and observed production data, or characterizes data misfit as a time shift. There are several benefits related to parameter estimation in the travel time domain; however, there is a limitation in the assumption of invariant streamline trajectories, and also in the definition of the optimal horizontal shift which defines the objective function magnitude. To address the limitations of the travel time inversion, He et al. (2002) introduced the Generalized Travel Time Inversion (GTTI). The improved calibration performance of this approach results from definition of the data misfit as the time shift at which the cross-correlation between the observed and simulated responses is maximized. Also in the GTTI, the sensitivities are time averaged, calculated as the expected value over a set of time intervals selected throughout the production history. Both improvements enable the application of streamline-based travel time inversion on field cases with complex reservoir heterogeneity and high-resolution production schedules.

3.2.3. Inversion Algorithm and Time-lapse Data Integration

Once the sensitivities for the production and time lapse seismic data are available, the data integration is performed using a single objective function that considers data types of two uniquely different spatial resolutions. One term of the objective function considers the production data, which represents a sparse data set in the sense that they present a reduced capacity to infer static properties with increasing distance from the well. The second term considers the seismic data which, although areally dense with a resolution of tens of meters, has associated multiple levels of uncertainty (Feng and Mannseth, 2010). The seismic data can be posed in several forms in the objective function. For example, the data can be defined as the absolute values of the state at a particular time, or as relative values of the state by computing the difference over survey intervals. In either case, the objective function can be augmented for inclusion of the initial state to constrain the inversion and improve non-uniqueness (e.g., Dong and

Oliver, 2005; Landa and Horne, 1997). In this study, after the sources of dynamic data and the different formulations of the seismic information are defined, we assemble the system of inverse modeling equations which are composed of the sensitivities, the data misfit and a set of regularization terms. The non-linear inverse problem is therefore posed as a linear system which we iteratively solve using a sparse least squares algorithm. At each iteration the algorithm updates the calibrated parameters, or reservoir heterogeneity defined at individual grid cells, to minimize the misfit in a least squares sense. The regularization terms are included to ensure spatial continuity and geologic realism (Yoon et al., 2001).

3.2.4. Illustration of the Procedure with a Two Dimensional Example

Before presenting the mathematical formulation of the proposed techniques, we first illustrate the major steps involved in the data integration procedure using a two-dimensional synthetic application. The calibrated reservoir model is characterized as a 50×50×1 cell lognormal permeability field with heterogeneity defined by maximum continuity in the north-east orientation (**Fig. 3.1**).
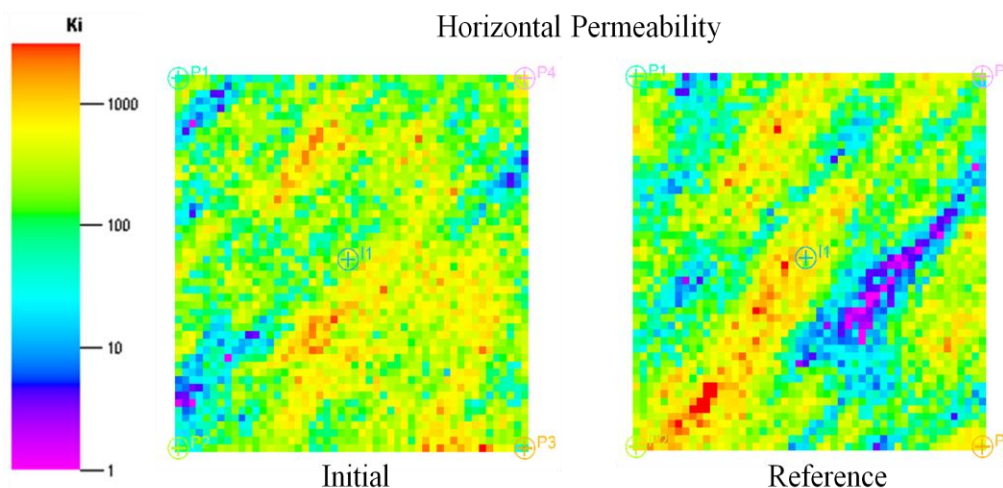
Fig. 3.1—Initial permeability and reference permeability used in the illustrative example.

The example involves reservoir production in a 5-spot pattern with four producers located at the corners and one central injector. In order to maintain pressure and minimize the effects of phase evolution, the reservoir is produced under voidage balance. Also, the injection program starts simultaneously with the production of the reservoir. The initial or prior permeability field applied for the history matching exercise is shown in **Fig. 3.1** together with the reference permeability heterogeneity that we attempt to approximately reproduce using the observed time-lapse seismic and production data. The temporal water front movement through the prior and reference models is shown in **Fig. 3.2**.
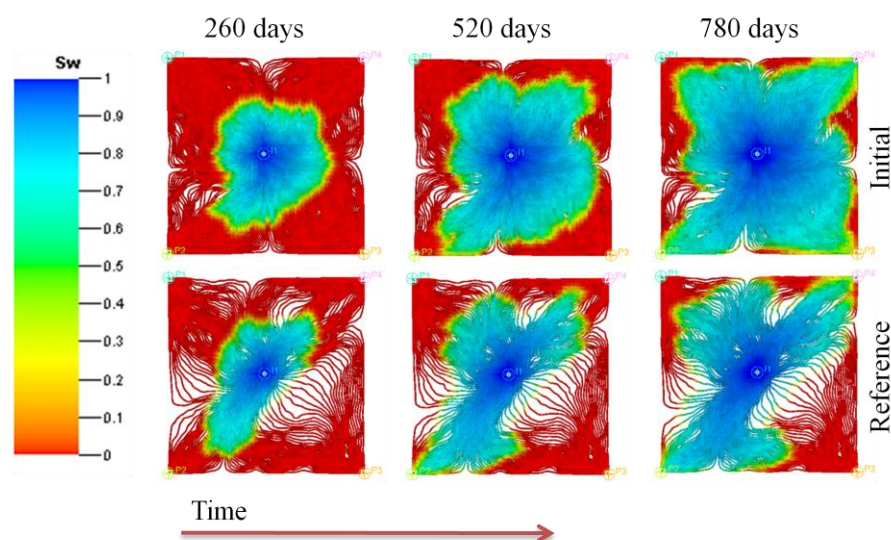
Fig. 3.2—Water front movement comparison between the initial and reference model in the streamline coordinate system.

Consistent with expectations, the underlying heterogeneity largely determines the difference in front evolution between the prior and reference models. The propagation of the water in the reference model depicts a preferential movement along the high permeability streak. On the contrary, frontal progression through the less heterogeneous prior model depicts a more radial distribution. In order to illustrate the different sources of dynamic data in the time lapse integration, we consider two different examples. In the first case the seismic data are expressed in the form of inverted water saturation changes

available after a geophysical seismic inversion. In the second case, the inversion is based on integration of seismic data in the form of maps of the elastic acoustic impedance. Both cases integrate seismic data alone and do include production data in the objective function.
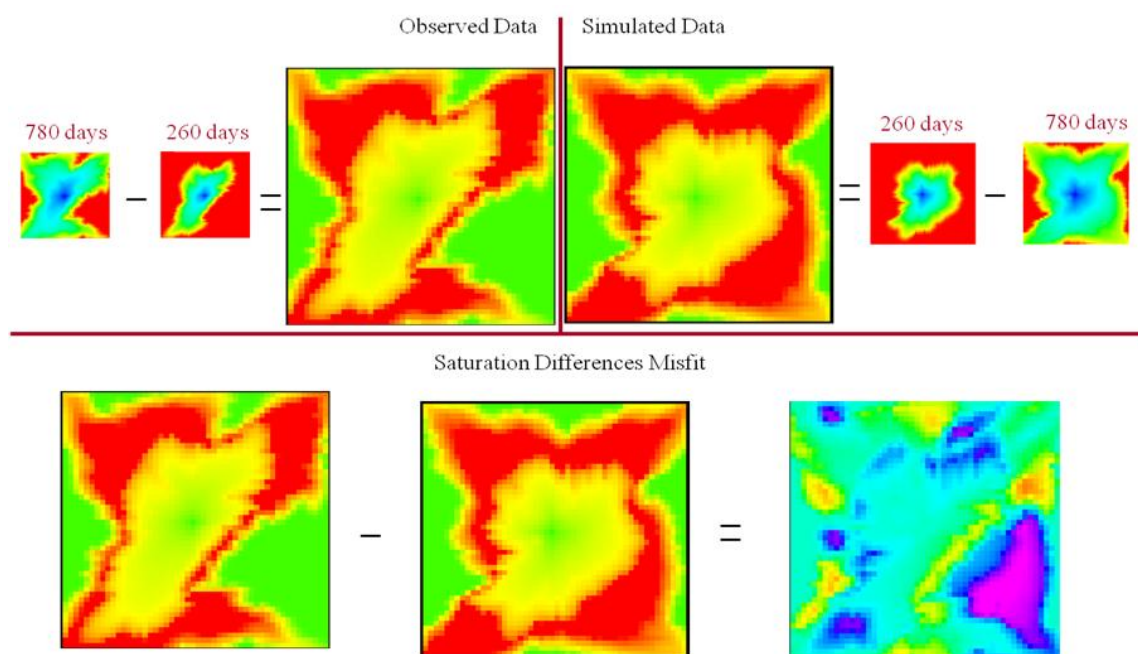
Fig. 3.3—Calculation of the seismic saturation changes and the seismic misfit.

Fig. 3.3 shows the how the seismic observation data are defined for the first case of saturation changes. The observed data set is computed as the change in water saturation between the time lapse intervals, at grid cell resolution, using the reference model. This saturation difference map therefore reflects how the static field properties influence the waterflood. The simulated data set is computed in the same manner although using the prior model. Therefore, the data misfit (i.e., objective function) is computed as the difference between the saturation change using the prior permeability model and the saturation change using the reference model, again at grid cell resolution. **Fig. 3.4** shows the results of the model calibration procedure, comparing the front evolution through the calibrated (prior) model against the reference (i.e., target) fluid movement. Notable results of the inversion procedure are an improved description of the front evolution at

the time of the base survey, and also an improvement in the prediction of consecutive surveys. The improvement in the location of the front evolution is based solely on integration of the change in water saturation maps, which reduces the effect of noise in the seismic data and also reduces the affects of poorly determined rock elastic parameters. Therefore, when the interpreted seismic attributes are subtracted, the fluid evolution is amplified.
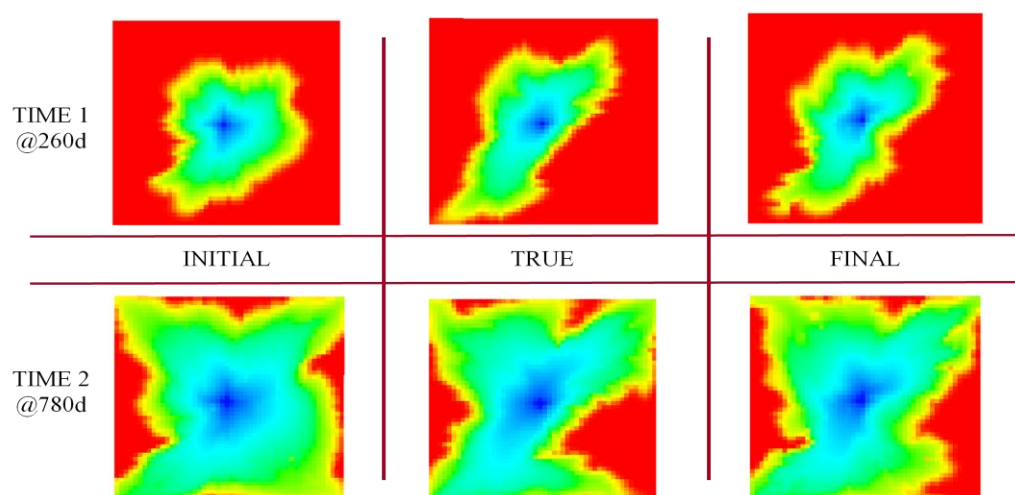
Fig. 3.4—Saturation evolution for the initial, reference and the calibrated model.

In the ideal scenario, i.e., in the theoretical application, the seismic data do not have associated noise and there is no ambiguity in the data related to the rock elastic parameters. In this case the seismic data prove useful in the improvement of production responses at the well level. In **Fig. 3.5** is plotted the water cut response at each producer over a production time of 2000 days. There is a marked improvement in the match quality of each well response that results from the integration of the seismic difference maps between the surveys at 280 and 780 days. The quality of the match is also preserved for times beyond the scope of the seismic interval, indicating that the forecast is also improved by seismic data integration.
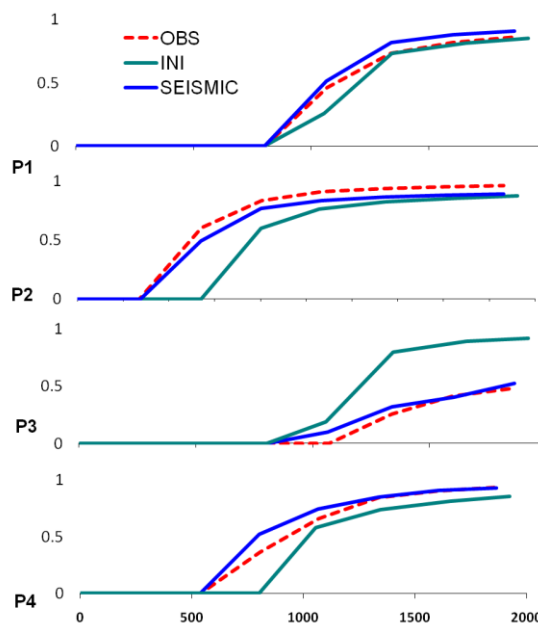
Fig. 3.5—Water cut responses at the production wells after seismic data integration.

In practical geophysical seismic inversion, it is more common to obtain maps of the rock acoustic impedance rather than of changes in water or gas saturation. We therefore investigate the performance of our proposed algorithm when the seismic data are provided as changes in acoustic impedance over some production period. For this exercise, the time-lapse change in acoustic impedance in the reference model, at grid cell resolution, is applied as the observation data set for calibration of the prior permeability model. This calibration dataset is shown in **Fig. 3.6**, and is also shown with added white noise that represents sources of uncertainty inherent to the geophysical seismic inversion. These data are applied in the inversion algorithm as is, without filtering or smoothing, to test the robustness of the algorithm, and also to assist in the understanding of the influence of noise on the calibrated model.

Objective Function Acoustic Impedance

Simulated   Observed   Misfit
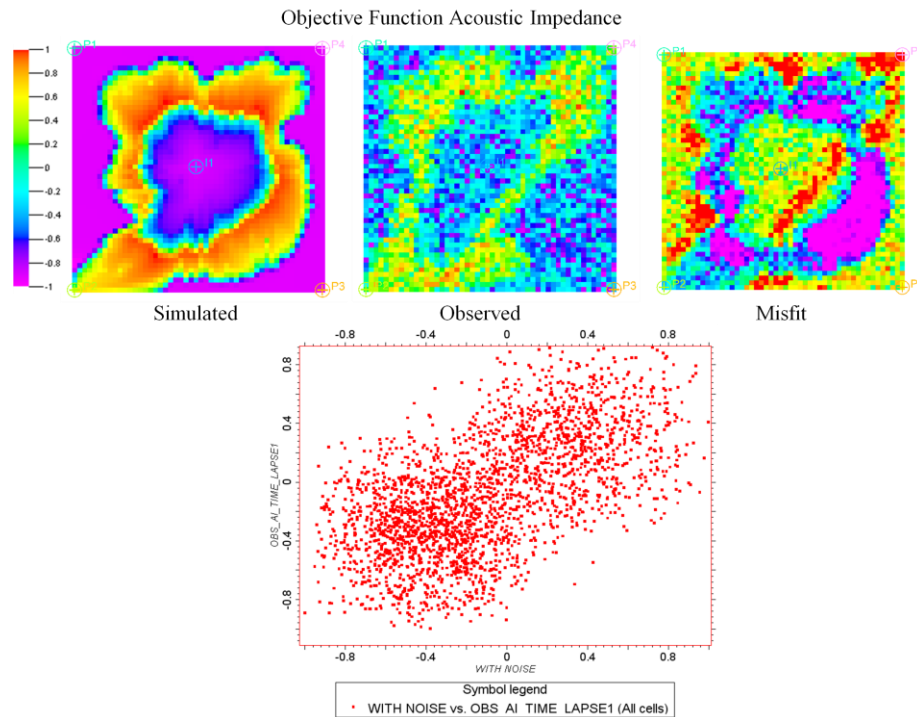
Fig. 3.6— (Top) Observed data in the form of changes in acoustic impedance, and (bottom) the uncorrelated noise added to the data.

Fig. 3.6 also presents the data misfit computed as the difference between the observed (from the reference model) and simulated (from the prior model) acoustic impedance maps over a period of 780 days. We use these data, or the difference in acoustic impedance between surveys, as the observation data set for the calibration of reservoir permeability heterogeneity.

Acoustic Impedance Differences

Initial   Reference   Final
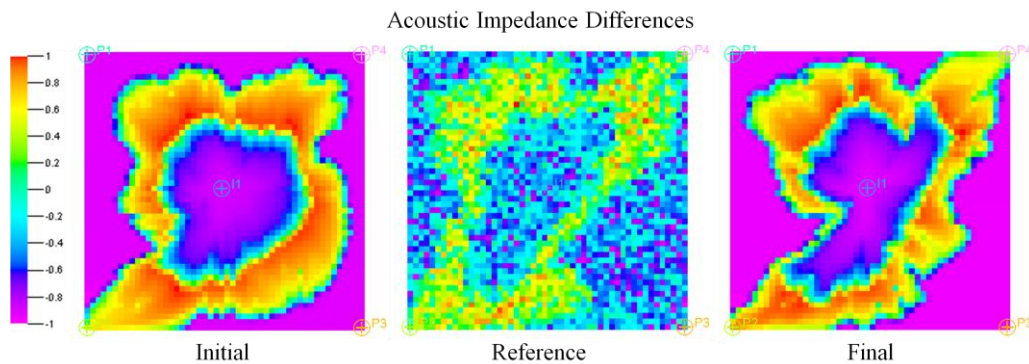
Fig. 3.7—Comparison of the acoustic impedance changes for the initial, reference and the calibrated model.

Fig. 3.7 shows a comparison of the changes in acoustic impedance corresponding to the permeability field before and after calibration, which required 40 iterations of the inversion algorithm. **Fig. 3.8** shows the changes in the evolution of the water saturation before and after the data integration. It is the evolution of the water saturation along the each streamline that forms the underlying basis of our inversion approach. That is to say, at each single cell it is the change in the water composition of the rock, characterized as a saturation front that is evolving through all streamlines intersecting the cell, that produces a change in its elastic properties. Both figures depict the ability of the time lapse seismic data, through inverse modeling, to effectively capture the water movement in the reference case, even when containing large levels of noise.
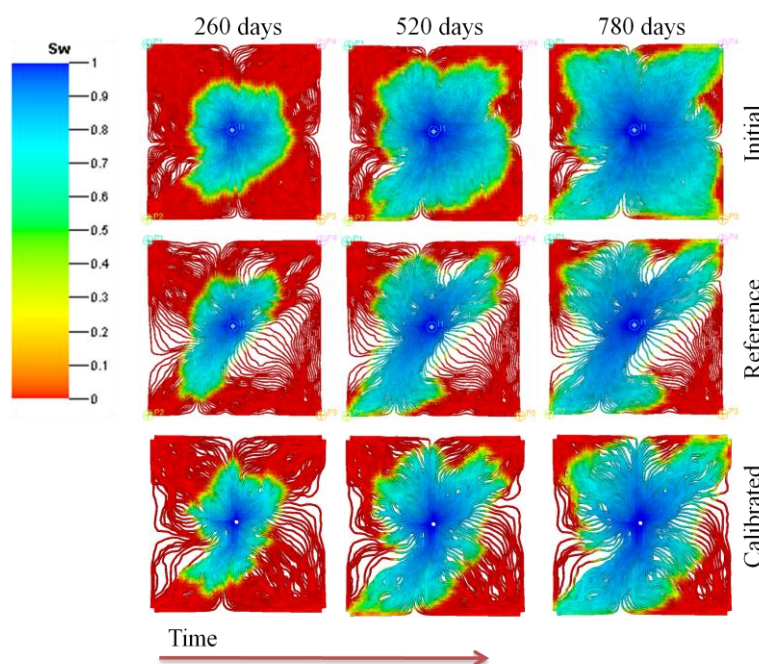
Fig. 3.8—Comparison of the water front movement for the initial, reference and calibrated model in the streamline coordinate system.

Another criterion for evaluation of the model calibration quality is achieved by comparing the changes needed in the model with the changes introduced after the history match. **Fig. 3.9** presents the calibrated permeability, which characterizes the underlying

heterogeneity of the model, and its several primary characteristics that are associated with the reference permeability. In particular, there is a low permeability barrier present in the reference model with a northeast orientation that is captured after the integration of the changes in acoustic impedance. The proper identification of this and other primary heterogeneity features reveals that the single-term objective function, enforcing only the changes observed in the time lapse seismic evolution, enable the characterization of heterogeneity that also influence production responses. We assess this capacity from inspection of match quality improvement in the water cut at the producers. **Fig. 3.10** shows a mild deterioration in the match quality in comparison to **Fig. 3.5**, which is the result of the uncorrelated noise present in the acoustic impedance changes, and also the variation in the field pressure captured by modification of the stiffness of the rock. The combined effect introduces a non-linearity between the rock elastic properties and the heterogeneity that is more difficult to resolve or calibrate than for the case of the saturation maps, although there is still overall improvement in the water cut responses. The predictability of the model is also reduced by the use of changes in acoustic impedance in comparison to the use of saturation changes.

Calibrated Permeability   Changes Needed   Changes Made
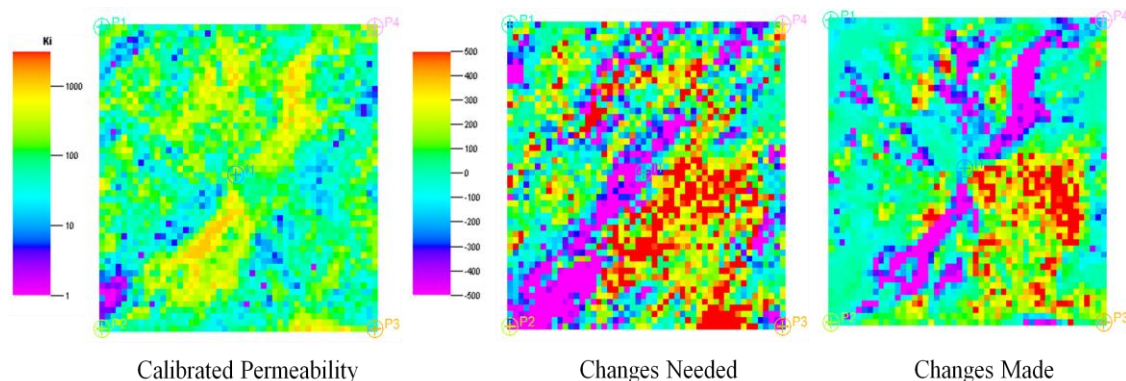
Fig. 3.9—Final permeability after the data calibration, for references the changes needed in the permeability model and the changes introduced after the history matching.
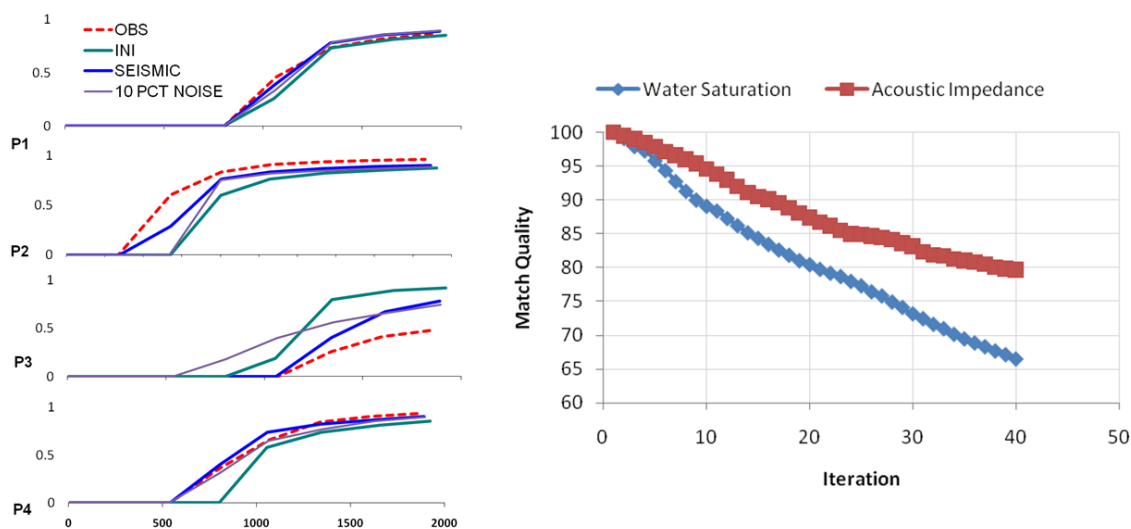
Fig. 3.10—Left the history matching results for the water cut response after the seismic inversion, on the right the performance of the minimization procedure.

3.3. Mathematical Approach

The streamline techniques are based on a Lagrangian approach that decomposes the physical domain into a series of one-dimensional equations characterized by the streamline geometry and the travel time along the streamline, or time of flight. Within the streamline domain the determination of changes in the state resulting from a perturbation in the underlying heterogeneity is remarkably inexpensive. These streamline sensitivities, which relate time of flight to perturbations in transport properties such as permeability and porosity, are based on the reasonable assumption that small changes in these properties do not affect the streamline trajectory. The extension of these sensitivities to other production responses (e.g. water and gas arrival time) requires only the determination of partial derivatives obtained from the mass conservation law for the water and gas phases in the streamline coordinates. The streamlines can also be used to account for changes in the phase composition at a fixed location. In the streamline coordinates the saturation along the streamlines can be expressed as a functional dependency of a self similar variable such that a perturbation of the state of a phase composition can be directly correlated with a perturbation in the

arrival time along the streamline. The self similarity assumptions can be extended for problems with changes in the streamline geometry that originate from variations in the field boundary conditions or from the effect of transverse, diffusive forces that are unrelated to the streamline coordinate system. In this section we will cover the details related to the time of flight sensitivities, including the transport behavior associated with the arrival of the water phase at the producers, the saturation of water along streamlines, and changes in water saturation in the streamline domain. We then establish the inverse problem as the minimization of an objective function using a damped least squares algorithm to solve for the model updates.

3.3.1. Sensitivity for the Arrival Time of a Neutral Tracer

The derivation of the analytical streamline sensitivities is based on the simplicity of the transport equations when expressed in a Lagrangian representation. The key element is a coordinate transformation from the physical domain to the streamline domain that is based upon the bi-streamfunctions and an additional time of flight coordinate. Streamlines are, by definition, the tangential curves to the instantaneous velocity field and, under steady state conditions, equivalent to pathlines of individual particles traveling through a continuous system. We can define a streamline that is everywhere tangential to the velocity field by introducing the bi-streamfunctions, ψ and χ (Datta-Gupta and King, 2007), as

$$\vec{u} = \nabla \psi \times \nabla \chi$$ ....(3.1)

An important underlying concept behind our approach is the concept of 'time of flight', τ, which is defined simply as the travel time of a neutral tracer along the streamline trajectory Σ, or as

$$\tau(x, y, z) = \int_{\Sigma} s(r)dr$$ ....(3.2)

The variable s(r) is called the "slowness" and is defined as the reciprocal of the Darcy velocity divided by porosity (Datta-Gupta and King, 2007),

$$s(r) = \frac{\phi(r)}{u_t}$$ ....(3.3)

A streamline is defined by the intersection of a constant value of ψ with a constant value of χ. In the streamline perspective we need to define a transformation operation from the physical (Eulerian) to the streamline (Lagrangian) domain. This transformation is characterized by the Jacobian,

$$\left\| \frac{\partial(\tau, \psi, \chi)}{\partial(x, y, z)} \right\| = (\nabla \psi \times \nabla \chi) \cdot \nabla \tau = \vec{u} \cdot \nabla \tau = \phi$$

For sensitivity computations we are primarily interested in defining the streamline trajectories. The saturations in each cell from the finite difference solution are mapped along these streamlines to relate the saturation changes to the changes in reservoir properties, thereby defining the parameter sensitivities.

Assuming that small changes in the reservoir parameters will not shift the streamline paths (i.e., assuming negligible changes in the pressure and velocity field), a perturbation in the time of flight can be written as follows,

$$\delta\tau = \int_{\Sigma} \delta s(r) dr$$ ....(3.4)

And

$$\partial s(r) = \frac{\partial s}{\partial k} \delta k + \frac{\partial s}{\partial \phi} \delta\phi$$ .... (3.5)

The slowness derivatives are given by the following (Vasco et al., 1999),

$$\frac{\partial s}{\partial k} = -\frac{s(r)}{k} \quad \dotfill (3.6)$$

And

$$\frac{\partial s}{\partial \phi} = -\frac{s(r)}{\phi} \quad \dotfill (3.7)$$

3.3.2. Sensitivity for the Arrival Time of Water

We can write the mass balance equation for two phase incompressible flow as

$$\frac{\partial S_w}{\partial t} + \frac{\partial F_w}{\partial S_w}\frac{\partial S_w}{\partial \tau} = 0 \quad \dotfill (3.8)$$

Considering a small volume of water that travels along the streamline we define a perturbation in the state variable

$$\delta S_w(\tau,t) = \frac{\partial S_w}{\partial t}\delta t + \frac{\partial S_w}{\partial \tau}\delta \tau = 0 \quad \dotfill (3.9)$$

That yields the following functional dependency between the arrival of a neutral tracer and the arrival of the water phase,

$$\delta t = \left(-\frac{\partial S_w}{\partial \tau} \middle/ \frac{\partial S_w}{\partial t}\right)\delta \tau \quad \dotfill (3.10)$$

Combining Eq. (3.10) with the mass balance for the water phase (He et al., 2002) finally provides the useful relationship between travel time (or physical time) and time of flight,

$$\frac{\partial F_w}{\partial S_w} = -\frac{\partial S_w}{\partial t} \middle/ \frac{\partial S_w}{\partial \tau} \quad \dotfill (3.11)$$

$$\delta t = \frac{\delta \tau}{\left(\frac{\partial F_w}{\partial S_w}\right)} \quad \text{...}(3.12)$$

3.3.3. Sensitivities of the Time Lapse Saturation Differences of Water Saturation

In order to calculate sensitivities for the water saturation at a particular location along the streamline, we recognize that the streamlines are the characteristic curves of Eq. (3.8). We are interested in determination of the functional relationship between the streamline coordinates (i.e., geometry and time of flight) and the saturation distribution along the streamline. A self-similar variable enables a reduction in the number of independent variables such that

$$S_w(\tau,t) = S_w(\eta)$$
$$\text{...}(3.13)$$

Where η is the self similar variable and is defined as

$$\eta = \frac{\tau}{t}$$
$$\text{...}(3.14)$$

Therefore, a perturbation in the saturation along a streamline can be written as

$$\delta S_w(\eta) = \frac{\partial S_w}{\partial \eta}\frac{\partial \eta}{\partial \tau}\delta \tau$$
$$\text{...}(3.15)$$

Or, expanded in terms of the primary variables, as

$$\delta S_w\left(\frac{\tau}{t}\right) = \frac{1}{t}S'_w\,\delta \tau$$
$$\text{...}(3.16)$$

In the previous equation we assume that the streamlines do not vary during the time interval between the base and the monitoring surveys. This is a strong assumption

because there are a myriad of factors that can affect the velocity field and therefore the geometry of the streamline field. To substantiate this assumption we extend the concept utilized in streamline simulation, where transport calculations along the streamlines are defined over time intervals of invariant streamline geometry. In our particular case we assume that the saturation not only depends on the dimensionless location of the front along the streamlines, represented by the time of flight over the simulation time variable, but also on the previous state of the saturation, or the (physical) time at which the streamline geometry was refreshed using a new set of fluxes from finite difference simulation. These assumptions are formulated as

$$S_w^n = S_w^n \left(\frac{\tau}{t}, S_w^{n-1} \right)$$ .... (3.17)

From this is it possible to perturb the state of the saturation at time n as a function of the streamline geometry and the dimensionless position of the water front along the streamline. It is important to understand that the perturbation is also dependent on the state of the saturation at the previous time step when the streamlines were regenerated, that is,

$$\delta S_w^n = \frac{1}{t} S_w'^n \delta\tau + \frac{\partial S_w^n}{\partial S_w^{n-1}} \delta S_w^{n-1}$$ ....(3.18)

A recursive relationship is therefore defined in which a perturbation of the saturation state at time n is expressed directly in terms of a perturbation at the previous time step n-1, and therefore to all M time steps between the base survey and the current monitoring survey. The recursion backwards in time may be terminated early if a point in time is reached at which the velocity field is no longer perturbed. The recursion is formulated as

$$\delta S_w^n = \frac{1}{t} S_w'^n \delta\tau + \frac{\partial S_w^n}{\partial S_w^{n-1}} \left[\frac{1}{t} S_w'^{n-1} \delta\tau + \frac{\partial S_w^{n-1}}{\partial S_w^{n-2}} \left[\cdots \frac{\partial S_w^{n-M}}{\partial S_w^0} \frac{1}{t} S_w'^0 \delta\tau \right] \right]$$ ....(3.19)

We further make the reasonable assumption that changes in the background saturation are slow relative to adjustment of the streamline geometry during the pressure updates, which permits the use of self-similarity within the time steps of constant streamline geometry. Also, rather than correcting the saturation front for changes in the streamline geometry ($\partial S_w^{n-1}/\partial S_w^{n-2}$), we correct the state directly using the phase saturations solution of the finite difference simulator. Thus, the sensitivity metric defined as the change in saturation with respect to permeability during the time lapse interval is formulated as

$$\frac{\delta \Delta S_w}{\delta k} = \sum_{i=1}^{n} \left(\frac{1}{t} S_w' \frac{\delta \tau}{\delta k} \right)_i - \left(\frac{1}{t} S_w' \frac{\delta \tau}{\delta k} \right)_0 \quad \text{.................................(3.20)}$$

3.3.4. Petro Elastic Model and Sensitivities of the Acoustic Impedance

The elasticity of the reservoir rock and, therefore, its ability to propagate mechanical waves is determined by the rock matrix properties, the pore fluids and the reservoir pressure. For low frequency waves, the Gassmann's equation (Gassmann, 1951) is adequate for representation of the elasticity of the bulk rock volume. The equation relates the bulk modulus of the porous rock, also called the bulk modulus of the frame $\mathbf{K_{fr}}(\phi)$, which is a function of porosity and the lithostatic pressure, the bulk modulus of the structural rock $K_{dry/grains}(\phi_c)$, which is an intrinsic property of the rock configuration and can be assumed to be constant under varying conditions, such as variations in the fluid occupying the porous space, and finally the fluid bulk modulus $K_f(S_w, S_o, S_g, P, T)$, which is a function of the elastic properties of the complete mixture. The Gassmann's equation is

$$K_{sat} = K_{fr} + \frac{\left[1 - \dfrac{K_{fr}}{K_{grains}}\right]^2}{\phi\left[\dfrac{1}{K_f\left(S_w, S_o, S_g\right)} - \dfrac{1}{K_{grains}}\right] + \dfrac{1}{K_{grains}}\left[1 - \dfrac{K_{fr}}{K_{grains}}\right]} \quad\text{............................(3.21)}$$

The composite fluid bulk modulus, K_f, is calculated from the properties of the fundamental components and using the Rouss average or harmonic average of the properties weighted by the relative amount of each individual component. The Rouss average guarantees the lowest value of the modulus obtained by combining the individual elements (Mavko et al., 1998). The formulation is

$$K_f = \left(\sum_{i=o,g,w} \frac{S_i}{K_i}\right)^{-1} \quad\text{...(3.22)}$$

In the case of our field application (Norne reservoir model), the dependency of the frame modulus, K_{fr}, with respect to the porosity of the rock has been determined by laboratory observations made on cores and is expressed as the linear equations

$$K_{fr} = a - \varphi \cdot b$$
$$G_{fr} = c - \varphi \cdot d \quad\text{...(3.23)}$$

The density, ρ, is computed as the weighted average of the densities of the individual components of the rock

$$\rho = (1 - \varphi) \cdot \rho_{fr} + \phi\left(\sum_{i=o,g,w} S_i \rho_i\right) \quad\text{...............................(3.24)}$$

With the density and bulk modulus of the saturated rock, the compressional and shear velocities can be estimated under the assumptions of an isotropic media and of

insensitivity of the shear modulus to the fluid inside the porous media. The compressional or p-wave velocity, Vp, is estimated as

$$V_p = \sqrt{\frac{1}{\rho}\left(K_{sat}\frac{4}{3}G_{fr}\right)}$$ ....(3.25)

The seismic impedance, Z, can be written in terms of Vp as

$$Z = \rho V_p = \sqrt{\rho\left(K_{sat}\frac{4}{3}G_{fr}\right)}$$ ....(3.26)

From the above relationships, the acoustic impedance is a function of the reservoir static parameters, such as porosity, and also of the changes of fluid composition of the rock, that is,

$$\frac{\partial Z}{\partial k} = \frac{\partial Z}{\partial S_w}\frac{\partial S_w}{\partial k} + \frac{\partial Z}{\partial S_g}\frac{\partial S_g}{\partial k} + \frac{\partial Z}{\partial P}\frac{\partial P}{\partial k}$$ ....(3.27)

In this research we study waterflooded reservoirs and therefore consider only the contribution of the changes in water front movement to the changes in acoustic impedance. This assumption simplifies the derivation of our sensitivities and is adequate for our field application where the majority of the changes in acoustic impedance are related to changes in the saturation content of the rock (El Ouair et al., 2005).

3.3.5. Joint Integration of Seismic and Production Data

We perform the data integration using a deterministic approach in which we minimize a penalized misfit function composed of the seismic data misfit and additional regularization terms. The regularization terms consist of a 'norm' constraint and a 'roughness' constraint and are introduced to preserve the spatial continuity and the geological realism in the updated model. In this manner, the model calibration is a

balance between reducing the data misfit and minimizing the changes to the prior model, thereby maintaining geologic consistency. The penalized misfit function $f(\delta\mathbf{k})$ is defined as

$$f(\delta\mathbf{k}) = \theta\left\|\delta\mathbf{d}_{seis} - \mathbf{G}_{\mathbf{seis}}\delta\mathbf{k}\right\| + (1-\theta)\left\|\delta\mathbf{d}_{prod} - \mathbf{G}_{\mathbf{prod}}\delta\mathbf{k}\right\| + \beta_1\left\|\delta\mathbf{k}\right\| + \beta_2\left\|\mathbf{L}\delta\mathbf{k}\right\| \quad\text{.............(3.28)}$$

In Eq. (3.28), $\delta\mathbf{d}_{seis}$ is the vector of the misfit between the change in acoustic impedance derived after a geophysical seismic inversion and the change in simulated acoustic impedance. $\mathbf{G}_{\mathbf{seis}}$ is the sensitivity matrix containing the partial derivatives of the changes in acoustic impedance with respect to the reservoir parameters, i.e., grid cell permeabilities. The production information is incorporated to an extent controlled by a weighting factor θ, which is defined from the degree of confidence in the seismic data. In fact, based on the amount of noise and the resolution of the seismic information, a weight can be selected such that the seismic information is applied as a second smoothness constraint (Feng and Mannseth, 2010). The quantity δk is the vector of changes in the reservoir permeability. The first penalty term is the 'norm' constraint that minimizes deviation from the prior model. The second penalty term is the 'roughness' constraint, where the operator L computes the second difference of each cell permeability and has an effect analogous to the imposition of a prior variogram or covariance constraint (He et al., 2002). An objective function minimum is obtained using an iterative least-squares solution of the augmented linear system of equations given by Eq. (3.29),

$$\begin{pmatrix} \mathbf{G}_{seis} \\ \mathbf{G}_{prod} \\ \beta_1\mathbf{I} \\ \beta_2\mathbf{L} \end{pmatrix}\delta\mathbf{k} = \begin{pmatrix} \delta\mathbf{Z} \\ \delta\mathbf{d}_{prod} \\ 0 \\ 0 \end{pmatrix} \quad\text{..(3.29)}$$

where the scalars β_1 and β_2 determine the relative strengths of the 'norm' and 'smoothness' constraints. While the selection of these weights can be somewhat

subjective, they are minimally enforced only to the extent that implausible geologic features resulting from updates along streamline trajectories are avoided.

3.4. Results and Discussions

In this section we discuss the application of our proposed methodology to a field scale semi-synthetic example, the Brugge reservoir model, and also to the Norne field case. The Brugge field is a comparative example designed by TNO (a Dutch research organization) to compare different history matching and production optimization strategies. The case study was constructed with the objective of incorporating realistic operational conditions and geological features (Peters et al., 2010). The effectiveness of the proposed time lapse seismic inversion algorithm is tested in this application where a series of reservoir management activities including infill drilling of producers and injectors, and also changes in reservoir driving mechanisms as a result of aquifer depletion, are performed between the time span of the base and monitoring surveys. The model provides a good test scenario for our proposed inversion algorithm because the varying field conditions result in highly variable streamline geometries throughout the production time. The second application considers the Norne field, operated by Statoil and located offshore in the Norwegian Sea, providing field production data beginning from 1997 and also a set of repeated seismic surveys available for the E-segment of the reservoir. The base survey was acquired in 2001 and two monitoring surveys were completed in 2003 and 2004. The Norne reservoir model brings the complexity of the seismic inversion together with the uncertainty associated with the inversion of the seismic attributes to rock elastic parameters. In particular, the Norne model presents a strong candidate to test the applicability of our proposed technique because the changes in acoustic impedance are mainly considered to result from changes in the water saturation of the rock (El Ouair et al., 2005).

3.4.1. Brugge Field Seismic Data Integration

The Brugge reservoir represents a typical North Sea Brent-type field. The structure consists of an east-west elongated half-dome with an interior fault with moderate throw. The reservoir model has a corner-point grid with more than 60,000 active grid cells, twenty producers located in the dome, and ten infill water injectors located in the surrounding aquifer that, in addition to the aquifer, provide pressure support. The prior facies structure represents a fluvial environment constructed trough sequential indicator simulation and contains a channelized zone in the bottom of the reservoir. The permeability is populated deterministically using a correlation with porosity. **Fig. 3.11** shows the location of the producers, injectors and interior north-east fault, together with the prior permeability, porosity and net to gross mapped onto the grid. Further details of the geologic description and the static and fluid properties of the reservoir can be found in Peters et al. (2010).

Production data are given in the form of water and oil rates, and also bottom-hole pressure, at each of the twenty producers over a ten year period. The reservoir is produced above the bubble point with the fluid modeled as a dead oil. Inverted 4D seismic data are provided over the 10 year history matching period in the form of water saturation changes. The data were provided as a geocellular property and averaged vertically within the four primary formations (Scheld, Maas, Wall and Schie) that constitute the reservoir. This saturation difference is provided with uncorrelated noise. **Fig. 3.12** shows the saturation changes for the reservoir after 10 years of production. In this inversion exercise, we use this data set as the seismic observation with the intent of calibrating permeability heterogeneity to minimize the difference of the observed and simulated changes. For flow simulation we use the ECLIPSE 100 black oil simulator.
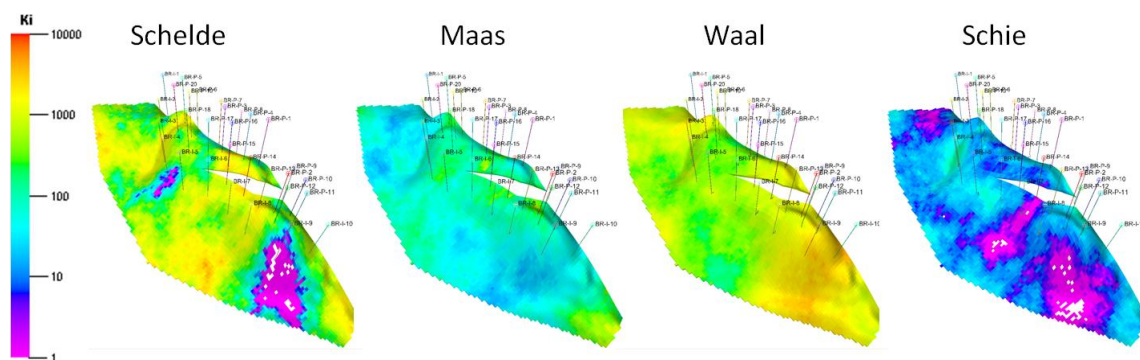
Fig. 3.11—Permeability distribution for the different geologic zones in the Brugge reservoir.
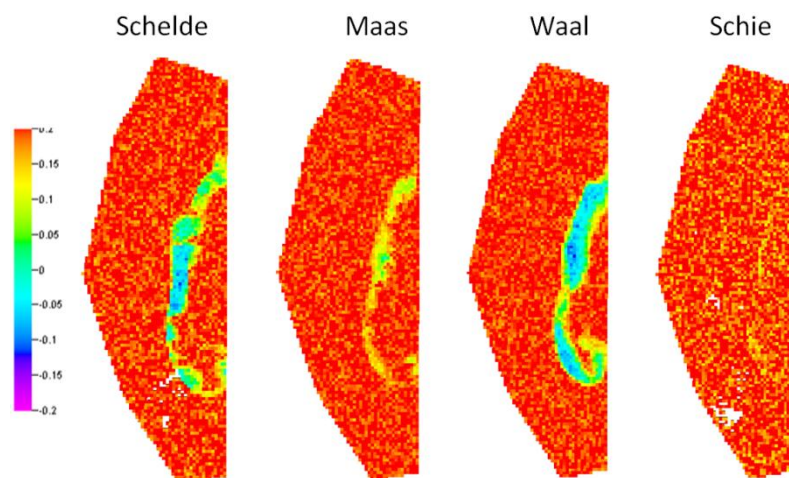
Fig. 3.12—Seismic derived saturation changes averaged over the 4 different zones of the reservoir.

The production schedule begins with production at a limited number of producers. **Fig. 3.13** shows the main events that modify the streamline geometry as the reservoir evolves from the start of production, depicted as the streamline field at different points in time through the ten year history. The first noticeable event, which considerably alters streamline trajectories, is the drilling of infill producers close to the dome. Later at about six hundred days, the reservoir begins to lose pressure support and the water injection program is initiated with the completion of infill injectors at the periphery of the reservoir. The main reason for this intervention is to maintain reservoir production above the bubble point. A large adjustment to reservoir flow behavior is made at eight hundred

days when the aquifer support is depleted and the producers establish pressure communication primarily with the injectors. This event forces the streamline field to significantly evolve as the reservoir driving mechanisms are fundamentally altered.

In order to calibrate the model to reproduce the changes in water saturation observed in the time lapse seismic data, we run the forward simulator, trace streamlines and simultaneously calculate the sensitivities of the saturation changes with respect to the permeability at grid cell resolution. In order to deal with the noise present in the observed data, we perform the inversion algorithm using several different threshold values of saturation change, i.e., any values in the observation data below this cut off are ignored during the inversion. After defining the data misfit, a sensitivity-based minimization of the objective function is performed using a sparse least squares algorithm. **Fig. 3.14** at the left shows the results of the minimization after 40 iterations and using three different threshold values which effectively filter the influence of noise from the observed data. Also shown is the reduction in the amount of data available when larger filtering thresholds are applied. This reduction in the amount of observation data propagates through the inversion workflow in the form of a slower convergence rate as shown in **Fig. 3.15**. At the right in **Fig. 3.14**, the permeability updates are presented and appear targeted following the same direction of continuity that is present in the initial model; however, the calibration significantly reduces the differences between the observed and simulated results.
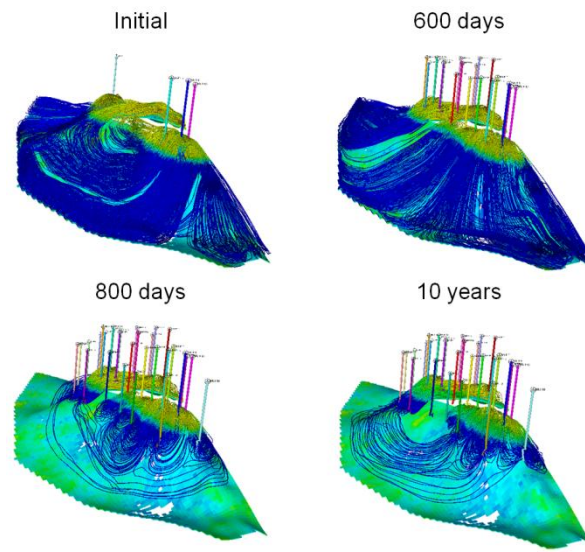
Fig. 3.13—Reservoir dynamics during the production time of the Brugge reservoir.
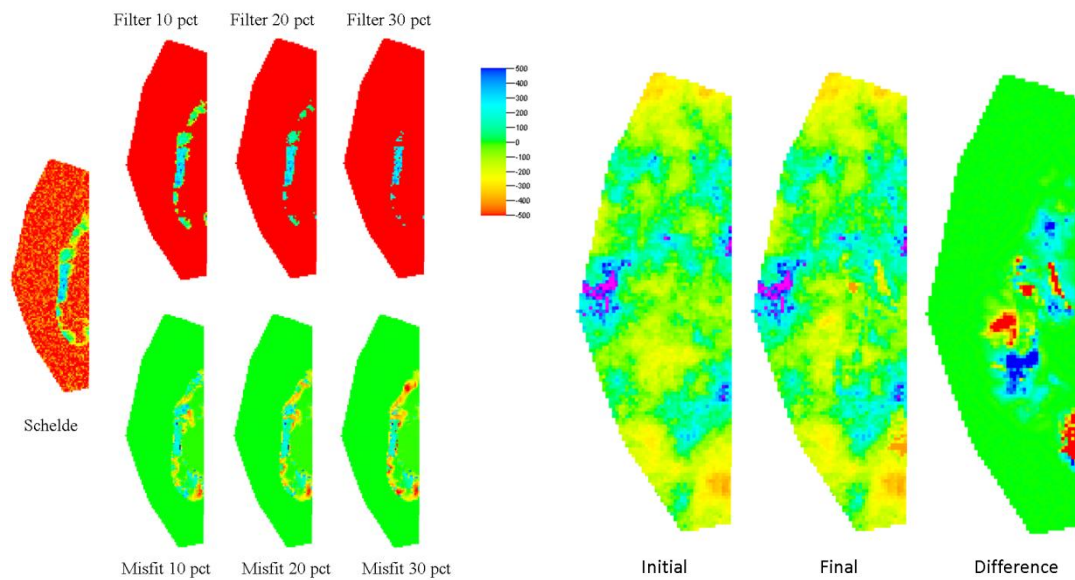
Fig. 3.14—Results of the history matching procedure. Left, data misfit after data calibration for the Schelde reservoir zone with different levels of filtering in the observed data. Right, permeability update for Schelde zone after data calibration.
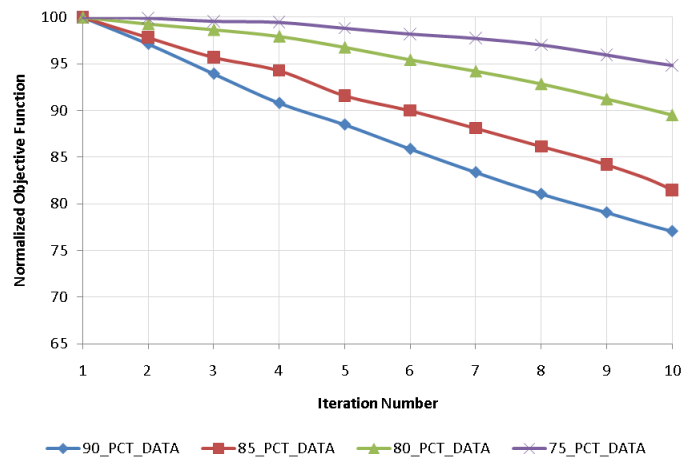
Fig. 3.15—Match quality for different values of the filtering in the inversion algorithm.

Fig. 3.16 at left shows the water cut response at each producer before and following the seismic data integration. Only wells are shown at which the water cut misfit improved by performing the calibration using the seismic data alone. It is evident that the use of only the seismic data is insufficient to improve the water cut response at all of the wells. Therefore, the production data are used for a joint inversion together with the seismic data. In **Fig. 3.16** is shown the water cut history match corresponding to the joint inversion for all of the wells. The majority of the wells show an improvement in match quality except for producer P-16. This well is located near the interior fault boundary at a location of complex flow behavior and shows improvement in the water cut response only upon larger, geologically inconsistent changes in the underlying heterogeneity. As a final step we assess the impact of the model calibration on reservoir management. Following the same methodology applied by Idrobo et al. (2000), we estimate the drainage volume for some of the producers before and after the calibration (**Fig. 3.17**). The correct representation of these volumes as affected by the producers is essential information for the determination of infill locations.
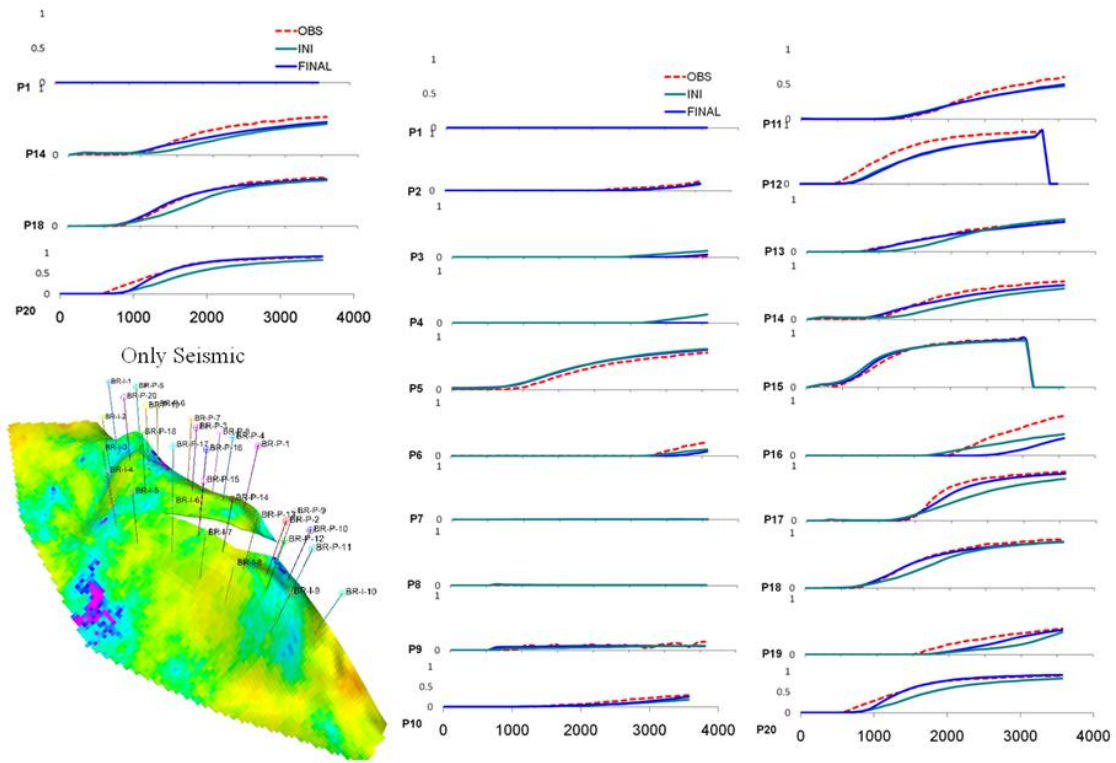
Fig. 3.16— (Left) Improvement in the water cut response for selected wells following the inversion using only the seismic data, and (right) the history matched water cut at each producer following the joint inversion.
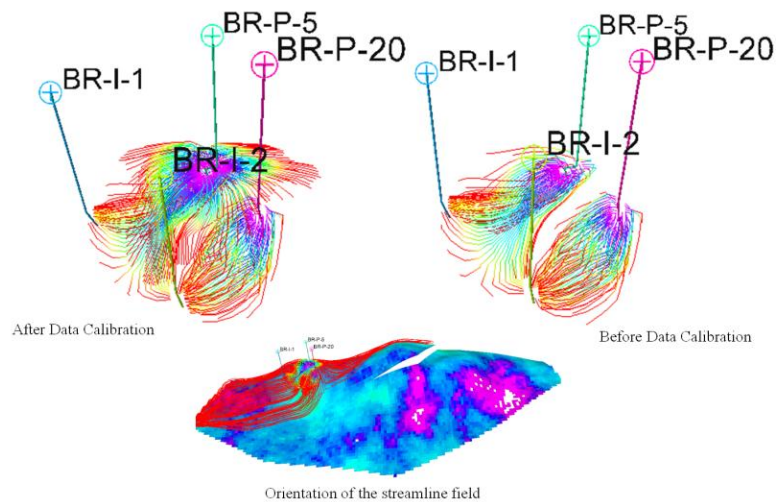
Fig. 3.17—Streamline time of flight, beginning from selected producers, indicates the drainage volume of the producers.

3.4.2. Norne Field Seismic Data Integration

The Norne field is an offshore reservoir located in the northern part of Norway. The field was discovered in 1991 and production started in 1998. The Norne contains multiple faults and is geologically partitioned into several segments. Segments C, D and E constitute the Garn formation which contains the largest hydrocarbon accumulation in the reservoir, with a gas cap of approximately 75 meters. The other segment, G, is a secondary leg of the reservoir that is mostly an oil accumulation. The reservoir rocks are lower to middle Jurassic sandstones of a high quality, with an average porosity of 25 percent and permeability in the range of 200 to 2000 mD. The reservoir model consists of more than one-hundred twenty thousand cells and contains two different rock types separated by a shale layer that hydraulically disconnects the stratigraphic layers above and below. The first rock type comprises the upper part of the reservoir (layers 1 to 3) and is saturated mostly by gas, while the second type is located mainly below the shale barrier (layers 5 to 22) and is saturated by oil accumulations and the aquifer. **Fig. 3.18** shows the top horizon of the reservoir and the respective segments (C, D, E, G) and wells. **Fig. 3.18** also shows the initial phase distribution accompanied by the porosity and permeability cellular properties for the initial model.
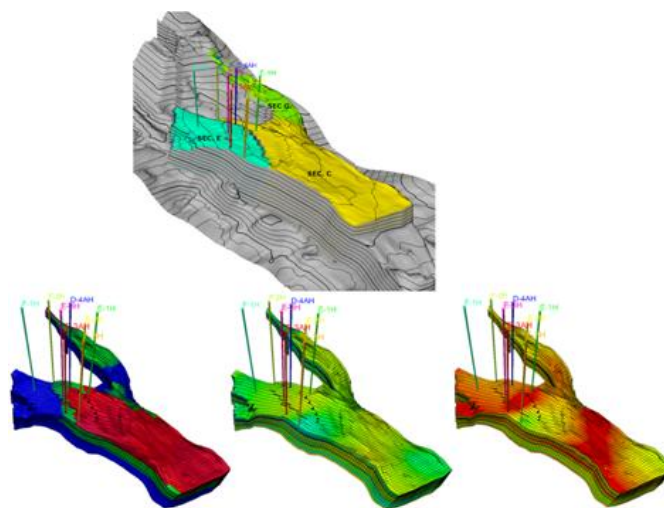
Fig. 3.18—Top surface of the Norne reservoir indicating the different segments. In the bottom the initial fluids in place, horizontal permeability and initial porosity.

The production data include water, oil and gas rates in addition to bottom hole pressure. These data are provided exclusively for the wells located in the E segment; therefore, we will concentrate the calibration of the reservoir model over this segment, thus defining our case study. **Fig. 3.19** shows the location of the three producers (E3H, E2H, E3AH) and two injectors (F1H, F3H), together with their hydraulic connectivity depicted by streamline trajectories that are colored per injector-producer pair. This graphic is an essential tool for visualization of the affect of faults and barriers on the flow geometry. In addition to the production data, a set of 4D seismic surveys was acquired over the years 2001, 2003 and 2004. The seismic data were externally processed and provided for use in model calibration as post stack volumes of the reflection amplitude together with the corresponding horizons for the top and base of the reservoir. Seismic volumes of the differences in reflection amplitude were additionally provided with interpreted horizons used for identification of movement in the water oil contact.

The first step in our data calibration procedure is to invert the seismic volumes of reflection amplitude to changes in acoustic impedance. **Fig. 3.20** shows the results of the geophysical inversion and the upscaling of the seismic volume from the seismic grid resolution (25m x 25m) to the reservoir grid resolution (100m x 100m). Collocation of the seismic data in the reservoir grid allows us to perform a grid-by-grid evaluation of the match quality during the calibration procedure. **Fig. 3.20** also shows the extent of the seismic volume of the E segment compared to the size of the entire reservoir. Considering the small time span between the consecutive surveys, it is reasonable to assume that the porosity did not vary as a result of subsidence of the reservoir. Thus, we assume that only the acoustic impedance varied as the result of changes in fluid phase saturations or pressure in the reservoir. In support of this assumption, the inverted seismic volume indicates the rise of the water oil contact in the E segment (**Fig. 3.20**). The red color in the graphic is associated with a positive change in acoustic impedance. Therefore, we can infer that these changes are produce by an incremental increase in the

stiffness of the rock during the production interval. In this case, the increment in the saturated bulk modulus is produce by an increase in the water saturation.
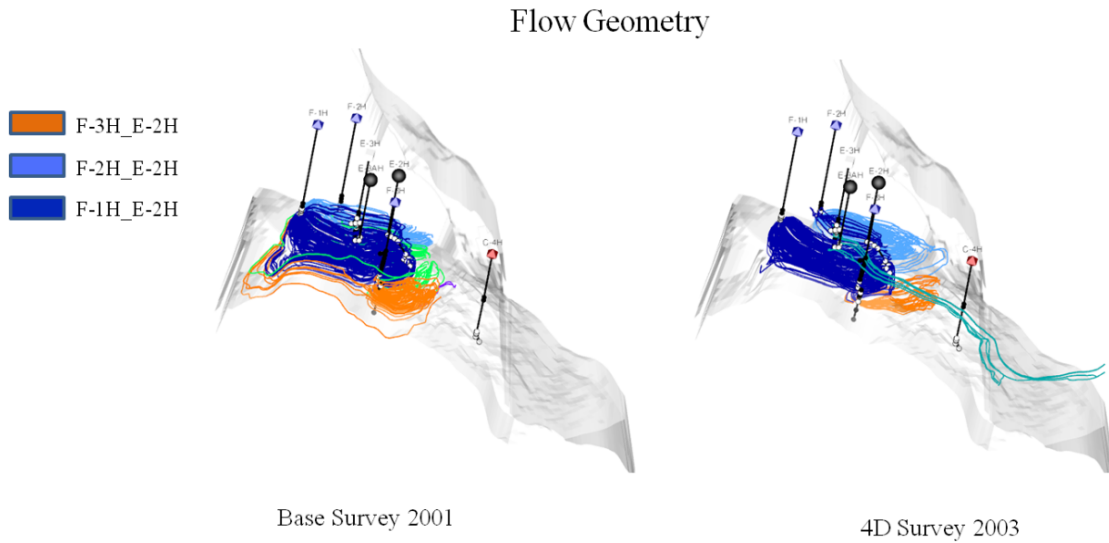
Fig. 3.19—Flow Geometry for the surveys at 2001 and 2003.
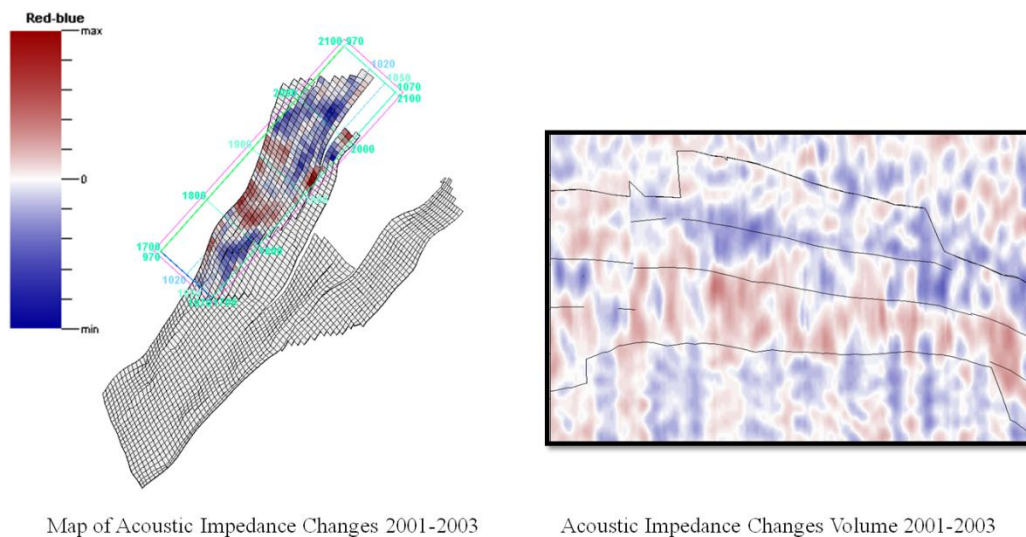
Fig. 3.20—Changes in the acoustic impedance of the rock, the red color indicates hardening of the rock and the blue color softening associated with changes in pressure or gas saturation.

The next step is to calculate the acoustic impedance using the results from the reservoir simulator. For this purpose we use the PEM and the state of the saturation and pressure. We calculate the differences in the acoustic impedance between the times when the seismic surveys were acquired. **Fig. 3.21** shows the influence of the water saturation, gas saturation and the porosity in the calculation of the absolute impedance. From these results we observe that porosity is the parameter that has the largest impact on determination of the elastic properties of the saturated rock. Porosity is a poorly resolved parameter that carries high levels of uncertainty. Therefore, defining the data integration in terms of changes in acoustic impedance allows us to emphasize the effect of changes resulting from the fluid evolution in the reservoir, while minimizing the effect of the uncertain static parameters.

PEM Bulk Modulus as a function of the fluid saturation and porosity

Maps of the Acoustic Impedance for some Selected Layers
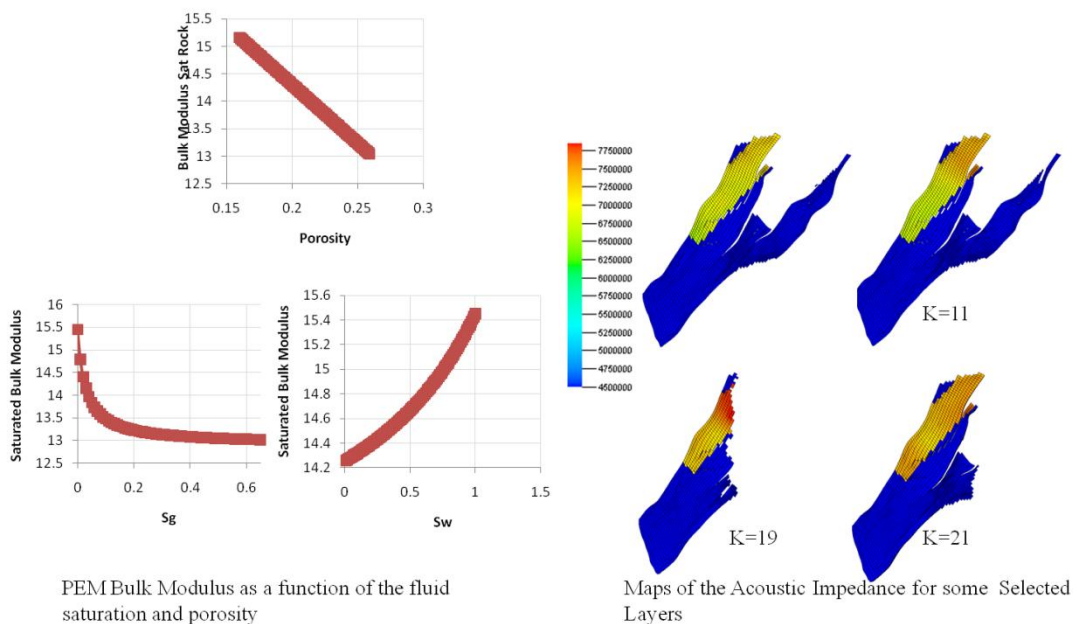
Fig. 3.21—PEM for the Norne reservoir and the absolute acoustic impedance calculated on the reservoir grid.

Our strategy of history matching the Norne data consists of a hierarchical approach that is performed in a sequential manner. First we calibrate the global parameters, and then we history match the production responses at the well level. The observed seismic and

the simulated responses are then defined on the same grid, from which we at last define the match quality as a cost function that is minimized using a gradient-based approach that updates the reservoir parameters on a cell-by-cell basis. **Fig. 3.22** shows the results of the history matching procedure using the well and seismic data. A zone of compaction is clearly identified that is characterized by an increment in the acoustic impedance in the seismic volume. In this figure the water saturation changes over the same period of time are also shown using the same grid alignment. Notable is the estimation of the water oil contact in the initial model (i.e., the model calibrated at the well level); through the seismic data calibration the extent of the changes in water saturation are fine tuned for improved consistency with the observed increment in the acoustic impedance. This behavior is more clearly observed when we compare the changes in acoustic impedance after the data calibration in a layer-by-layer basis. **Fig. 3.23** shows the extent of the modifications to the acoustic impedance for selected layers.
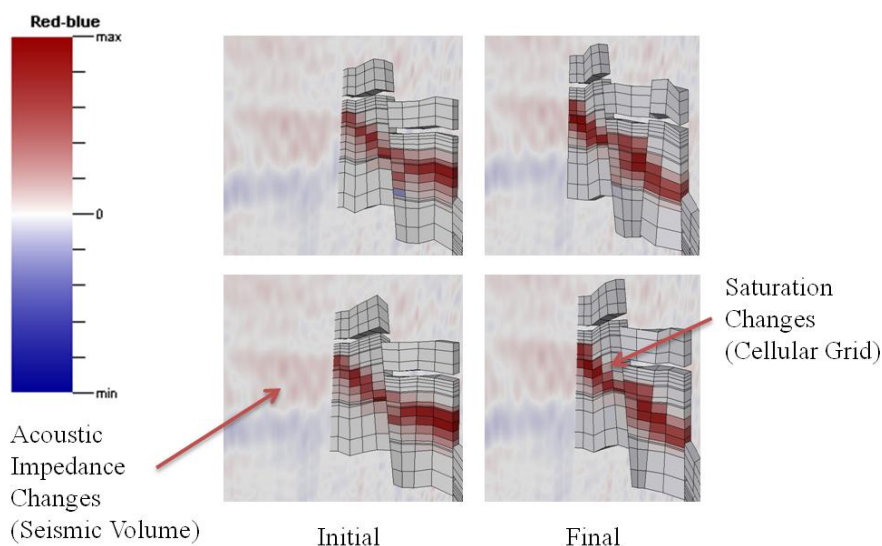
Fig. 3.22—Results of the data calibration procedure, comparison of the water saturation changes in the reservoir grid to the positive changes of acoustic impedance in the seismic volume.

In **Fig. 3.23** we have averaged the changes in acoustic impedance over the interval between layers five and nine, and also separately between layers eleven and thirteen. It is observed that the majority of negative changes are located in the area affected by

compaction. These areas experience a reduction in acoustic impedance, located especially in areas that are fully saturated with water. The reason for this reduction in the bulk modulus is not related to changes in the saturation at those cells, but rather by changes in the average pressure over that area. We have to emphasize that neither our sensitivities nor the rock physics model are capable of capturing this reduction in the acoustic impedance related to changes in field pressure thus we will concentrate in the positive changes.

In previous history matching exercises (Osdal et al., 2006; El Ouair et al., 2005), researchers have used inverted 4D seismic data in the form of changes in acoustic impedance over the production interval. After assisted history matching of the well responses and 4D seismic data, they concluded that the vast majority of the observable changes in acoustic impedance over the E segment were related to replacement of the oil by water. This makes our results consistent with those available in the literature. Furthermore, we can conclude that with the limited effect of gas replacing oil or water in the E segment, any reduction in the acoustic impedance must be related to changes in the formation pressure. Reconciling the model to the pressure effects involves the calibration of larger global parameters that are more related with the energy and compartmentalization of the reservoir. The calibrated parameter along this exercise is the permeability field which does not have a significant impact on the field pressure (Yin et al, 2010).

Finally we want to assess the quality of our history match measured at the well level. **Fig. 3.24** shows the responses for the water, oil and gas production rates before and after the calibration procedure. The observed response of the field is also included. A careful look at the rates before and after calibration highlights the improvement over the match quality achieved by our automated history matching algorithm.
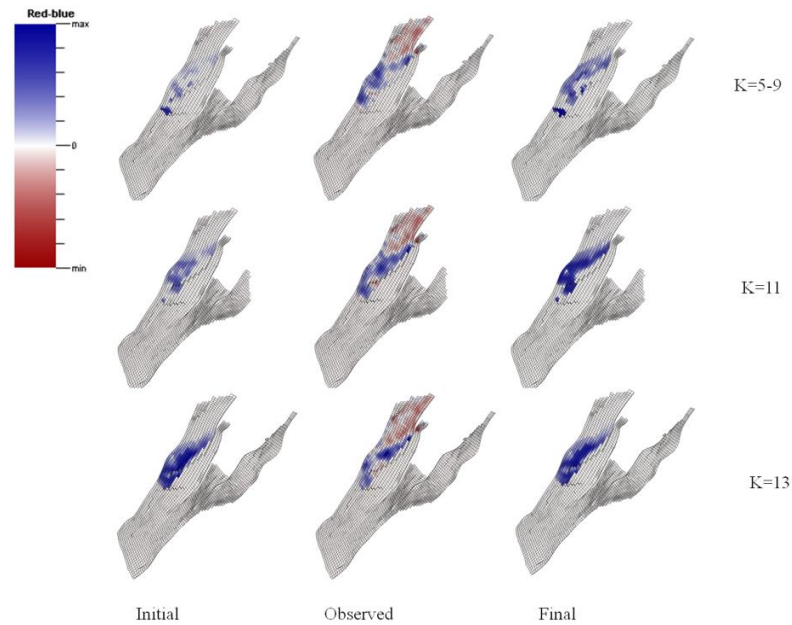
Fig. 3.23—Changes in acoustic impedance in a layer by layer basis for the initial, observed and the calibrated model.
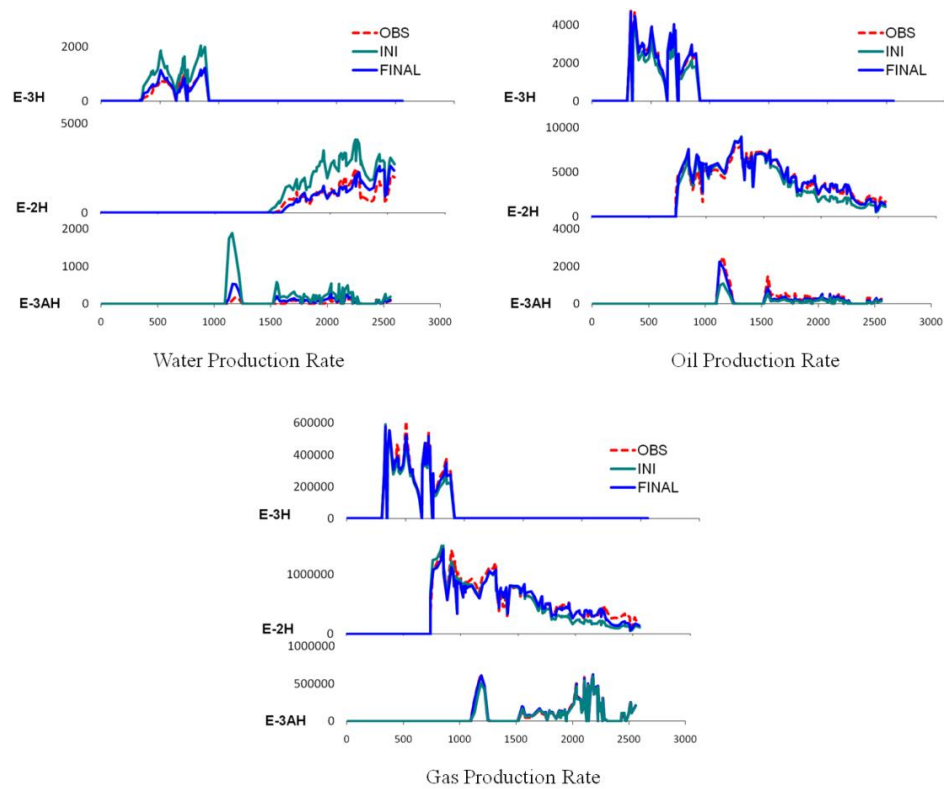
Fig. 3.24—Final response at the well levels after data calibration.

3.5. Chapter Summary

We have developed an efficient approach for the model calibration using 4D seismic and production data in high resolution models. The algorithm is able to reconcile the model with different data types such as changes in acoustic impedance or fluid saturation. The technique is based on a deterministic procedure for the minimization of an objective function that can include seismic and production data simultaneously using a gradient-based minimization that utilize streamline derived sensitivities of production and seismic responses with respect to continuous reservoir parameters.

Through the use of synthetic examples we have shown the value of the seismic data to calibrate reservoir models. This is especially evident in cases that are free of noise and there are no additional levels of non-linearity between the seismic data and the states predicted by the reservoir simulator. In some idealized cases the seismic data integration algorithm was able to calibrate the well responses. We have also shown the impact of the noise in the seismic data reflected in some deterioration in the match quality at the well; nonetheless, our algorithm is able to reproduce the main features observed in the seismic data.

A notable advantage of our technique is the efficiency in the computation of sensitivities, making our algorithms particulary suitable for large field applications and complex geological descriptions. Additionally, we have demonstrated that our algorithm is capable of representing complex dynamic evolution. Our field scale synthetic application has exhibited improvement in the representation of the water phase front and in the production responses for some wells. We have also performed the inversion procedure using simultaneously the seismic and production data, successfully matching the front evolution and the fractional flow responses. Upon calibration of the underlying heterogeneity, we have investigated the effects of incorporating the dynamic data in the estimation of the drainage volume.

The power of our proposed methodology was finally demonstrated through the application to the E-sector of the Norne field. The algorithm was able to improve the positive changes in the acoustic impedance, fine tuning the vertical estimation of the water oil contact and improving the vertical location of the water front. The automatic history matching algorithm in combination with good engineering judgment (understanding the benefits and limitation of our proposed techniques), shows promising results to exploit the benefits of the 4D seismic data for quantitative calibration of reservoir models.

CHAPTER IV

USE OF TIME-LAPSE SEISMIC DATA FOR HETEROGENEITY
CHARACTERIZATION DURING CO2 SEQUESTRATION IN SALINE AQUIFERS[*]

The effects of heterogeneity in Carbon Capture and Storage (CCS) in saline aquifers have been investigated extensively and are known to have important bearings on the storage capacity of the aquifer. In CCS projects, the time-lapse seismic survey has been proposed as a valuable tool for monitoring of CO2 movement. However, the potential of the time-lapse seismic data for heterogeneity characterization and geologic model updating has not been fully explored. One of the biggest challenges in the quantitative use of time-lapse seismic data during CCS is the complex movement of the CO2 influenced by compositional effects, geochemical reactions, phase changes and gravity segregation.

In this work, we first introduce compositional streamlines to understand and visualize the flow and transport of CO2 in the presence of mineral precipitation/dissolution, residual trapping and buoyancy effects. To start with, individual component fluxes are generated by a finite difference fully implicit compositional simulator incorporating all the relevant physics of CO2 sequestration. The fluxes are then utilized in novel streamline tracing algorithms to generate phase and component streamlines depicting the movement and the trapping of CO2 in the aquifer. Next, we utilize the compositional streamlines to determine the sensitivity of the time-lapse seismic attributes specifically, interpreted saturation differences, to changes in reservoir properties such as permeability

and porosity. The sensitivities are then used in an inverse modeling algorithm to calibrate the geologic model to time-lapse seismic data. The outcome is an improved description of permeability heterogeneity that is consistent with the 4-D seismic response and improved predictions of the CO_2 storage capacity.

We have investigated the benefits of time-lapse seismic data integration in improving the performance assessment of CO_2 sequestration using examples involving CO_2 injection under realistic conditions. The first example examines the value of the 4-D seismic data integration in the estimation of storage capacity. The second example systematically studies the impact of viscous to gravity ratio on the performance of time-lapse seismic monitoring and heterogeneity characterization during CCS.

4.1. Chapter Introduction

Carbon sequestration in brine aquifers faces many different challenges in both engineering and economical aspects. There are several sources of uncertainties associated with the injection of CO_2 in deep saline aquifers. Engineering problems such as the leakage of CO_2 can compromise the integrity of fresh waters, ecosystems and the health of populations exposed to high concentration of CO_2 (Ha-Duong and Keith, 2003; Gasda et al., 2004). There are also economic threats associated with legal disputes and fines imposed by regulatory agencies.

Monitoring, verification and accounting (MVA) are the activities directed to determine the location of the injected CO_2 and the presence of possible leaks in order to provide public assurance. Many techniques have been developed for monitoring the performance of CO_2 injection projects and the migration of CO_2 in geologic formations. Time lapse seismic surveillance data is one of the most mature and effective techniques for monitoring changes in the fluid saturation and pressure and has been extensively used by the oil industry.

The viability of time lapse seismic data as a monitoring tool has been investigated in laboratory and field experiments (Wang and Nur 1986; Wang 1997; Korneev et al 2004; Hovorka et al 2006; Daley et al 2008). The characteristics of seismic responses under the complex compositional and geochemical interactions of the injected CO2 in geologic formations have been modeled by Kumar et al. (2008). Also, the effectiveness of traditional rock physics models to invert the seismic responses into changes in the acoustic impedance of the rock during CO2 sequestration has been investigated by Vanorio et al. (2010).

In petroleum reservoir characterization, the time lapse seismic data has been a valuable source of information to calibrate reservoir models using automatic history matching procedures. Because of the high spatial density, seismic data can help estimate and constrain reservoir properties beyond the wells. For example, time lapse observations have been used to infer reservoir properties such as porosity and permeability during reservoir characterization (Huang et al, 1997; Vasco et al., 2004; Dong and Oliver, 2005).

There are many previous studies related to the integration of seismic data for calibrating reservoir simulation models. Huang and Kelkar (1996) integrated production and seismic data using the simulated annealing method to improve history matching. Landa and Horne (1997) used 4D seismic data to calibrate reservoir models to production data by changing porosity and permeability. Waggoner et al. (2003) used seismic history matching to incorporate 4D seismic data for a gas condensate reservoir in the Gulf of Mexico. Their objective was to match acoustic impedance by using a rock physics model. Input to the rock physics model e.g. porosity and saturation were changed to calibrate reservoir models to production data. Kretz et. al (2004) used a gradual deformation of petro-physical properties to calibrate reservoir flow model with 4D seismic data.

Fanchi (2003) used Han-Eberhart-Phillips petro-physical algorithm which is an extension of the Gassmann model to generate seismic attributes from flow simulation. The rapid generation of seismic attributes (P- impendence) helped compare observed seismic data with the simulated seismic data. Yamamoto et al. (2004) used 4D seismic survey to monitor a CO2 miscible injection in the Weyburn field, Canada. They also used the seismic data to characterize the reservoir and calibrate the flow model to production and P-impendence data. A joint objective function incorporating normalized P-impendence and production data was used to quantify the data misfit during the history matching process.

Among the many available techniques developed for history matching time lapse seismic responses, the approach proposed by Vasco et al. (2004) offers great promise to overcome the challenges of large field applications and complex geologic descriptions. This technique utilizes a trajectory based approach that takes advantage of the streamlines associated with fluid flows and semi-analytic solutions of the transport equations along streamlines. The fluid saturation is related to a self-similar variable that allows for calculation of the parameter sensitivities using a single forward simulation. The parameter sensitivities relate changes in the time-lapse response because of small changes in reservoir properties and are a crucial part of the seismic data integration procedure. Compared to petroleum-related applications, there are relatively few applications dealing with automatic history matching of time lapse seismic data in CCS projects. The focus of this work is centered on the inversion of the interpreted time lapse seismic responses for quantitative interpretation of the movement of the CO2 plume in the subsurface, specifically in saline aquifers (Chadwick et al, 2005, Chadwick et al, 2010; Delepine et al, 2011). A crucial element in our work is accounting for the gravity segregation of the injected CO2 and the resulting implications on the quantitative interpretation of the time-lapse seismic response.

We present a streamline-based method for 4-D seismic data integration in the presence of gravity segregation as in the case of CO2 sequestration. The method takes advantage of the convective nature of the injection process by linking the location of the CO2 front along streamlines and the aquifer parameters, specifically porosity and permeability. Non-convective processes such as dissolution, precipitation and phase trapping are included in the simulation model and their effects on the distribution of the CO2 plume are fully accounted for using a finite-difference compositional simulator and streamline tracing algorithms that utilizes the phase fluxes from the compositional simulator. Gravity segregation of CO2 plays an important role and the shape of the CO2 plume will be influenced by the competition between the viscous and gravity forces (Stone, 1982; Jenkins, 1984; Nordbotten et al, 2005; Silin et al 2009). Compositional streamlines are used in order to characterize the motion of different phases, and to account for the upward movement of the injected CO2.

The outline of this work is as follows. First, we introduce the general procedure for the seismic data integration into high-resolution aquifer models. We then illustrate the workflow using a two-dimensional synthetic example. This is followed by a review of the mathematical formulations of our proposed technique. We discuss the underlying assumptions of self similarity and the fundamentals of the time-lapse seismic derived sensitivities for propagation of the CO2 front. Next, we introduce the compositional streamline tracing. By utilizing streamline tracing in a compositional finite difference simulator, we are able to incorporate all the relevant physics in the CCS process. The technique is further tested and the results of seismic data integration in a 3-D heterogeneous deep saline aquifer are presented. This application highlights the benefits of calibrating the model with the dynamic time-lapse information to improve the estimate the storage capacity of the aquifer. Finally, we investigate the effect of the gravity segregation on the performance of our proposed approach to characterize the aquifer and infer permeability heterogeneity.

4.2. Approach

In this section we briefly outline the major steps in our approach for integrating time lapse seismic data in CCS projects and illustrate the procedure using a 2D example.

4.2.1. Compositional Flow Simulation of CO2 Sequestration

There are a variety of physical and chemical mechanisms that interact together when modeling the CO2 sequestration process. The CO2 is normally injected under supercritical conditions but depending on the pressure, temperature and salinity of the brine, it can exist either as a gas or liquid phase. The injected CO2 can also initiate a variety of chemical reactions resulting from the acidification of the aquifer brine and precipitate in a solid form of carbonate mineral. Eventually, over a long period of time, mineral precipitation can induce changes in the formation modifying transport properties like porosity and permeability (Kumar et al., 2008). Although CO2 mineralization is the most effective method of CO2 sequestration, it occurs over very long time scales. Other mechanisms by which CO2 is sequestered in the reservoir are structural trapping, residual trapping and dissolution in reservoir brine. Structural trapping of CO2 is dependent on the quality and integrity of the structural seal. This is one of the major uncertainties of CCS projects. Residual trapping is related to immobile phase trapping of CO2 as the CO2 rises up because of buoyancy and travels through the water phase. This residual trapping is dependent on rock-fluid properties such as permeability, relative permeabilities and also the phase behavior of the reservoir fluids and the injected CO2. Dissolution of CO2 in reservoir brine is typically small (about 3–7% by mass) and depends on the salinity of reservoir brine and reservoir pressure and temperature (Leonenko and Keith, 2008). We have used a commercial compositional simulator (Eclipse300TM) with the CO2 sequestration option that allows us to model all of the three above-mentioned mechanisms of CO2 sequestration. The CO2 storage model includes three phases: A CO2 rich phase, a H2O rich phase and a solid phase. The CO2

rich phase is mostly in the gaseous state while H2O-rich phase is mostly in the liquid state. The solid state consists of salts, for example, CaCl2 and NaCl. Phase splitting between CO2 and H2O is modeled after Spycher and Preuss (Spycher et. al, 2003). Salts are present in the liquid as well as the solid phase. All the relevant geochemical reactions arising from the acidification of brine from the injected CO2 and salt precipitation are modeled. Mobility reduction because of solid precipitation is also accounted for. In this work, we have used four components in the compositional simulation which are CO2, H2O, NaCl and CaCl2.

4.2.2. Compositional Streamline Tracing

We have used a compositional finite-difference simulator to model CO2 sequestration in the aquifer. Given the component fluxes from the simulator, we reconstruct the phase fluxes in order to trace the total velocity streamlines relating the CO2 plume movement and the 'time of flight' which is simply the travel time of a neutral tracer along the streamlines (Datta-Gupta and King, 2007). After we compute the time of flight, we can calculate sensitivities of this variable with respect to reservoir parameters. We will discuss the procedure for the compositional streamline tracing and sensitivity computations in more detail in the mathematical model section.

4.2.3. Sensitivity of Time-Lapse Attributes to Reservoir Properties

The streamline methodology to integrate seismic attributes into high resolution models is based on the analytical relationship between the arrival time of a propagating fluid front and the reservoir properties like porosity and permeability (Vasco et al, 2004). Using an asymptotic solution for the propagation of a two phase front, it is possible to find a self similar variable along the characteristic curves that has the property of transforming the spatial domain from an Eulerian representation to a Lagrangian perspective (Vasco and Datta-Gupta, 2001). This technique is very efficient and requires a single forward

simulation to calculate the sensitivities (Vasco, 2004). In this work, we derive analytic sensitivities which are partial derivatives of the time-lapse response with respect to reservoir properties of interest. These sensitivities are an integral part of our proposed methodology.

4.2.4. Inversion Algorithm and Time-lapse Data Integration
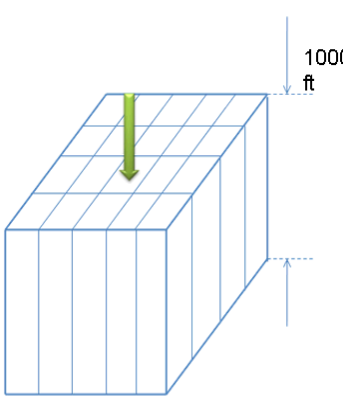
Once the sensitivities are calculated, the data integration is performed utilizing an iterative least squares minimization of the differences in the interpreted saturation of CO2 between two consecutive seismic surveys. To ensure spatial continuity and geologic realism, the misfit function is augmented by additional regularization terms (Yoon et al., 2001.). We assume that the time-lapse seismic data has been inverted and interpreted in terms of saturation differences. Hence, the data misfit is calculated as differences in CO2 saturation between surveys (Feng and Mannseth, 2010).

4.3. Illustration of the Procedure Using a 2D Example

The mathematical details of our formulation will be discussed in the next section. Before that, we first illustrate the major steps in our proposed approach using a two dimensional example. The example consists of a deep saline aquifer with one injector in the center which is perforated all the way through the formation. The geological model consists of a two dimensional 50x50 cellular grid with a lognormal permeability distribution having a north-east direction of continuity (**Fig. 4.1**). The parameters used in the compositional simulation are given in Table 1 representing 2D model of an aquifer.

The example involves the injection of CO2 generated from a 1000 MW coal power plant. We ensure sufficient injection capacity through transmissibility and pore volume multipliers applied to the periphery of the aquifer model. Because of dissolution of CO2 in the brine, we expect the formation of acids and mineral precipitation. The initial

permeability field used for history matching is shown in **Fig. 4.1** along with the reference permeability field that we will attempt to reproduce using the time-lapse seismic data. The CO2 plume movements for the initial model and the reference model are shown in **Fig. 4.2**. As expected, the difference in the direction of continuity of the permeability field significantly affects the direction of propagation of the CO2 front. **Fig. 4.3** shows the CO2 saturation distribution for the base survey and the second survey after a period of 5 years for both the initial and the reference model. In the same figure, we have also shown the changes in CO2 saturation.

TABLE 1— SIMULATION PARAMETERS FOR COMPOSITIONAL SIMULATION AND THE 2D MODEL OF AQUIFER

Simulation Parameters

Parameter	Value
Aquifer Depth	6000 feet
Thickness	1000 feet
Grid DX / DY	32.808 feet / 32.808 feet
NX / NY / NZ	50 / 50 / 1
Aquifer Temperature	110 Deg. F
Pressure @ 6000 ft	2500 psi
Rate of Injection	45 mmscfd
Maximum BHP Pressure	4000 psi
Water Density	75 lb / ft3
Water Viscosity	1.15 cp @ 2500 psi
Salinity (PPM)	268000

Model of Aquifer

1000 ft

Fig. 4.1—Initial and reference permeability fields for the two dimensional CO2 injection case.
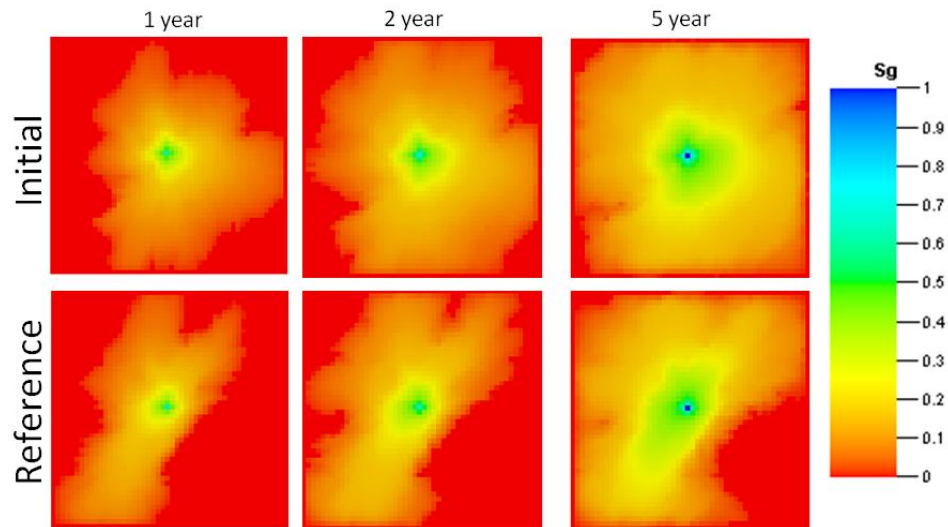
Fig. 4.2—Comparison of the movement of the CO2 plume saturation between the reference model and the initial model.

For inversion purposes, the saturation changes from the reference model are considered to be the data derived from time-lapse seismic surveys and will be used to update the initial permeability distribution. The data misfit consisting of the difference between the observed (from the reference model) and simulated (from the initial model) changes in the saturation front over a period of 5 years is shown in the **Fig. 4.4**. We will use this data in the inversion algorithm in order to calibrate the flow properties viz. permeability.
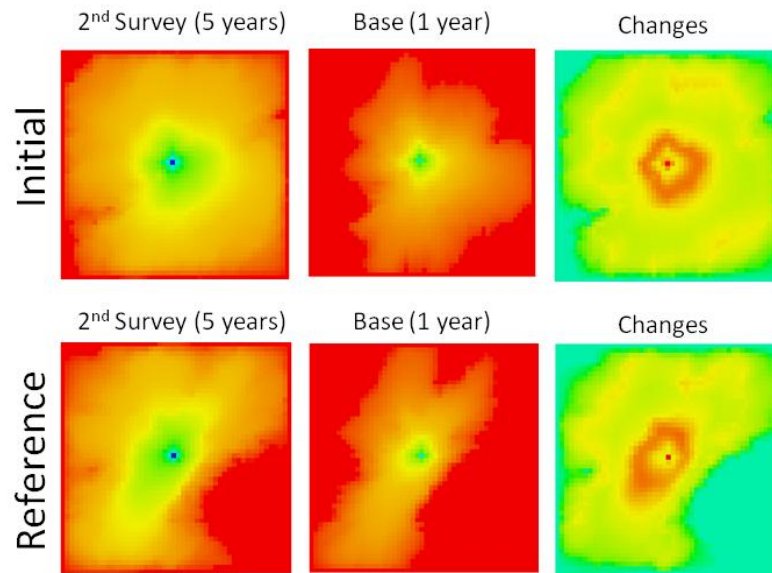
Fig. 4.3—Saturation differences between the surveys acquired after five years of injection and the base survey.

Fig. 4.5 shows the performance of the objective function and the convergence of the inversion algorithm with iterations. The changes in the initial permeability field for various iterations are also seen in this figure. We can see that the final updated permeability field resembles the reference field in many respects. For example, the low permeability barrier in the reference model is now clearly visible. We can conclude that the algorithm is targeting the places where the heterogeneity needs to be adjusted to match the time-lapse saturation differences. Furthermore, majority of the large-scale features present in the reference model are being captured through the inversion process.
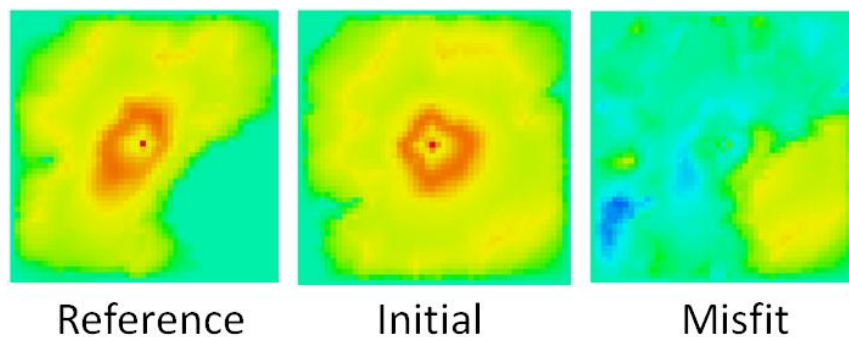
Fig. 4.4—Data misfit between the simulated and observed saturation differences.
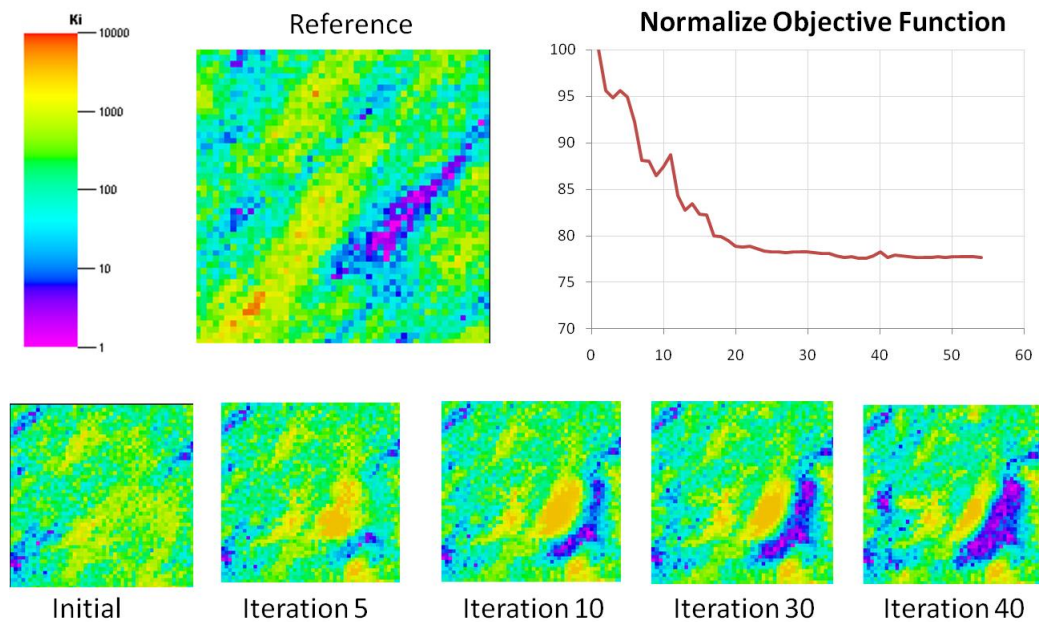
Fig. 4.5—Changes in the initial permeability field at various iteration and objective function performance.

This feature is notable because the permeability heterogeneity has a strong influence on the plume evolution and the capacity of the aquifer to sequester CO2. **Fig. 4.6** shows the changes in the evolution of the plume before and after the data integration. **Fig. 4.7** displays the same evolution using CO2 saturation along the streamlines which form the underlying basis of our inversion approach. It can be clearly seen from both of these figures that the time lapse seismic data integration has been effective in capturing the CO2 plume movement in the reference case.
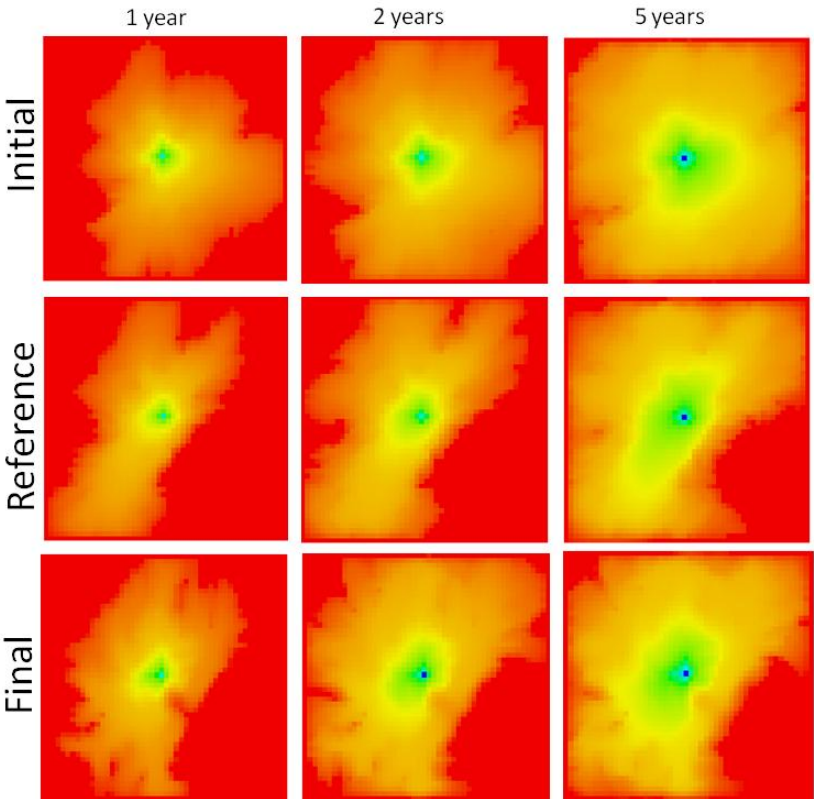
Fig. 4.6—Comparison of gas saturations for initial, observed and final over the years.
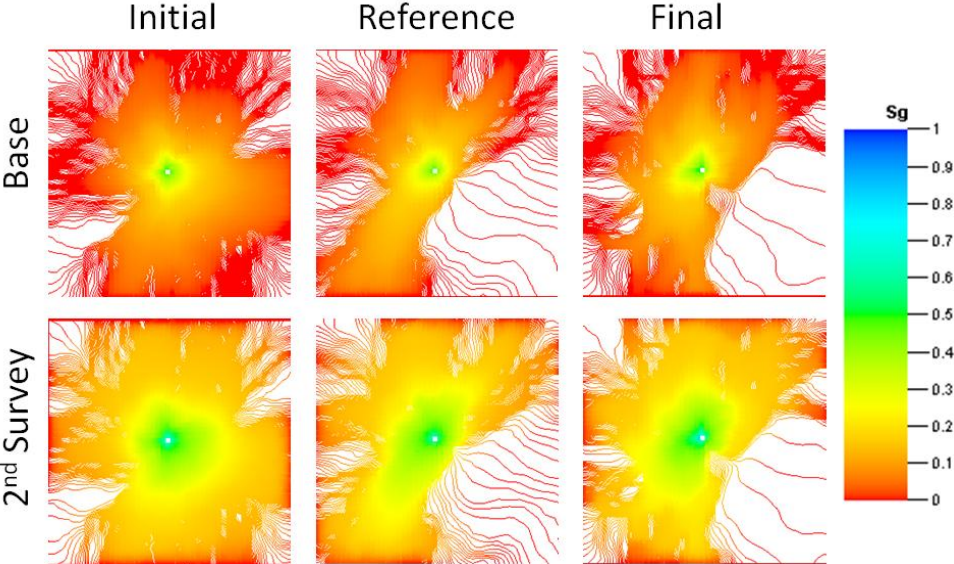
Fig. 4.7—Comparison of gas saturations on streamlines for initial, observed and final cases over the years.

4.4. Mathematical Approach

The advantages of the streamline techniques are related to our ability to efficiently calculate parameter sensitivities utilizing the relationship between the streamline time of flight and reservoir heterogeneity. In this section we will cover the details related to the calculation of sensitivities of CO2 saturation with respect to reservoir parameters such as porosity and permeability, the tracing of streamlines and computing time of flight in compositional simulation and minimization of the objective function for data integration.

4.4.1. Sensitivities of the Time-lapse Saturation Differences

As mentioned before, for modeling CO2 sequestration in the aquifer, we have used a commercial finite-difference simulator that incorporates all the major underlying physical mechanisms. These include the effects of gravity, capillarity, residual trapping and the precipitation and dissolution reactions arising from the acidification of brine. For computing sensitivities of CO2 saturation with respect to reservoir properties, we first define the streamline coordinates based on the fluid fluxes from the finite difference simulator.

We make a few simplifying assumptions for sensitivity calculations. We want to emphasize that these assumptions are limited to sensitivity calculations only and do not apply to the CO2 transport calculations in the finite-difference simulation. These simplifying assumptions allow us to compute the sensitivities analytically leading to significant savings in computation time. The primary assumptions behind the sensitivity calculations are incompressible flow and negligible role of gravity and capillarity between successive updates of the sensitivities. As we will see later, one of the consequences of these assumptions are more frequent updates of streamlines and sensitivity computations when the viscous to gravity ratio is high and there are more rapid changes in the CO2 saturation distribution.

Our sensitivity calculations are based upon a coordinate transformation from physical space to a coordinate system following the flow directions. This transformation is based upon the bi-streamfunctions and an additional time of flight coordinate. We can define a streamline which is everywhere tangential to the velocity field by introducing the following bi-streamfunctions, ψ and χ (Bear, 1988; Datta-Gupta and King, 2007).

$$\vec{u} = \nabla \psi \times \nabla \chi$$ ....(4.1)

A streamline is defined by the intersection of a constant value for ψ with a constant value for χ. For sensitivity computations we are primarily interested in defining the streamline trajectories. The saturations from the finite difference calculations will be mapped along these streamlines in order to relate the saturation changes to the changes in reservoir properties, defining the parameter sensitivities.

An important underlying concept behind our approach is the concept of 'time of flight', τ which is defined simply as the travel time of a neutral tracer along the streamline trajectory r,

$$\tau(x, y, z) = \int_{\Sigma} s(r)dr$$ ....(4.2)

Where the variable $s(r)$ is called the "slowness" and is defined as the reciprocal of the Darcy velocity divided by porosity (Datta-Gupta and King, 2007),

$$s(r) = \frac{\phi(r)}{u_t}$$ ....(4.3)

The main purpose of introducing the time of flight coordinate is that the 3-D spatial gradients assume a very simple form in the streamline time of flight coordinates. Let us now consider the 3-D convective transport equation of CO2 assuming incompressible flow,

$$\phi \frac{\partial S_c}{\partial t} + \vec{u}_t \cdot \nabla F_c = 0$$ ....(4.4)

Where F_c is the fractional flow of CO2. With the introduction of the (τ, ψ, χ) coordinates, we have the following operator identity for transformation from the physical space to the streamline coordinates (Datta-Gupta and King, 2007),

$$\vec{u}_t \bullet \nabla = \phi \frac{\partial}{\partial \tau}$$ ....(4.5)

Convection-driven flow now reduces to one dimensional spatial gradient along streamlines. The governing transport Eq. (4.4) can then be written as,

$$\frac{\partial S_c}{\partial t} + \frac{\partial F_c}{\partial \tau}$$ .... (4.6)

Although our saturation calculations will fully account for gravity effects through the finite difference simulation, for sensitivity computations we will mainly consider the convective part and ignore the effects of gravity during the time interval of sensitivity computations. Eq. (4.6) is invariant with respect to coordinate scaling which indicates the existence of a self-similar variable that can reduce the time-space dependence of the CO2 evolution to a simple ordinary differential equation. Eq. (4.7) describes the functional dependence of the solution along the new variable (Bear, 1988).

$$S_c(\tau, t) = S_c\left(\frac{\tau}{t}\right)$$ .... (4.7)

We can now express a perturbation in the CO2 saturation as a perturbation in the time of flight,

$$\delta S_c\left(\frac{\tau}{t}\right) = \frac{1}{t} S_c{}'\left(\frac{\tau}{t}\right)\delta\tau$$ .... (4.8)

Where

$$S_c{}' = \frac{\partial S_c(\tau/t)}{\partial(\tau/t)}$$ .... (4.9)

Assuming that small changes in the reservoir parameters will not shift the streamline paths (negligible changes in the pressure/velocity field), a perturbation in the time of flight can be written as follows,

$$\delta\tau = \int_\Sigma \delta s(r)dr$$ .... (4.10)

And

$$\partial s(r) = \frac{\partial s}{\partial k}\delta k + \frac{\partial s}{\partial \phi}\delta\phi$$ .... (4.11)

The slowness derivatives are given by the following (Vasco et al., 1999),

$$\frac{\partial s}{\partial k} = -\frac{s(r)}{k}$$ .... (4.12)

And

$$\frac{\partial s}{\partial \phi} = -\frac{s(r)}{\phi}$$ .... (4.13)

Both the slowness and the reservoir properties are available along streamlines and can be readily integrated. The only remaining term in Eq. (4.8) is $S_c{}'$ which is computed by numerical perturbation from the fractional flow relationship.

The sensitivities derived above integrate the convective effects only and are applicable for a limited time interval over which gravity segregation can be considered negligible. However, for time lapse saturation integration we are interested in the saturation evolution over an extended period of time over which gravity and other physical mechanisms will influence the CO2 saturation distribution. To account for these effects, we subdivide the total time period into smaller time intervals for sensitivity calculations. We assume that at any particular time n, the saturation of the CO2 is not only a function of the time of flight and time as given in the self-similar solution, but also the previous states of saturation at time $n-1$,

$$S_c^n(\tau, t, S_c^{n-1}) = S_c^n\left(\frac{\tau}{t}, S_c^{n-1}\right)$$ .... (4.14)

Therefore, a perturbation in the saturation distribution is going to be tied to the historical states of the evolution of the CO2 plume.

$$\delta S_c^n\left(\frac{\tau}{t}, S_c^{n-1}\right) = \frac{1}{t} S_c^{n\prime}\left(\frac{\tau}{t}\right) \delta\tau + \frac{\partial S_c^n}{\partial S_c^{n-1}} \delta S_c^{n-1}\left(\frac{\tau}{t}, S_c^{n-2}\right)$$ .... (4.15)

Based upon on the magnitude of the transverse effects from gravity, we may need to consider a smaller time interval and consequently an increased number of perturbations throughout the different states from the time n up to the time n_o which is the initial time

for the CO2 injection or the previous seismic survey time. This leads to the following repeated application.

$$\delta S_c^n\left(\frac{\tau}{t}, S_c^{n-1}\right) = \frac{1}{t} S_c^{n'}\left(\frac{\tau}{t}\right)\delta\tau + \frac{\partial S_c^n}{\partial S_c^{n-1}}\left(\cdots + \frac{\partial S_c^1}{\partial S_c^0}\delta S_c^0\left(\frac{\tau}{t}\right)\right)$$ .... (4.16)

In our implementation, we assume that the successive changes in saturations between two time intervals do not differ significantly i.e. $\left(\partial S_c^n / \partial S_c^{n-1}\right) \cong 1$. This avoids saving of saturation from previous time intervals and leads to considerable savings in computation time and storage. The sensitivity expression now takes the simplified form given by,

$$\delta S_c^n\left(\frac{\tau}{t}, S_c^{n-1}\right) = \sum_{t=n_0}^{n}\left(\frac{1}{t} S_c{}'\left(\frac{\tau}{t}\right)\delta\tau\right)_t$$ .... (4.17)

4.4.2. Compositional Streamline Tracing

Streamline trajectories form the underlying basis for the sensitivity calculations described above. The CO2 saturation sensitivities are defined as 1-D integrals along streamlines. In this section, we briefly describe the tracing of streamlines in compositional modeling of CO2 sequestration. The streamline tracing is carried out using the extended Pollock (1988) approach proposed by Jimenez et al. (2007) for corner-point cells using iso-parametric transformation from the physical coordinate (x,y,z) to the unit cube coordinates (α, β, γ). This approach has two important elements: First the volumetric flux, rather than velocity, is interpolated within the grid-cell; second, the Jacobian of transformation $J(\alpha, \beta, \gamma)$ to the unit cube, instead cell volume, is used to relate volumetric flux and velocity.

Jimenez et al, (2007, 2010) used a pseudo time of flight, T for simplifying the streamline tracing method so that time of flight can be calculated by rigorously accounting for the spatially varying Jacobian within the corner point cell. The pseudo time of flight is defined as follows:

$$dT = \frac{1}{\phi} \frac{d\tau}{J(\alpha,\beta,\gamma)} = \frac{d\alpha}{dQ_1(\alpha)} = \frac{d\beta}{dQ_2(\beta)} = \frac{d\gamma}{dQ_3(\gamma)}$$ .... (4.18)

Where Q_1, Q_2, Q_3 are the volumetric fluxes in the x, y, z directions respectively.

The streamline trajectories are obtained by integrating the above equation in all three directions. For example, the integral in the α direction is given as follows:

$$\int_0^{T_E} dT = \int_{\alpha_0}^{\alpha} \left(\frac{d\alpha}{dQ_1(\alpha)} \right) = \int_{\alpha_0}^{\alpha} \left(\frac{d\alpha}{\alpha_1 + c_1\alpha} \right)$$ .... (4.19)

Solving the above integral we get:

$$T_E = \frac{1}{c_1} \ln\left(\frac{a_1 + c_1\alpha}{a_1 + c_1\alpha_0} \right)$$ .... (4.20)

Identical constructions will arise for the β and γ directions. The actual pseudo time of flight T is given by the minimum over allowable edges (Jimenez et al., 2007).

$$\Delta T = Min \ Positive \left(\Delta T_E, \Delta T_W, \Delta T_F, \Delta T_B, \Delta T_T, \Delta T_B \right)$$ .... (4.21)

Once the pseudo time of flight T is known, the exit coordinate of the particle can be easily calculated. For example, by rearranging Eq. (4.20), we can get the α coordinate of the exit point,

$$\alpha_e = \alpha_0 + (\alpha_1 + \alpha_0 c_1)\left(\frac{e^{c_1 T} - 1}{c_1}\right)$$ .... (4.22)

Knowing the unit space coordinates (α, β, γ), we can use tri-linear interpolation to transform the unit coordinates into the physical space (Jimenez et al., 2007). The last step is to convert pseudo time of flight T to the actual time of flight τ. This is given by the following integral,

$$\tau = \phi \int_0^T J(\alpha(T), \beta(T), \gamma(T)) dT$$ .... (4.23)

As mentioned before, we have used a compositional simulator for modeling CO2 sequestration. Compositional simulators typically provide the flux of individual components in different phases. The flow rate of component 'c' embedded in the phase p into cell 'i' from the neighboring cell 'n' i.e. Q_{Pni}^c is given as follows (Eclipse300TM)

$$Q_{Pni}^c = T_{ni}(M_p^c) dP_{Pni}$$ .... (4.24)

Where T_{ni} is the transmissibility between the cells, dP_{Pni} is the potential difference and M_p^c is the generalized mobility of component c in the phase p given as

$$M_p^c = x_p^c k_{rp}(S_p)\frac{b_p^m}{\mu_p}$$ .... (4.25)

Where the fluid mobility M_p^c is evaluated in the upstream cell for each phase separately.

Eq. (4.24) and Eq. (4.25) are used for tracking component c in phase p. So, for tracking a particular component, the component flux in all the phases is summed up. For phase tracking, the fluxes of all the components are summed up for that particular phase. The streamlines are traced based on total fluxes (sum of all phase fluxes) leading to continuous trajectories.

4.4.3. Seismic Data Integration

We perform the data integration using a deterministic approach in which we minimize a penalized misfit function composed of the seismic data misfit and additional regularization terms. The regularization terms consist of a 'norm' constraint and a 'roughness' constraint and are introduced to preserve the spatial continuity and the geological realism in the updated model. Thus, the model calibration is a trade-off whereby we want to reduce the data misfit (within some specific tolerance) while minimizing the changes to the prior model to maintain geologic consistency. The penalized misfit function $F(\delta R)$ is defined as follows:

$$F(\delta R) = \|\delta d - G\delta R\| + \beta_1\|\delta R\| + \beta_2\|L\delta R\| \quad (4.26)$$

In Eq. (4.26) δd is the vector of the misfit between the seismically-derived saturation differences and the simulated saturation differences. Also, G is the sensitivity matrix containing the partial derivatives of the changes in saturation of CO_2 with respect to the reservoir parameters viz. grid-block permeabilities. The quantity δR is the vector of changes in the reservoir property. In Eq. (4.23) the first penalty term is the 'norm' constraint that minimizes deviation from the prior model. The second penalty term is the

'roughness' constraint. The operator L is a second spatial difference and is analogous to imposing a prior variogram or covariance constraint. (He et al, 2002). The minimum is obtained by an iterative least-square solution of the augmented linear system of equations given by Eq. (4.27)

$$\begin{pmatrix} G \\ \beta_1 I \\ \beta_2 L \end{pmatrix} \delta R = \begin{pmatrix} \delta d \\ 0 \\ 0 \end{pmatrix}$$ .... (4.27)

where the scalars β1 and β2 determine the relative strengths of the 'norm' and 'roughness' constraints. The selection of these weights can be somewhat subjective although there are guidelines in the literature (Parker, 1994). In general, the inversion results will be sensitive to the choice of these weights

4.5. Results and Discussions

In this section we discuss the application of our proposed method to a 3D example. The 3D example is designed to illustrate the effectiveness of the time lapse seismic inversion when there is significant vertical migration of CO_2 arising from gravity segregation. The 3D model consists of 10 layers with 100ft. each and uses the same rock and fluid properties as the 2D model (Table 2). On comparing Table-1 and Table-2, we see that the primary difference between the 2D and the 3D example is the vertical resolution.

As in the 2D example, we impose constant flux boundaries by applying transmissibility and pore volume multipliers to the periphery of the aquifer model. As expected, for the 3D example the injected CO_2 at the center rises vertically because of buoyancy forces. This is clearly visible from the streamline patterns in **Fig. 4.8**. The CO_2 plume rises like a fountain and this movement is very well captured using streamlines derived from the total fluid flux tracing as discussed in the previous section. The fluid fluxes are obtained

from a fully compositional finite difference simulator for CO2 sequestration that includes all the relevant physical and chemical mechanisms. In **Fig. 4.9** we have shown a vertical cross-section displaying CO2 plume migration in the initial and the reference model. It is apparent that the injected CO2 rises vertically very rapidly because of buoyancy. This represents a challenge for seismic inversion as most of the gas saturation changes are predominantly in top layers. This also requires taking smaller time intervals for sensitivity calculations to capture the effects of gravity segregation.

TABLE 2—SIMULATION PARAMETERS FOR COMPOSITIONAL SIMULATION AND THE 3D MODEL OF AQUIFER

Simulation Parameters

Parameter	Value
Aquifer Depth	6000 feet
Thickness	1000 feet
Grid DX / DY	32.808 feet / 32.808 feet
NX / NY / NZ	50 / 50 / 10
Aquifer Temperature	110 Deg. F
Pressure @ 6000 ft	2500 psi
Rate of Injection	45 mmscfd
Maximum BHP Pressure	4000 psi
Water Density	75 lb / ft3
Water Viscosity	1.15 cp @ 2500 psi
Salinity (PPM)	268000

Model of Aquifer

1000 ft

100 ft

After 1 Month   After 2 Months   After 6 Months   After 1 Year
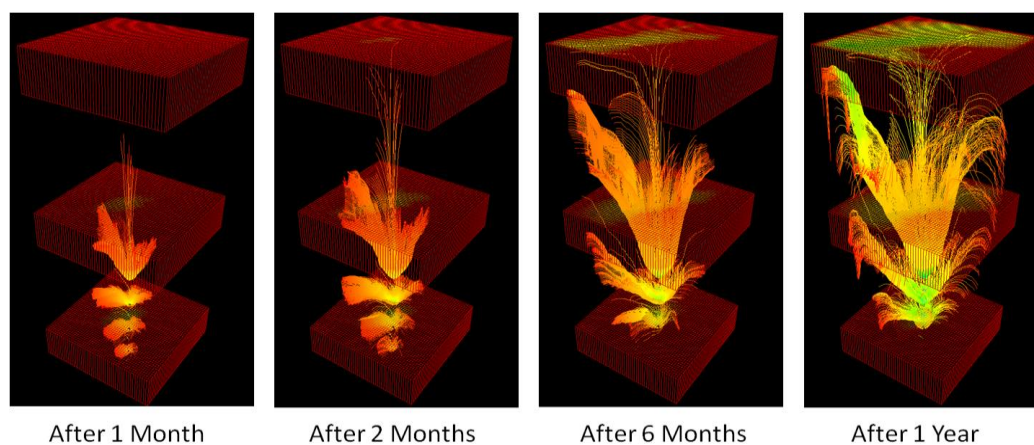
Fig. 4.8—Streamlines showing buoyancy effects of injected CO2.

Fig. 4.10 shows the difference in gas saturation between the initial and the reference cases over a period of 5 years for each of the 10 layers. As expected, majority of the saturation changes are in the top layers (layers 1 through 4). We will use these saturation differences as data misfit in the inversion algorithm in order to calibrate the flow properties, specifically grid block permeabilities in this case.
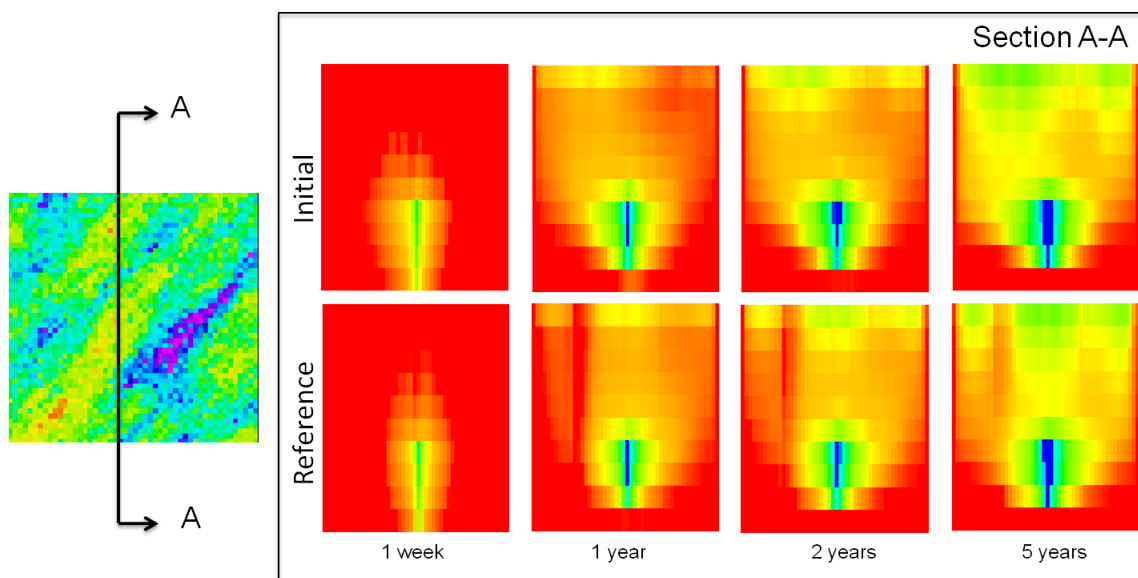
Fig. 4.9—Vertical cross-section showing CO2 plume migrating upwards over the years.

Fig. 4.11 shows the reduction in the data misfit and convergence of the inversion algorithm with iterations. The reference permeability (same in all layers) and the difference between the reference and the initial permeability can also be seen in this figure. Note that the difference represents the changes needed in the initial permeability field for all the layers. **Fig. 4.11** shows the changes to the initial permeability in the top five layers. Recall that the majority of the saturation changes were in the top layers and that is where we mostly expect the permeabilites to change. Comparing **Fig. 4.10** and **Fig. 4.11**, we can see that much of the changes in the initial permeability field are similar to the changes required. Thus, we can conclude that the algorithm is targeting the spatial locations where the heterogeneity needs to be adjusted. Furthermore, we can also see

that some of the large-scale permeability trends present in the reference model are being captured via inversion of the time-lapse saturation changes.
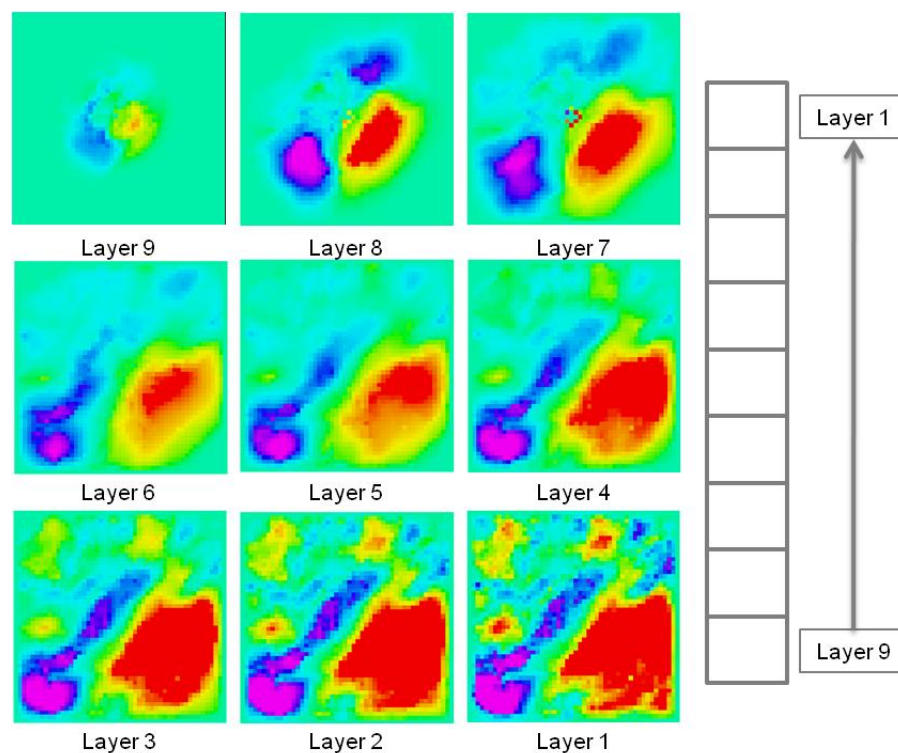
Fig. 4.10—Layerwise gas saturation difference between observed and simulated cases over the years.

Fig. 4.12 shows the changes in the evolution of the CO2 plume before and after the data integration. It can be clearly seen that the time lapse seismic data integration helps in capturing the CO2 plume movement which now better resembles the reference case.
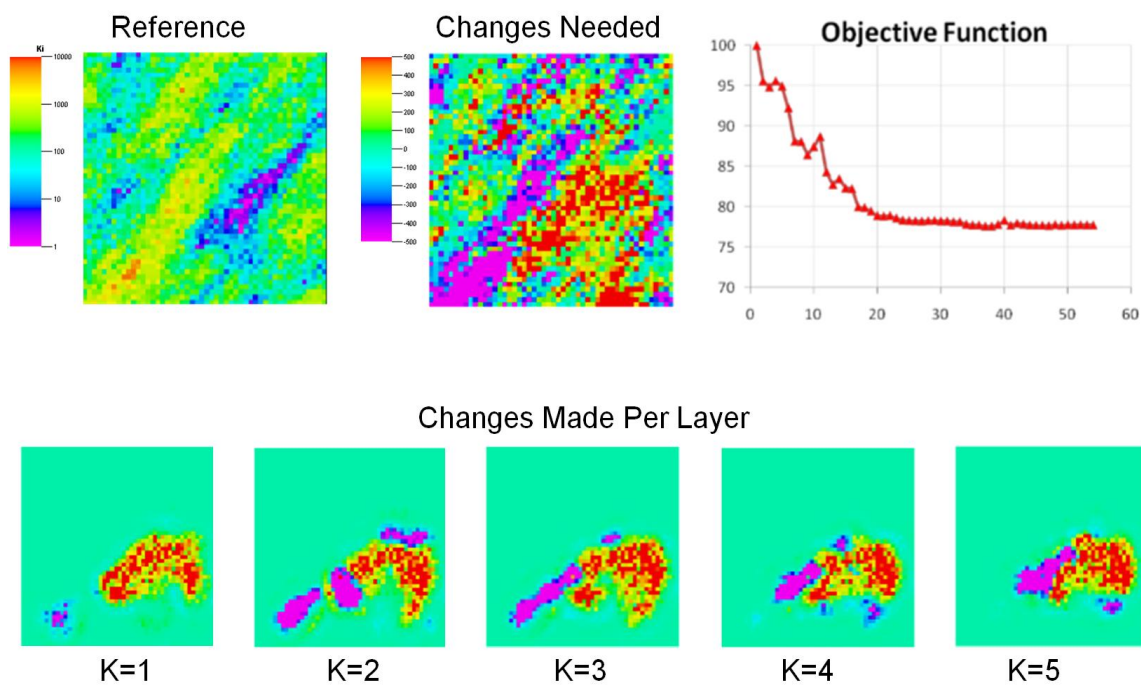
Fig. 4.11—Layer-wise changes made during seismic inversion.
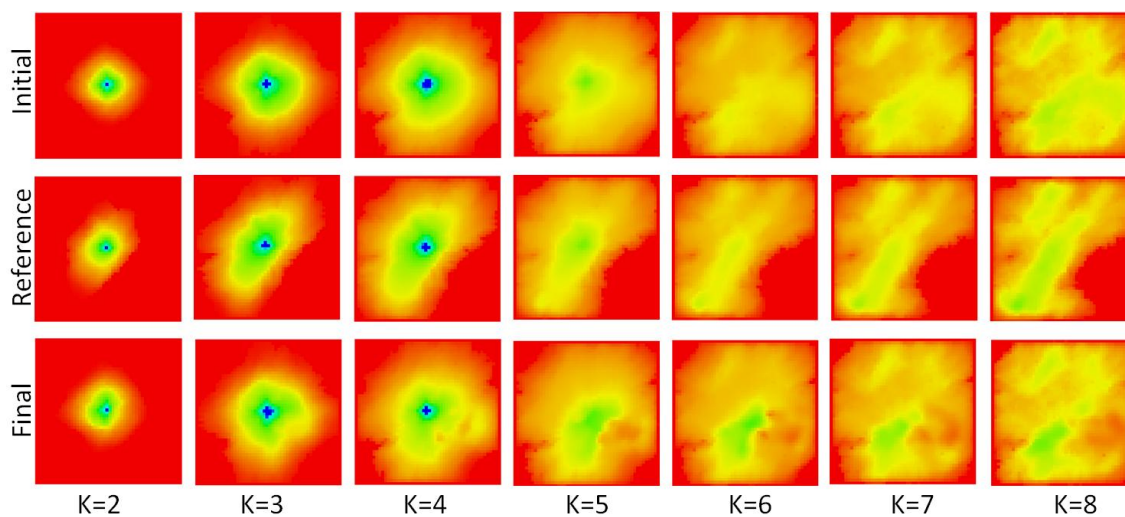
Fig. 4.12—Layer-wise comparison of gas saturations for initial, observed and final cases.

4.5.1. Value Addition in Forecasting the CO2 Sequestration Capacity of the Aquifer

The role of time-lapse seismic data in monitoring of CO2 sequestration has been well-recognized. However, the use of time-lapse data in permeability characterization and improved estimates of CO2 storage capacity has been relatively unexplored. A critical outcome of aquifer model calibration for carbon sequestration and storage is in the improved forecast of how much CO2 can be sequestered in the future. The economics of CCS projects is dependent to a large extent on proper forecasting of CO2 storage capacity.
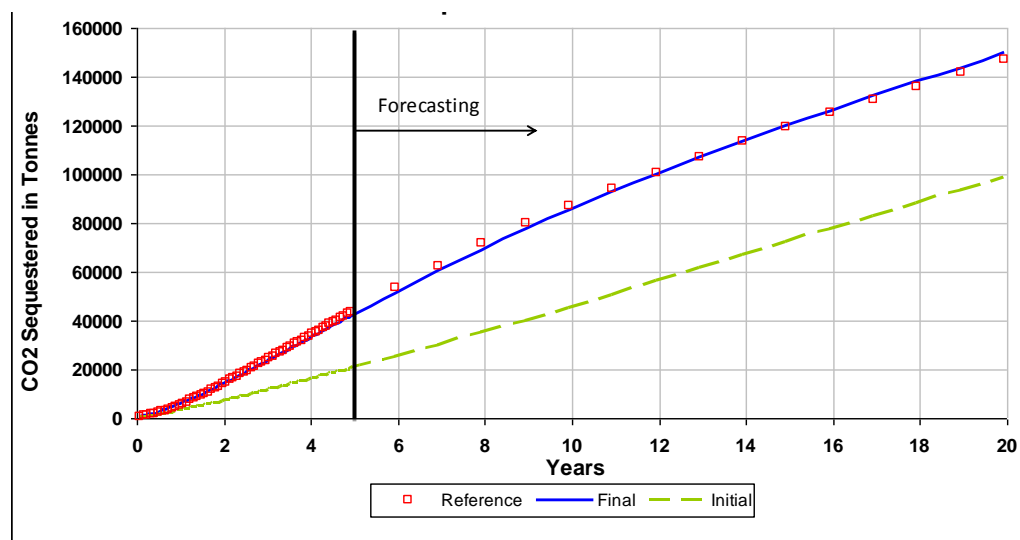
Fig. 4.13—CO2 sequestered with time for initial, observed and final cases over the time.

Fig. 4.13 shows the importance of dynamic model calibration for CCS projects, specifically the utility of time lapse seismic inversion as discussed in this work. As explained before, the time lapse seismic inversion was carried out based on seismic data at the beginning of the project and after five years. We predicted the amount of CO2 sequestered for 15 years with and without the seismic data integration. It can be seen that

amount of CO2 sequestered (dissolved + residually Trapped) is severely under-predicted by initial permeability model as compared to the reference model. This indicates very large discrepancy in the initial model in terms of its dynamic performance compared to the reference model and the importance of model calibration using dynamic data. The updated model after time-lapse seismic inversion shows very good match with the reference model in terms of the amount of CO2 sequestered. The results clearly show the value of time-lapse seismic data integration to improve predictive capabilities of CO2 sequestration models.

4.5.2. Impact of Viscous to Gravity Ratio (VGR) on the Time-lapse Seismic Integration

One of our objectives in this work is to evaluate the effectiveness of time-lapse seismic data in the presence of gravity segregation of the injected CO2. The extent of gravity segregation of CO2 is largely a function of the viscous to gravity ratio defined as follows (Stone (1982); Jenkins (1984)):

$$VGR = \frac{Q_t}{\Delta\rho A k_v \left(\lambda_c + \lambda_w\right)} \dots\dots\dots\dots\dots\dots\dots\dots\dots\dots\dots\dots\dots\dots\dots\dots\dots(4.28)$$

Where A is the cross-section area of injection, λ_c and λ_w are CO2 and water mobilities, respectively, and $\Delta\rho$ is the density difference between CO2 and water.

We have studied the impact of various CO2 injection rates corresponding to different viscous gravity ratios on the performance of the inversion algorithm. The results are shown in **Fig. 4.14**. For all the cases, we have kept a fixed time step interval of 1 year for computing the sensitivity of time-lapse seismic derived saturation differences changes in the permeability distribution. It can be seen that for a fixed time-step, the inversion algorithm converges faster for lower viscous to gravity ratios, i.e., lower injection rates.

For very high VGR, a slower convergence and even an increase in the objective function are seen, indicating that more frequent updating of the sensitivity is required. This is to be expected because of the rapidly changing CO2 saturation and streamline patterns in the cases with high VGR. In general, the higher the change in saturation between two streamline tracing intervals, the more difficult it is for streamlines to accurately describe the relation between the location of the CO2 plume and the changes in the reservoir parameters. Thus, the higher the VGR the, smaller should be the timesteps for our proposed time lapse data integration method so that the movement of CO2 can be captured by streamlines effectively.
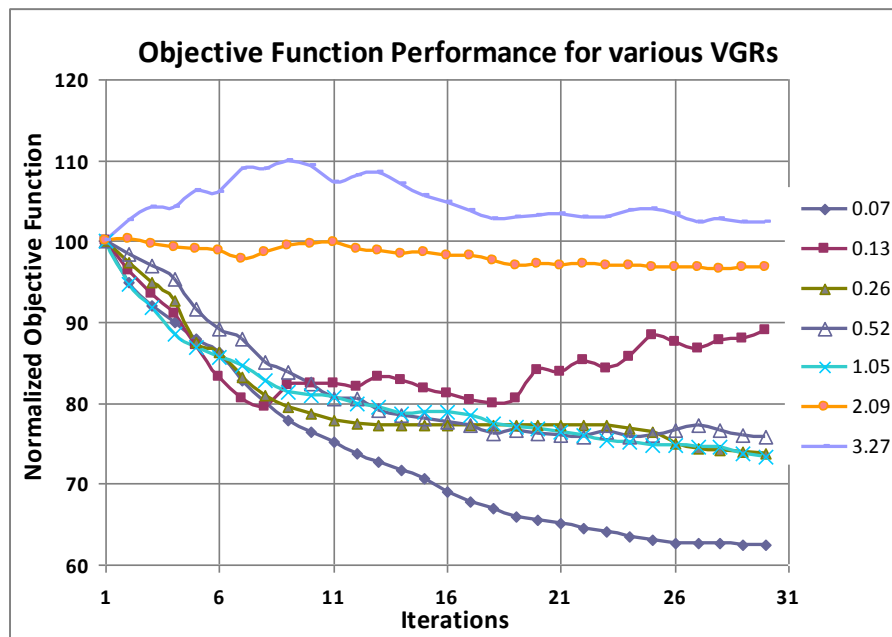
Fig. 4.14—Objective function performance for various viscous gravity ratios using a fixed timestep interval (1 yr).

4.6. Chapter Summary

We have demonstrated the utility of time lapse seismic data integration for aquifer characterization during CCS projects and also for improved predictions of CO2 storage capacity. Specifically, we have shown that the streamline based seismic inversion is

successful in calibrating 3D aquifer models in the presence of gravity segregation of the injected CO2. The streamline-based approach is particularly appealing because of the analytic computation of the sensitivity of time-lapse saturation differences with respect to reservoir properties. This leads to significant savings in computation time and offers great potential in terms of large-scale field applications. Although our forward simulation accounted for all the dominant physical mechanisms, the sensitivity calculations are approximate because of the underlying assumptions. Nevertheless, these approximate sensitivities seem to be adequate for data integration purposes and did not result in any significant convergence issues. We have also shown that streamline based seismic inversion improves the prediction of the amount of CO2 sequestered which can help in the economic planning of carbon sequestration projects. Finally, we have studied the impact of viscous to gravity ratio (VGR) on the performance of the inversion procedure.

CHAPTER V

CONCLUSIONS AND RECOMMENDATIONS

This study develops an integrated approach for model calibration using production and seismic data simultaneously. The technique is based on a deterministic procedure for the minimization of a data misfit cost function, using a gradient-based method where the sensitivity of a reservoir response (e.g., grid cell saturation change, acoustic impedance and fractional flow at a producer) to perturbations in the model parameters is calculated analytically using the streamline geometry and properties. A notable advantage of the technique is the ability to incorporate the dynamic effects of changing field conditions resulting, for example, from infill drilling, alternating drive mechanisms or reservoir management. Another advantage is the flexibility of the sensitivity formulation to different data types. For example, the seismic data can be applied as either changes in water saturation or accoustic impedance, and the data can also contain uncorrelated noise associated with the uncertainty in the geophysical data and inversion. The technique is not limited to black oil models but can also be applied to compositional simulation. Finally, the streamline-based approach is extended in the case of CO2 injection with non-convective effects such as dissolution and precipitation. The algorithm is able to calibrate models with different levels of viscous to gravity forces. In the specific case of CO2 sequestration, the importance of this work is highlighted by the finding that the calibrated heterogeneity significantly impacts the predicted storage capacity of open aquifers.

5.1. Summary

The major findings and concluding remarks of this research are summarized in the following sub-sections.

5.1.1 Production Data Integration

In the established approach of streamline based history matching, the Generalized Travel Time Inversion (GTTI), we have highlighted the limitations of the cross correlation function to calculate the time shift that defines the data misfit term per well. The presence of discontinuities and non-monotonicity in the observed history introduces levels of complexity in the production data that cannot be resolved in the traditional GTTI approach. The presence of such behavior leads to an erroneous estimation of the misfit time and also to a slow convergence rate in the minimization of the cost function. In this study we proposed a re-sampling procedure that preserves the desirable features of the streamline techniques while improving the estimation of the data misfit and the match quality after model calibration. The proposed technique is robust and relatively insensitive to the threshold values used to resample the data. Moreover, the approach retains unique features of streamline models that make them particularly well-suited for production data integration into high resolution geologic models.

The proposed approach is applied to a real field application with active reservoir management and a highly detailed production history, together with well recompletions that frequently change the boundary conditions. The results of the minimization using the proposed approach show a faster convergence rate and an improvement in the match quality on a well by well basis, compare to the traditional GTTI approach. Also, the streamline visualization techniques are proven to be a valuable tool for evaluating the changes introduced to the prior model during calibration to the dynamic data. Finally, the streamline-based dynamic data integration can be applied as a diagnostic tool to evaluate structural uncertainties in the high-resolution geologic model.

5.1.2. Seismic Data Integration

We have developed a streamline based history matching technique that can utilize high resolution areal information from consecutive (i.e., 4D) seismic surveys. The seismic data can be expressed as either the difference in saturation or acoustic impedance derived after a geophysical seismic inversion, both at grid cell resolution. Our approach is able to reproduce the complex dynamic evolution of fluid transport in the reservoir by calibration of a prior high resolution geologic model using efficiently derived seismic sensitivities. We have specifically applied this approach to resolve the location of the water saturation fronts at the cell level, thereby improving the response of the fractional flow at the well level relative to field measurements. The quality of the calibrated model is related to the level of noise associated with the seismic data.

The application of the proposed inversion approach to field cases has demonstrated that the incorporation of the seismic data only can be insufficient to calibrate the responses at the well level. In these cases, seismic data are, therefore, utilized simultaneously with the available production information. An added benefit of the inclusion of seismic data in the inversion is the apparent improvement in the geologic realism of the calibrated heterogeneity even in the cases where the seismic information contains large levels of noise or uncertainty.

5.1.3. Compositional Seismic Data Integration

Seismic data can be a valuable source of data for the calibration of aquifer or reservoir models that simulate CO_2 injection. Time-lapse seismic surveys can be used in order to better estimate the underlying heterogeneity, improving the predictive capability of the model, especially in relation to the CO_2 storage capacity of the reservoirs. The streamline based sensitivity calculation was modified to incorporate non convective effects such as dissolution and precipitation. In order to incorporate transverse effects the

streamline field has to be regenerated more frequently and the multiphase saturations are mapped from the results of a finite difference compositional simulator.

Our approach has demonstrated the relevance of the viscous-gravity ratio in the calibration of the underlying heterogeneity in aquifers under CO2 injection. This reflects the dominance of the gravity forces in the dynamics and evolution of the plume. Despite the complexity and nonlinearity of these processes, the streamline formulation shows promising results, targeting the changes in the calibrated parameter field and reproducing the main features in the reference model.

5.2. Recommendations

The use of seismic data for quantitative calibration of reservoir models is a task of considerable difficulty. Perhaps one of the most challenging steps is the integration of two different disciplines that need to interact for the successful use of the seismic data. Reservoir Engineers and Geophysicists need to work in a collaborative environment with mutual understanding of each other's disciplines. This is of special relevance because the majority of the modern approaches for calibrating the reservoir model with seismic data rely on observation data that are derived as the result of an independent seismic inversion that too suffers, from non-uniqueness and ill-posedness.

Nevertheless, the advantages of incorporating high resolution areal information make the task of identifying new strategies for improvement of the effectiveness of the collaborative work between these two disciplines a worthwhile exercise. The reservoir engineer cannot blindly use the inverted parameters from a seismic volume as observation data without carefully considering the validity and the consequences of this information in terms of reservoir development and management. Thus, the Reservoir Engineer needs to understand the benefits and limitation of 4D seismic data in order to make an effective use of this type of information. Automatic history matching routines

like the ones proposed in this thesis are essential to bridge the gap between these disciplines. They empower the engineer with tools that assist the history matching procedure and are useful for critical evaluation of the reservoir heterogeneity and flow dynamics.

Even with the benefits of our techniques in terms of speed and minimal targeted changes in the reservoir model, the user must be aware of the limitations and simplifications related to our proposed approaches. We need to develop a better understanding of the vertical resolution of seismic information and the effects of upscaling or downscaling, in both the vertical and horizontal orientations, required for compatibility of the seismic grid with the resolution of the reservoir simulator. While we have included the effects of the pressure changes in the time lapse seismic inverted attributes, our technique is limited to a convective phenomena characterized by a sharp interface in a slowly changing background saturation. Furthermore, even when the effects of gravity segregation and dissolution were successfully treated, they were limited to a predominantly two phase system. There is still critical research required for a more complete understanding of the dynamics, interactions and influence of multiple phases on acoustic impedance signatures, and other related seismic attributes.

REFERENCES

Arenas, E., Kruijsdijk, V. and Oldenziel, T. 2001. Semi-automatic history matching using the pilot point method including time-lapse seismic data. Presented at the SPE Annual Technical Conference and Exhibition, New Orleans, 30 September - 3 October. doi:10.2118/71634-MS.

Arts, R., Brevik, I., Eiken, O., Sollie, R., Causse, E. and Van Der Meer, B. 2000. Geophysical methods for monitoring marine aquifer CO_2 storage–Sleipner experiences. Presented at the 5 th International Conference on Greenhouse Gas Control Technologies, Cairns, Australia, August 2000.

Bear, J. 1988. *Dynamics of fluids in porous media*. New York: Dover Publications.

Behrens, R., Condon, P., Haworth, W., Bergeron, M., Wang, Z. and Ecker, C. 2002. 4D seismic monitoring of water influx at bay marchand: The practical use of 4D in an imperfect world. *SPE Reservoir Evaluation and Engineering* **5** (5): 410-20. SPE 79961-PA. doi: 10.2118/79961-PA.

Behrens, R., MacLeod, M., Tran, T. and Alimi, A. 1998. Incorporating seismic attribute maps in 3D reservoir models. *SPE Reservoir Evaluation & Engineering* **1** (2): 122-6. SPE 36499-PA. doi: 10.2118/36499-PA.

Brun, B., Gosselin, O. and Barker, J. 2001. Use of prior information in gradient-based history-matching. Presented at the SPE Reservoir Simulation Symposium, Houston, Texas, 11-14 February. doi: 10.2118/66353-MS.

Chadwick, A., Williams, G., Delepine, N., Clochard, V., Labat, K., Sturton, S., Buddensiek, M.L., Dillen, M., Nickel, M. and Lima, A.L. 2010. Quantitative analysis of time-lapse seismic monitoring data at the Sleipner CO_2 storage operation. *The Leading Edge* **29** (2): 170-7. doi: 10.1190/1.3304820.

Chadwick, R.A., Arts, R. and Eiken, O. 2005. 4D seismic quantification of a growing CO_2 plume at Sleipner, North Sea. *Geological Society, London, Petroleum Geology Conference series* **6**: 1385-99. doi: 10.1144/0061385.

Cheng, H., Datta-Gupta, A. and He, Z. 2005a. A comparison of travel-time and amplitude matching for field-scale production-data integration: Sensitivity, nonlinearity, and practical implications. *SPE J* **10** (1): 75-90. SPE 84570-PA doi: 10.2118/84570-PA.

Cheng, H., Kharghoria, A., He, Z. and Datta-Gupta, A. 2005b. Fast history matching of finite-difference models using streamline-based sensitivities. *SPE Reservoir Evaluation & Engineering* **8** (5): 426-36. SPE 89447-PA. doi: 10.2118/89447-PA.

Cheng, H., Oyerinde, A., Datta-Gupta, A. and Milliken, W. 2007. Compressible streamlines and three-phase history matching. *SPE Journal* **12** (4): 475-85. SPE 99465-PA. doi: 10.2118/99465-PA.

Cheng, H., Wen, X.H., Milliken, W.J. and Datta-Gupta, A. 2004. Field experiences with assisted and automatic history matching using streamline models. Presented at the SPE Annual Technical Conference and Exhibition, Houston, Texas, 26-29 September. doi: 10.2118/89857-MS.

Clifford, P., Robert, T., Parr, R., Moulds, T., Tim, C., Allan, P. and Phil, S. 2003. Integration of 4D seismic data into the management of oil reservoirs with horizontal wells between fluid contacts. Presented at the Offshore Europe Conference, Aberdeen, United Kingdom, 2-5 September. doi:10.2118/83956-MS.

Cooper, M., Westwater, P., Thorogood, E., Kristiansen, P. and Christie, P. 2005. Foinaven active reservoir management: Towed streamer and buried sea - bed detectors in deep water for 4D seismic. *SEG Technical Program Expanded Abstracts* **18** (1): 1632-5. doi: 10.1190/1.1820841.

Dadashpour, M., Kleppe, J. and Landro, M. 2007. Porosity and permeability estimation by gradient based history matching using time-lapse seismic data. Presented at the SPE Middle East Oil and Gas Show and Conference, Kingdom of Bahrain, 11-14 March. doi:10.2118/104519-MS.

Daley, T.M., Myer, L.R., Peterson, J.E., Majer, E.L. and Hoversten, G.M. 2008. Time-lapse crosswell seismic and VSP monitoring of injected CO_2 in a brine aquifer. *Environmental Geology* **54** (8): 1657-65. doi: 10.1007/s00254-007-0943-z.

Datta-Gupta, A. and King, M. 2007. *Streamline simulation: Theory and practice*, 11th edition. Richardson, Texas: Society of Petroleum Engineers.

Datta-Gupta, A., Kulkarni, K.N., Yoon, S. and Vasco, D.W. 2001. Streamlines, ray tracing and production tomography: Generalization to compressible flow. *Petroleum Geoscience, 7, SUPP* **7** (SP1): S75-86.

Datta-Gupta, A., Seongsik, Y., Barman, I. and Vasco, D.W. 1998. Streamline-based production-data integration into high-resolution reservoir models. *Journal of Petroleum Technology* **50** (12): 72-6.

Delépine, N., Clochard, V., Labat, K. and Ricarte, P. 2011. Post-stack stratigraphic inversion workflow applied to carbon dioxide storage: Application to the saline aquifer of Sleipner field. *Geophysical Prospecting* **59**: 132-44. doi: 10.1111/j.1365-2478.2010.00905.x.

Dong, Y. and Oliver, D. 2005. Quantitative use of 4D seismic data for reservoir description. *SPE Journal* **10** (1): 91-9. SPE 84571-PA doi: 10.2118/84571-PA.

Eastwood, J., Lebel, P., Dilay, A. and Blakeslee, S. 1994. Seismic monitoring of steam-based recovery of bitumen. *Leading Edge* **13** (4): 242-51.

El Ouair, Y., Lygren, M., Osdal, B., Husby, O. and Springer, M. 2005. Integrated reservoir management approach: From time-lapse acquisition to reservoir model Update at the Norne Field. Presented at the International Petroleum Technology Conference, 21-23 November. doi:10.2523/10894-MS.

Fahimuddin, A., Aanonsen, S. and Skjervheim, J.A. 2010. 4D seismic history matching of a real field case with enkf: Use of local analysis for model updating. Presented at the SPE Annual Technical Conference and Exhibition, Florence, Italy, 19-22 September. doi:10.2118/134894-MS.

Falcone, G., Gosselin, O., Maire, F., Marrauld, J. and Zhakupov, M. 2004. Petroelastic modelling as key element of 4D history matching: A field example. Presented at the SPE Annual Technical Conference and Exhibition, Houston, Texas, 26-29 September. doi:10.2118/90466-MS.

Fanchi, J.R. 2001. Time-lapse seismic monitoring in reservoir management. *The Leading Edge* **20** (10): 1140-7. doi: 10.1190/1.1487246.

Fanchi, J.R. 2003. The Han - Eberhart - Phillips model and integrated flow modeling. *Geophysics* **68** (2): 574-6. doi: 10.1190/1.1567227.

Feng, T. and Mannseth, T. 2010. Impact of time-lapse seismic data for permeability estimation. *Computational Geosciences* **14** (4): 705-19. doi: 10.1007/s10596-010-9182-6.

Foster, D. 2007. The BP 4D story: Experience over the last 10 years and current trends. Presented at the International Petroleum Technology Conference, Dubai, U.A.E., 4-6 December. doi:10.2523/11757-MS.

Gasda, S.E., Bachu, S. and Celia, M.A. 2004. Spatial characterization of the location of potentially leaky wells penetrating a deep saline aquifer in a mature sedimentary basin. *Environmental Geology* **46** (6): 707-20. doi: 10.1007/s00254-004-1073-5.

Gassmann, F. 1951. Elastic waves through a packing of spheres. *Geophysics* **16** (4): 673-85. doi: 10.1190/1.1437718.

Gill, P.E., Murray, W. and Wright, M.H. 1981. *Practical optimization*, 1st edition. London: Academic Press.

Gosselin, O., Aanonsen, S., Aavatsmark, I., Cominelli, A., Gonard, R., Kolasinski, M., Ferdinandi, F., Kovacic, L. and Neylon, K. 2003. History matching using time-lapse seismic (HUTS). Presented at the SPE Annual Technical Conference and Exhibition, Denver, Colorado, 5-8 October. doi:10.2118/84464-MS.

Gosselin, O., van den Berg, S. and Cominelli, A. 2001. Integrated history-matching of production and 4D seismic data. Presented at the SPE Annual Technical Conference and Exhibition, New Orleans, Louisiana, 30 September-3 October. doi:10.2118/71599-MS.

Ha-Duong, M. and Keith, D.W. 2003. Carbon storage: The economic efficiency of storing CO_2 in leaky reservoirs. *Clean Technologies and Environmental Policy* **5** (3): 181-9. doi: 10.1007/s10098-003-0213-z.

He, Z., Yoon, S. and Datta-Gupta, A. 2002. Streamline-based production data integration with gravity and changing field conditions. *SPE Journal* **7** (4): 423-36. SPE 81208-PA. doi: 10.2118/81208-PA.

Hohl, D., Jimenez, E. and Datta-Gupta, A. 2006. Field experiences with history matching an offshore turbiditic reservoir using inverse modeling. Presented at the SPE Annual Technical Conference and Exhibition, San Antonio, Texas, 24-27 September. doi: 10.2118/101983-MS.

Hovorka, S.D., Benson, S.M., Doughty, C., Freifeld, B.M., Sakurai, S., Daley, T.M., Kharaka, Y.K., Holtz, M.H., Trautz, R.C. and Nance, H.S. 2006. Measuring permanence of CO_2 storage in saline formations: The Frio experiment. *Environmental Geosciences* **13** (2): 105-21. doi: 10.1306/eg.11210505011.

Huang, X. and Kelkar, M. 1996. Reservoir characterization by integration of seismic and dynamic data. Presented at the SPE/DOE Improved Oil Recovery Symposium, Tulsa, Oklahoma, 21-24 April. 10.2118/35415-MS.

Huang, X., Meister, L. and Workman, R. 1997. Reservoir characterization by integration of time-lapse seismic and production data. Presented at the SPE Annual Technical Conference and Exhibition, San Antonio, Texas, 5-8 October. doi:10.2118/38695-MS.

Idrobo, E., Choudhary, M. and Datta-Gupta, A. 2000. Swept volume calculations and ranking of geostatistical reservoir models using streamline simulation. Presented at the SPE/AAPG Western Regional Meeting. doi: 10.2118/62557-MS.

Jenkins, M.K. 1984. An analytical model for water/gas miscible displacements. Presented at the SPE Enhanced Oil Recovery Symposium, Tulsa, Oklahoma, 15-18 April. doi: 10.2118/12632-MS.

Jenkins, S., Waite, M. and Bee, M. 1997. Time - lapse monitoring of the Duri steamflood: A pilot and case study. *The Leading Edge* **16** (9): 1267-73.

Jimenez, E., Datta-Gupta, A. and King, M. 2010. Full-field streamline tracing in complex faulted systems with non-neighbor connections. *SPE Journal* **15** (1): 7-17. SPE 113425-PA. doi: 10.2118/113425-PA.

Jimenez, E., Sabir, K., Datta-Gupta, A. and King, M. 2007. Spatial error and convergence in streamline simulation. *SPE Res Eval & Eng* **10** (3): 221-32. SPE 92873-PA. doi: 10.2118/92873-PA.

Johnstad, S., Seymour, R. and Smith, P. 1995. Seismic reservoir monitoring over the Oseberg field during the period 1989-1992. *First Break* **13** (5): 169-83.

Khazanehdari, J., Yi, T. and Curtis, T. 2005. Production history-matching using time-lapse seismic. Presented at the SPE Annual Technical Conference and Exhibition, Dallas, Texas, 9-12 October 2005. doi:10.2118/97100-MS.

Kjelstadli, R., Lane, H., Johnson, D., Barkved, O., Buer, K. and Kristiansen, T. 2005. Quantitative history match of 4D seismic response and production data in the Valhall field. Presented at the Offshore Europe, Aberdeen, United Kingdom, 6-9 September. doi:10.2118/96317-MS.

Korneev, V.A., Goloshubin, G.M., Daley, T.M. and Silin, D.B. 2004. Seismic low-frequency effects in monitoring fluid-saturated reservoirs. *Geophysics* **69** (2): 522-32. doi: 10.1190/1.1707072.

Kretz, V., Le Ravalec-Dupin, M. and Roggero, F. 2004. An integrated reservoir characterization study matching production data and 4D seismic. *SPE Reservoir Evaluation & Engineering* **7** (2): 116-22. SPE 88033-PA. doi: 10.2118/88033-PA.

Kumar, A., Datta-Gupta, A., Shekhar, R. and Gibson, R. 2008. Modeling time lapse seismic monitoring of CO2 sequestration in hydrocarbon reservoirs including compositional and geochemical effects. *Petroleum Science and Technology* **26** (7): 887-911.

Landa, J. and Horne, R. 1997. A procedure to integrate well test data, reservoir performance history and 4-D seismic information into a reservoir description. Presented at the SPE Annual Technical Conference and Exhibition, San Antonio, Texas, 5-8 October. doi:10.2118/38653-MS.

Landa, J., Horne, R., Kamal, M. and Jenkins, C. 2000. Reservoir characterization constrained to well-test data: A field example. *SPE Reservoir Evaluation & Engineering* **3** (4): 325-34. SPE 65429-PA. doi: 10.2118/65429-PA.

Landro, M., Digranes, P. and Strønen, L. 2001. Mapping reservoir pressure and saturation changes using seismic methods possibilities and limitations. *First Break* **19** (12): 671-7.

Landro, M., Solheim, O.A., Hilde, E., Ekren, B.O. and Stronen, L.K. 1999. The Gullfaks 4D seismic study. *Petroleum Geoscience* **5** (3): 213-26. doi: 10.1144/petgeo.5.3.213.

Leonenko, Y. and Keith, D.W. 2008. Reservoir engineering to accelerate the dissolution of CO2 stored in aquifers. *Environmental science & technology* **42** (8): 2742-7. doi: 10.1021/es071578c.

Li, R., Reynolds, A. and Oliver, D. 2003. History matching of three-phase flow production data. *SPE Journal* **8** (4): 328-40. SPE 87336-PA. doi: 10.2118/87336-PA.

Lumley, D. and Behrens, R. 1998. Practical issues of 4D seismic reservoir monitoring: What an engineer needs to know. *SPE Reservoir Evaluation & Engineering* **1** (6): 528-38. SPE 53004-PA. doi: 10.2118/53004-PA.

Lumley, D.E. 2001. Time-lapse seismic reservoir monitoring. *Geophysics* **66** (1): 50-3. doi: 10.1190/1.1444921.

Luo, Y. and Schuster, G.T. 1991. Wave - equation traveltime inversion. *Geophysics* **56** (5): 645-53. doi: 10.1190/1.1443081.

Lygren, M., Husby, O., Osdal, B., El Ouair, Y. and Springer, M. 2005. History Matching using 4D seismic and pressure data on the Norne field. Presented at the EAGE 67th Conference and Exhibition, Madrid, Spain, 13 - 16 June.

Marple Jr, S.L. 1987. *Digital spectral analysis with applications*, 1st edition. Englewood Cliffs, New Jersey.: Prentice-Hall.

Mavko, G., Mukerji, T. and Dvorkin, J. 1998. *The rock physics handbook*. Cambridge, UK: Cambridge University Press Cambridge.

McCormick, G.P. and Tapia, R.A. 1972. The gradient projection method under mild differentiability conditions. *SIAM Journal on Control* **10** (1): 93-8. doi: 10.1137/0310009.

Nordbotten, J.M., Celia, M.A. and Bachu, S. 2005. Injection and storage of CO_2 in deep saline aquifers: Analytical solution for CO_2 plume evolution during injection. *Transport in Porous Media* **58** (3): 339-60. doi: 10.1007/s11242-004-0670-9.

Nur, A. 1989. Four-dimensional seismology and (true) direct detection of hydrocarbons; the petrophysical basis. *The Leading Edge* **8** (9): 30-6.

Nur, A., Tosaya, C. and Vo-Thanh, D. 1984. Seismic monitoring of thermal enhanced oil recovery processes. *SEG Technical Program Expanded Abstracts* **3** (1): 337-40. doi: 10.1190/1.1894015.

O'Donovan, A., Smith, S. and Pal, K. 2000. Foinaven 4D seismic-dynamic reservoir parameters and reservoir management. Presented at the SPE Annual Technical Conference and Exhibition, Dallas, Texas, 1-4 October. doi:10.2118/63294-MS.

Oliver, D.S., Reynolds, A.C., Bi, Z. and Abacioglu, Y. 2001. Integration of production data into reservoir models. *Petroleum Geoscience* **7** (S): S65-73. doi: 10.1144/petgeo.7.S.S65.

Osdal, B., Husby, O., Aronsen, H.A., Chen, N. and Alsos, T. 2006. Mapping the fluid front and pressure buildup using 4D data on Norne Field. *The Leading Edge* **25** (9): 1134-41. doi: 10.1190/1.2349818.

Oyerinde, A., Datta-Gupta, A. and Milliken, W. 2009. Experiences with streamline-based three-phase history matching. *SPE Reservoir Evaluation & Engineering* **12** (4): 528-41. SPE 109964-PA. doi: 10.2118/109964-PA.

Parker, R.L. 1994. *Geophysical inverse theory*, Princeton, New Jersey: Princeton University Press.

Peters, L., Arts, R., Brouwer, G., Geel, C., Cullick, S., Lorentzen, R., Chen, Y., Dunlop, N., Vossepoel, F. and Xu, R. 2010. Results of the Brugge benchmark study for flooding optimization and history matching. *SPE Reservoir Evaluation & Engineering* **13** (3): 391-405. SPE 119094-PA. doi: 10.2118/119094-PA.

Pollock, D.W. 1988. Semianalytical computation of path lines for finite - difference models. *Ground Water* **26** (6): 743-50. doi: 10.1111/j.1745-6584.1988.tb00425.x.

Pullin, N., Matthews, L. and Hirsche, W. 1987. Techniques applied to obtain very high-resolution 3-D seismic imaging at an Athabasca tar sands thermal pilot. *The Leading Edge* **6** (12): 10-5.

Qassab, H., M. Khalifa, R., Afaleg, N., Ali, H., Kharghoria, A., He, Z., Lee, S.H. and Datta-Gupta, A. 2003. Streamline-based production data integration under realistic field conditions: Experience in a giant Middle-Eastern reservoir. Presented at the SPE Annual Technical Conference and Exhibition, Denver, Colorado, 5-8 October. doi: 10.2118/84079-MS.

Reynolds, A.C., He, N. and Oliver, D.S. 1999. Reducing uncertainty in geostatistical description with well testing pressure data. *Reservoir Characterization–Recent Advances* (71): 149-62.

Silin, D., Patzek, T. and Benson, S.M. 2009. A model of buoyancy-driven two-phase countercurrent fluid flow. *Transport in Porous Media* **76** (3): 449-69. doi: 10.1007/s11242-008-9257-1.

Skjervheim, J.A., Evensen, G., Aanonsen, S.I., Ruud, B.O. and Johansen, T.A. 2007. Incorporating 4d seismic data in reservoir simulation models using ensemble kalman filter. *SPE J* **12** (3): 282-92. SPE 95789-PA. doi: 10.2118/95789-PA.

Spycher, N., Pruess, K. and Ennis-King, J. 2003. CO_2-H_2O mixtures in the geological sequestration of CO_2. I. Assessment and calculation of mutual solubilities from 12 to 100 C and up to 600 bar. *Geochimica et Cosmochimica Acta* **67** (16): 3015-31. doi: 10.1016/S0016-7037(03)00273-4.

Stone, H. 1982. Vertical, conformance in an alternating water-miscible gas flood. Presented at the SPE Annual Technical Conference and Exhibition, New Orleans, Louisiana, 26-29 September. doi: 10.2118/11130-MS.

Tura, A. and Lumley, D. 2000. Estimating pressure and saturation changes from time-lapse AVO data. Presented at the Offshore Technology Conference, Houston, Texas, 1-4 May. doi:10.4043/12130-MS.

Vanorio, T., Mavko, G., Vialle, S. and Spratt, K. 2010. The rock physics basis for 4D seismic monitoring of CO2 fate: Are we there yet? *The Leading Edge* **29** (2): 156-62. doi: 10.1190/1.3304818.

Vasco, D.W. 2004. Seismic imaging of reservoir flow properties: Time-lapse pressure changes. *Geophysics* **69** (2): 511-21. doi: 10.1190/1.1707071.

Vasco, D.W. and Datta-Gupta, A. 2001. Asymptotics, saturation fronts, and high resolution reservoir characterization. *Transport in Porous Media* **42** (3): 315-50. doi: 10.1023/A:1006788413831.

Vasco, D.W., Datta-Gupta, A. and Long, J.C.S. 1997. Resolution and uncertainty in hydrologic characterization. *Water Resources Research* **33** (3): 379-97. doi: 10.1029/96WR03301.

Vasco, D.W., Datta - Gupta, A., Behrens, R., Condon, P. and Rickett, J. 2004. Seismic imaging of reservoir flow properties: Time-lapse amplitude changes. *Geophysics* **69** (6): 1425-42. doi: 10.1190/1.1836817.

Vasco, D.W., Seongsik, Y. and Akhil, D.G. 1999. Integrating dynamic data into high-resolution reservoir models using streamline-based analytic sensitivity coefficients. *SPE Journal* **4** (4): 389-99. SPE 59253-PA. doi: 10.2118/59253-PA.

Waggoner, J., Cominelli, A., Seymour, R. and Stradiotti, A. 2003. Improved reservoir modelling with time-lapse seismic data in a Gulf of Mexico gas condensate reservoir. *Petroleum Geoscience* **9** (1): 61-71. doi: 10.1144/1354-079302-512.

Wang, Z. 1997. Feasibility of time - lapse seismic reservoir monitoring: The physical basis. *The Leading Edge* **16** (9): 1327-30. doi: 10.1190/1.1437796.

Wang, Z. and Nur, A.M. 1986. Effect of temperature on wave velocities in sands and sandstones with heavy hydrocarbons. *SPE Reservoir Engineering* **3** (1): 158-64. SPE 15646-PA. doi: 10.2118/15646-PA.

Wang, Z., Hirsche, W.K. and Sedgwick, G. 1991. Seismic monitoring of water floods?—a petrophysical study. *Geophysics* **56** (10): 1614-23. doi: 10.1190/1.1442972.

Williams, M.A., Keating, J.F. and Barghouty, M.F. 1998. The stratigraphic method: A structured approach to history matching complex simulation models. *SPE Reservoir Evaluation & Engineering* **1** (2): 169-76. SPE 38014-PA. doi: 10.2118/38014-PA.

Wu, Z. and Datta-Gupta, A. 2002. Rapid history matching using a generalized travel-time inversion method. *SPE Journal* **7** (2): 113-22. SPE 78359-PA. doi: 10.2118/78359-PA.

Yamamoto, H., Fanchi, J. and Davis, T. 2004. Integration of time-lapse seismic data into a flow model study of co2 injection into the weyburn field. presented at the spe annual technical conference and exhibition, Houston, Texas, 26-29 September. doi: 10.2118/90532-MS.

Yang, P.H. and Watson, A.T. 1988. Automatic history matching with variable-metric methods. *SPE Reservoir Engineering* **3** (3): 995-1001. SPE 16977-PA. doi: 10.2118/16977-PA.

Yin, J., Park, H., Datta-Gupta, A. and Choudhary, M. 2010. A hierarchical streamline-assisted history matching approach with global and local parameter updates. Presented at the SPE Western Regional Meeting, Anaheim, California, 27-29 May. doi:10.2118/132642-MS.

Yoon, S., Malallah, A., Datta-Gupta, A., Texas A&M U., Vasco, D. and Behrens, R. 2001. A multiscale approach to production-data integration using streamline models. *SPE Journal* **6** (2): 182-92. SPE 71313-PA. doi: 10.2118/71313-PA.

VITA

Alvaro Jose Rey Amaya received his Bachelor of Science degree in mechanical engineering from Universidad Industrial de Santander in 1999. He received a Master of Science degree in mechanical engineering from Universidad de los Andes 2001. He has worked in simulation and control of thermal processes and he has taught undergraduate courses in heat transfer and fluid mechanics at the Universidad Industrial de Santander. He entered the doctorate program in petroleum engineering at Texas A&M University in September 2007 and received his Doctor of Philosophy degree in August 2011. His research interests include fluid flow simulation and dynamic data integration of production and seismic data.

Mr. Rey Amaya may be reached at Chevron ETC Reservoir Simulation Support Team; San Ramon, CA 94583. His email is alvarojose.rey@gmail.com